UNIVERSITY OF OSLO

MASTER'S THESIS

Late Kinetic Decoupling of Dark Matter

Author:
Håvard Tveit IHLE

Supervisor:
Torsten BRINGMANN and
Øystein ELGARØY

A thesis submitted in fulfillment of the requirements
for the degree of Master of Science

in the

Cosmology Group
Institute of Theoretical Astrophysics

June 1, 2016

"The physics is theoretical, but the fun is real."

Sheldon Cooper

UNIVERSITY OF OSLO

Abstract

The Faculty of Mathematics and Natural Sciences
Institute of Theoretical Astrophysics

Master of Science

Late Kinetic Decoupling of Dark Matter

by Håvard Tveit IHLE

If dark matter, after it has become non-relativistic, scatters elastically with a relativistic heat bath particle, then the resulting pressure leads to acoustic oscillations that suppress the growth of overdensities in the dark matter fluid. If such an interaction can keep dark matter in kinetic equilibrium until keV temperatures, this effect then suppresses structure formation on scales roughly equal to dwarf galaxy scales and smaller, possibly addressing the *missing satellite problem*. The goal of this thesis is to study the possibilities for such late kinetic decoupling in particle models for dark matter.

Using the Boltzmann equation, we discuss the thermal decoupling process of dark matter in detail. In addition to discussing specific dark matter models, we also go into important general considerations and requirements for *late* kinetic decoupling, and models with dark radiation.

We summarize the results obtained in Bringmann et al., 2016, but go into more details on two specific models. First a model consisting of two real scalar particles, one dark matter particle, and one relativistic dark radiation particle, interacting through a 4-particle vertex. This model is of particular interest not only because it is so simple, but also because a large class of effective field theory models will also essentially map onto this model. When combining relic density constraints with late kinetic decoupling, we need very light dark matter $m_\chi \lesssim$ MeV. For these masses, the assumption that dark matter is highly non-relativistic during chemical decoupling breaks down. However, when the dust settles, we find that this is still a viable model for late kinetic decoupling.

We also study a model where a fermionic dark matter particle transforms in the fundamental representation of some $SU(N)$ gauge group. The scattering in the t-channel is so enhanced at low energies in this model, that kinetic decoupling does not happen until the dark radiation becomes non-relativistic. As we discuss, depending on what happens to the dark radiation temperature when it becomes non-relativistic, the resulting suppression of dark matter structures can be radically different. In any case these models seem to require a low value for the dark radiation temperature, which is hard to achieve in model building without new input.

Acknowledgements

First of all I would like to thank my excellent supervisor **Torsten Bringmann**, who is always helpful, and always challenges me. You encourage me when I need encouragement, and you discourage me when I need discouragement. Thanks also for having the idea for this project, which was a perfect match for me, and for all the constructive feedback I have received.

Thanks to my *other* supervisor, **Øystein Elgarøy**, for support and advice during this project.

I want to thank my collaborators **Torsten Bringmann**, **Parampreet Walia** and **Jörn Kersten**, it has been a pleasure working with you, and I have learned a lot from this project. A special thanks to **Jörn** for a fruitful and stimulating discussion on gauge boson polarization sums!

Thanks also to **Frode Kristian Hansen** for giving me work during the last summers, and for helpful advice and guidance.

Thanks to all the people I have met here at ITA over the years, both in the basement and at the institute in general. Thank you for making me like it here so much, and I look forward to staying here for at least four more years!

Thanks to **Morten**, **Morten** and **Anders** for all the fun we have had while teaching the computational physics course these last years!

A big thanks goes out to my aunts **Bodil & Janicke** for giving me real food once in a while!

Thanks also to my friend **Magne**, for making me do active stuff!

I am also grateful to my family for the unconditional love that they provide.

Contents

List of Abbreviations

DM	**D**ark **M**atter
CDM	**C**old **D**ark **M**atter
WDM	**W**arm **D**ark **M**atter
WIMP	**W**eakly **I**nteracting **M**assive **P**article
CD	**C**hemical **D**ecoupling
KD	**K**inetic **D**ecoupling
BE	**B**oltzmann **E**quation
DR	**D**ark **R**adiation
SM	**S**tandard **M**odel
CMB	**C**osmic **M**icrowave **B**ackground
QFT	**Q**uantum **F**ield **T**heory
BBN	**B**ig **B**ang **N**ucleosynthesis
LHC	**L**arge **H**adron **C**ollider

Introduction

In the past 20 years or so, a series of excellent experiments have made cosmology into a precision science, converging on the ΛCDM model of cosmology, which has been a huge success. In recent years, however, a few discrepancies between observations and cold dark matter (CDM) simulations at small (dwarf galaxy) scales have emerged. The main ones are the *missing satellites*, the *cusp/core* and the *too big to fail* problems. These small-scale problems motivate us to consider alternatives or extensions to the standard CDM paradigm.

Detailed simulations have shown that DM with a significant self-interaction can solve the cusp/core and the too big to fail problems. Acoustic oscillations in the DM fluid from interaction between DM and some relativistic heat bath particle, can also help address the missing satellites problem. For these acoustic oscillations to be relevant for structures the size of dwarf galaxies, however, we need for the kinetic decoupling (KD) to happen much later than in typical weakly interacting massive particle (WIMP) models. This late KD is what we are interested in here.

Kinetic equilibrium for DM is maintained by elastic scattering between DM and the heat bath particles. KD refers to the process when the elastic scattering between DM and the heat bath become too rare to keep the temperature of DM equal to the heat bath temperature and the temperature of DM starts to drop.

Many models that give rise to late KD also naturally gives rise to a significant DM self-interaction, which is also interesting, since self-interacting DM has the potential to also solve both the cusp/core and the too big to fail problem.

Relation of this Thesis to Bringmann et al., 2016

The main focus of my work for this masters project has been in classifying all the simplest particle models for DM that can give rise to such late KD. This work culminated in my contribution to the paper Bringmann et al., 2016, for which I, among other things, calculated the tree-level scattering processes relevant for KD. When writing this thesis then, I make an effort to not just repeat what is in the paper, but to have this thesis stand on its own as complementary to the results and work in the paper.

What I do in this thesis is that while I give a brief summary of the results in Bringmann et al., 2016, I do not discuss all the different models I have worked with in detail. Rather, I focus on two models that are very interesting, and, for different reasons, are not immediately amenable to the simple analytic analysis that works well for most of the models. These models require some special care and are dealt with in detail.

For more on the other models and specific results see Bringmann et al., 2016.

Outline of Thesis

This thesis is divided into five parts. First we go into the background physics relevant for this thesis. This includes an introduction to cosmology and structure formation (Ch. 1) as well as an introduction to thermodynamics and kinetic theory in an expanding universe (Ch. 2).

The second part is focused on DM. First we discuss the motivation and evidence for DM, as well as what we actually know about DM properties (Ch. 3). We introduce DM detection and self-interaction, before going into a thorough discussion of the decoupling of DM from the thermal heat bath. Here we allow for the possibility of two separate visible and dark heat baths. We discuss both chemical decoupling (CD) and KD in detail (Chs. 4 and 5).

The third part is specifically focused on *late* KD. First we discuss various ways late KD can be achieved, and related issues (Ch. 6). Then we discuss some important properties of the dark heat bath and dark radiation (DR), like the evolution of the relative temperature of the dark and visible sectors, and cosmological constraints on the amount of DR. After a summary of previous work (Ch. 7), we then go into a detailed discussion of two interesting particle models for DM and DR, and thermal decoupling in these models (Chs. 8 and 9).

The fourth part consists of a short discussion section (Ch. 10) as well as the conclusion. In the former we discuss the results of the models analyzed in Bringmann et al., 2016, as well as the models considered in this thesis, we discuss the plausibility of the models, and the motivation for going beyond CDM at all.

Quantum field theory is also central to the masters project, but as it is not as relevant to the discussion in this thesis, only a very brief introduction is given in App. A. The appendix also contain a note on some technicalities regarding the polarization sums for external gauge bosons that we had to deal with in this project (App. B).

Part I

Background Physics

Chapter 1

Cosmology

1.1 Friedmann-Robertson-Walker Cosmology

Because the universe appears to be, on large scales, homogeneous and isotropic, we can describe its large scale evolution completely by some simple equations. In the metric, the assumption of homogeneity and isotropy is implemented by requiring the spatial 3-space to be totally symmetric. This results in three possible spatial curvatures, closed, open and flat, all described by the Friedmann-Robertson-Walker metric

$$ds^2 = dt^2 - a^2(t)\left(\frac{dr^2}{1-kr^2} + r^2 d\Omega^2\right), \tag{1.1}$$

where $a(t)$ is the scale factor, $r,\ \theta$ and ϕ are the comoving coordinates in space and $k = a^2 R_S/6$ is the curvature parameter, where R_S is the Ricci curvature scalar in space. Note that k can take any real value[1], and the sign of k determines if the universe is open or closed. $k = 0$ corresponds to flat space.

Since our observations are consistent with a completely flat universe ($k/a^2 \ll H^2$) (Planck Collaboration et al., 2015), we will simply set $k = 0$ in the following. The metric for a spatially flat universe is given by

$$ds^2 = dt^2 - a^2(t)\left(dx^2 + dy^2 + dz^2\right). \tag{1.2}$$

We will treat a as dimensionless and let the comoving coordinates carry dimensions of length, and we will, unless stated otherwise, use the convention where $a_0 \equiv a(t_0) = 1$, where t_0 is the present time. In this case, if two galaxies have a comoving distance x, this *comoving* distance is given by the *physical* distance, $r_{\mathrm{P}}(t_0)$, between the galaxies today. If you want the distance at some other time, t, you have to multiply by the scale factor $a(t)$. Thus in general the physical distance is given by

$$r_{\mathrm{P}}(t) = a(t)\, x. \tag{1.3}$$

Let us also note a special feature of these spacetimes. If you look at a galaxy at a certain (physical) distance r_{P}, then it will be moving away from (towards) you, depending on how fast the universe is expanding (contracting). This velocity is proportional to the distance, and the proportionality

[1] In many texts the scale factor is defined such that k can only take the values -1, 0 and 1. In this case the comoving coordinates are dimensionless and $a(t)$ carries dimension of length. .

coefficient is called the *Hubble rate*, H

$$v_{\rm P} = \frac{dr_{\rm P}}{dt} = \dot{a}x = \frac{\dot{a}}{a} r_{\rm P} = H r_{\rm P}, \tag{1.4}$$

where we see that $H = \dot{a}/a$.

$H_0 \equiv H(t = t_0)$ is the current value of the Hubble rate, often called the Hubble constant. This is an important cosmological parameter, and is usually defined in terms of the dimensionless Hubble parameter, h, as follows

$$H_0 = 100\, h \frac{\rm km}{\rm s\ Mpc}. \tag{1.5}$$

1.1.1 Perfect Fluids

The requirements of spatial homogeneity and isotropy impose severe constraints on the various quantities, like scalar, vector or tensor fields that are relevant in cosmology. In particular, isotropy implies that any three-vector $\mathbf{v}$ must vanish (in the comoving frame), and homogeneity implies that any three-scalar ϕ must be a function only of time.

A perfect fluid is defined as a medium that has, at every point, a locally inertial frame of reference, moving with the fluid, where the fluid appears isotropic. The energy momentum tensor of such a fluid in this reference frame is given in terms of two scalars ρ and P (Weinberg, 2008, p. 521)

$$T^0_0 = \rho(t), \;\; T^0_i = 0, \;\; T^i_j = -\delta^i_j P(t). \tag{1.6}$$

This can be thought of as the equation defining the energy density, $\rho(t)$, and the pressure, $P(t)$, of a perfect fluid. In a frame with arbitrary velocity, the energy momentum tensor of a perfect fluid is thus given by

$$T^{\mu\nu} = (\rho + p) u^\mu u^\nu - g^{\mu\nu} P. \tag{1.7}$$

The conservation of energy and momentum ($T^{\mu\nu}_{;\mu} = 0$) then implies the following continuity equation

$$\frac{d\rho}{dt} = -3\frac{\dot{a}}{a}(\rho + P). \tag{1.8}$$

This is in general not solvable analytically, but can be solved easily for a fluid obeying an equation of state of the form

$$P = w\rho, \tag{1.9}$$

where w is a constant (in time). Usually we have $-1 \leq w \leq 1$, but this depends on the physical assumptions you want to make.[2] The solution in these simple cases is given by

$$\rho = \rho_0 a^{-3(1+w)}, \tag{1.10}$$

where $\rho_0 = \rho(t_0)$ and we have used the convention $a_0 = a(t_0) = 1$.

There are three special cases that will be very useful in describing our own universe.

[2] For a nice discussion of these issues see (Carroll, 2004, p. 174-177).

- Non-relativistic matter (simpliy called *matter*): $w = 0$ and $\rho_m = \rho_{m0}/a^3$. This is interpreted as the energy of each particle being constant ($E \simeq m$) and the number density scaling with the volume.
- Ultra-relativistic matter (called *radiation*): $w = 1/3$ and $\rho_r = \rho_{r0}/a^4$. Here, in addition to the number density scaling with the volume, the radiation wavelength increases ($\lambda \propto a$) and hence the energy decreases as $E \propto 1/a$, leading to the extra power of a in the denominator.
- Vacuum energy (called the *cosmological constant*): $w = -1$ and $\rho_\Lambda = \rho_{\Lambda 0}$. This is simply an energy contribution that is proportional to the volume of space, leading to a constant energy density.

In general the universe, at any given moment in time, will consist of several energy components, but as long as we can neglect the energy transfer between the different components, we can apply Eq. 1.8 separately to each of the components, simplifying things considerably. For now we will assume that we can simply neglect this energy-transfer, but we will discuss these issues in more detail when we get into early universe thermodynamics in chapter 2.1.

1.1.2 The Friedmann Equations

If we write out the Einstein equations of a perfect fluid in a spacetime described by the FRW metric, we obtain the two Friedmann equations

$$\left(\frac{\dot{a}}{a}\right)^2 = \frac{8\pi G}{3}\rho - \frac{k^2}{a^2}, \tag{1.11}$$

$$\frac{\ddot{a}}{a} = -\frac{4\pi G}{3}(\rho + 3P). \tag{1.12}$$

Here we should note that these equations are not independent of Eq. 1.8, but that each of the three can be derived from the two others.

Let us now look at the solution of the Friedmann equations in cases where a single energy component (with a constant w) dominates. In these cases we can solve the equations explicitly

$$a(t) = \left(\frac{t}{t_0}\right)^{\frac{2}{3(1+w)}}, \tag{1.13}$$

where we have set the value of t at witch $a = 0$ to 0 (this would correspond to starting the time at the *Big Bang*). Note that this only holds for $w > -1$. For $w = -1$, which corresponds to a universe with just a cosmological constant, we have no Big Bang, but we have an exponential expansion with a constant H

$$a(t) = e^{H(t-t_0)}. \tag{1.14}$$

Introducing the critical density, $\rho_c \equiv 3H^2/(8\pi G)$, the density required to have a completely flat universe, and using the solution to Eq. (1.8), we can rewrite Eq. 1.11 in the following convenient form

$$H^2 = H_0^2 \sum_i \frac{\Omega_i}{a^{3(1+w_i)}}, \tag{1.15}$$

where i denotes each of the different energy components, $\Omega_i \equiv \rho_i(t_0)/\rho_c(t_0)$ and we are also treating the curvature as an effective energy component with $\rho_k \equiv -3k^2/(8\pi G a^2)$. With these conventions we will always have $\sum_i \Omega_i = 1$.

As a special case let us consider the best model we have for our own universe, the ΛCDM - model. This is a model with three components, matter, radiation and a cosmological constant, with $\Omega_\Lambda \sim 0.7$, $\Omega_m \sim 0.3$, $\Omega_r \sim 5 \cdot 10^{-5}$ and $H_0 \sim 70$ km/(s Mpc).[3] Eq. 1.15 can then be written

$$H^2 = H_0^2 \left[\frac{\Omega_r}{a^4} + \frac{\Omega_m}{a^3} + \Omega_\Lambda \right]. \tag{1.16}$$

At the present time, the radiation component hardly contributes, while the matter and cosmological constant have contributions of the same order of magnitude. At earlier times $a \sim 10^{-1} - 10^{-3}$ the universe was matter dominated, and at $a \lesssim 10^{-4}$ the universe was radiation dominated.

1.2 Structure Formation

Until now we have looked at the evolution of the background universe. We have assumed that the universe is completely homogeneous and isotropic. Although these are very good assumptions in the early universe, and good assumptions today at large scales, the most interesting stuff are the inhomogeneities (like us!).

In this section we will relax the assumption of homogeneity, and discuss what happens to the small initial perturbations in density and pressure. We will mostly discuss linear perturbation theory, but will mention some qualitative features of non-linear structure formation and cosmological simulations.

1.2.1 Linear Perturbation Theory

The early universe was very homogeneous. This is evident from observations of the CMB which has relative fluctuations of order 10^{-5}. The good thing about this is that as long as the (relative) perturbations are small, we can use linear perturbation theory, making all the complicated non-linear equations for the dynamics of fluids in an expanding universe linear, and simple to deal with.

A very nice property of linear equations is that when we go to Fourier space, all the different modes decouple. This means that we can treat each mode, corresponding to each length scale, independently.

The equations describing the evolution of perturbations are the Einstein equations for GR

$$G_{\mu\nu} = 8\pi G T_{\mu\nu}, \tag{1.17}$$

and the Boltzmann equations for each species of particle

$$\frac{df_i}{d\lambda} = C[f_i]. \tag{1.18}$$

[3] If you want the current best values for these parameters see Planck Collaboration et al., 2015.

For a few simple cases, however, a good assumption is that the particle species evolves like an ideal fluid. This is valid for a non-relativistic DM species and for baryons after recombination. It is also a good approximation for radiation before recombination (Mo, Bosch, and White, 2010, p. 191).

For an ideal fluid we do not have to consider the full Boltzmann equation, but can use the local conservation of the energy momentum tensor $T^{\mu\nu}_{;\nu} = 0$.

Let us now define the perturbed quantities

$$\rho(\mathbf{x}, t) = \rho_0(t)\big[1 + \delta(\mathbf{x}, t)\big], \tag{1.19}$$

$$T^{\mu\nu} = T^{\mu\nu}_0 + [\delta T]^{\mu\nu}, \tag{1.20}$$

$$g^{\mu\nu} = g^{\mu\nu}_0 + [\delta g]^{\mu\nu}, \tag{1.21}$$

where 0 denotes unperturbed (background) quantities, and the perturbations are considered "small" (in the sense that e.g. $[\delta T]^{\mu\nu}/T^{\mu\nu} \ll 1$). Since we are free to choose any coordinates (gauge freedom), it is clear that these perturbations are not unique, but will be gauge dependent.

Let us deal with the metric first, since this affects everything else. $[\delta g]^{\mu\nu}$ is a symmetric four by four matrix, meaning that it has 10 independent functions. We can, however, remove four of these by choice of gauge (coordinates). This leaves six free functions. It is useful to classify these by how they transform under rotations and translations.

In the following, we will only deal with two scalar perturbations to the metric. There are also tensor and vector perturbations (or even more scalars, depending on the choice of gauge). The vector modes decay as the universe expands, even outside the horizon, and usually do not contribute to structure formation. Tensor modes (in gauges where they are defined as the divergenceless and traceless part of the metric perturbations) represent gravitational waves and only start to decay after they enter the horizon. They usually do not affect structure formation much, although primordial gravitational waves, if they are detected, would be a very interesting probe of inflation physics.

We will work in the *conformal Newtonian gauge*, which only includes the two scalar functions, Φ and Ψ. The metric in this gauge is given by

$$ds^2 = a^2(\eta)\Big[(1 + 2\Psi)d\eta^2 - (1 - 2\Phi)\delta_{ij}x^i x^j\Big], \tag{1.22}$$

where $\eta(t) = \int_0^t dt'/a(t')$ is called the *conformal time* and is equal to the comoving particle horizon of the universe at any given time.

As we see from the metric, Ψ corresponds to a time dilation, while Φ corresponds to an isotropic stretching of space. The reason this gauge has its name is that in the Newtonian limit, Φ corresponds directly to the Newtonian gravitational potential.

The perturbations in the energy momentum tensor, for a single species, can be written as

$$[\delta T]^{\mu}_{\nu} = \rho_0 \begin{pmatrix} \delta & -(1+w)v^j \\ (1+w)v^j & -w\delta\delta^i_j \end{pmatrix}, \tag{1.23}$$

where $w \equiv P_0/\rho_0 = c_s^2$ and $v^j \equiv a u^j = a\, dx^j/d\tau$. c_s^2 is the square of the adiabatic sound speed.

We are now ready to write down the equations we need to solve to study the evolution of these perturbations. As mentioned we will work in Fourier space e.g.

$$\delta_{\mathbf{k}}(t) = \frac{1}{V}\int \delta(\mathbf{x}, t)\exp\left(-i\mathbf{k}\cdot\mathbf{x}\right),$$

where $\mathbf{k}$ is the co-moving wave vector. We will stay in Fourier space for the rest of this section, so for brevity we will neglect the subscript $\mathbf{k}$ on the various quantities.

We only need two of the Einstein equations, since we only have the two scalar functions. We will use the time-time and the longitudinal traceless space-space parts of the equations giving us (Mo, Bosch, and White, 2010, p. 185)

$$k^2\Phi + 3\frac{a'}{a}\left(\Phi' + \frac{a'}{a}\Psi\right) = -4\pi G a^2[\delta T]^0_0, \tag{1.24}$$

$$k^2(\Phi - \Psi) = 0, \tag{1.25}$$

where $'$ denotes $d/d\eta$.

We see that for an ideal fluid, we simply have $\Psi = \Phi$, making our lives simpler.

We also get two equations from the conservation of energy and momentum (Mo, Bosch, and White, 2010, p. 186)

$$\delta' + (1+w)\left[ikv - 3\Phi'\right] = 0, \tag{1.26}$$

$$v' + \frac{a'}{a}(1-3w)v + ik\left(\frac{w\delta}{(1+w)} + \Psi\right) = 0, \tag{1.27}$$

where we have assumed that the velocities are irrotational ($v^i = vk^i/k$).[4]

1.2.2 Simplified Model

In order to study how perturbations evolve in the universe we will study a simplified model with two fluids, both assumed to behave like ideal fluids. We will have one radiation fluid denoted by γ and one non-relativistic DM fluid denoted by χ. The equations for this model is given by

$$\delta'_\chi + ikv_\chi = 3\Phi', \tag{1.28}$$

$$v'_\chi + \frac{a'}{a}v_\chi = -ik\Phi, \tag{1.29}$$

$$\delta'_\gamma + \frac{4}{3}ikv_\gamma = 4\Phi', \tag{1.30}$$

$$v'_\gamma + \frac{1}{4}ik\delta_\gamma = -ik\Phi, \tag{1.31}$$

$$k^2\Phi + 3\frac{a'}{a}\left(\Phi' + \frac{a'}{a}\Phi\right) = -4\pi G a^2\left[\rho^\chi_0\delta_\chi + \rho^\gamma_0\delta_\gamma\right]. \tag{1.32}$$

[4]This is a good assumption for two reasons. First, $\nabla\times\mathbf{v} \sim 1/a$ in the linear regime, meaning that, since there are no sources of vorticity in the equations, that the curl of the velocity can be neglected at late times. Also, since only the divergence of the velocity field contributes to the equation for the overdensity, if any vorticity were there, it would not affect structure formation (in the linear regime).

Initial Conditions

In very early times ($\eta \to 0$) we are in the strongly radiation dominated phase and $\rho_0^\chi \delta_\chi \ll \rho_0^\gamma \delta_\gamma$. We can then rewrite Eq. 1.32 as

$$\left(\frac{a}{a'}\Phi' + \Phi\right) = -\frac{\delta_\gamma}{2}, \tag{1.33}$$

where we have used Eq. 1.11 for a flat radiation dominated universe. We will show that Φ is essentially constant in the deep relativistic era, so the derivative term is also negligible and we get

$$\delta_\gamma(\eta = 0) = -2\Phi_0, \tag{1.34}$$

where $\Phi_0 \equiv \Phi(\eta = 0)$.

We can also combine Eqs. 1.28 and 1.32 and get

$$\delta_\chi - \frac{3}{4}\delta_\gamma = \text{constant}. \tag{1.35}$$

We will chose the set this constant to zero. This choice correspond to isentropic initial conditions and is a common choice (Dodelson, 2003). This gives us

$$\delta_\chi(\eta = 0) = -\frac{3}{2}\Phi_0. \tag{1.36}$$

The velocities at early times are negligible.

Super-Horizon Evolution

As long as we are on super-horizon scales ($k\eta \ll 1$) we can make the same argument as in last section meaning that

$$\delta_\chi = \frac{3}{4}\delta_\gamma. \tag{1.37}$$

Eq. 1.32 is then given by

$$3\frac{a'}{a}\left(\Phi' + \frac{a'}{a}\Phi\right) = -4\pi G a^2 \rho_0^\chi \delta_\chi \Big[1 + \frac{4}{3y}\Big], \tag{1.38}$$

where we have introduced the variable $y \equiv a/a_{\text{eq}} = \rho_0^\chi/\rho_0^\gamma$ where a_{eq} is the scalefactor at matter radiation equality. Writing Eq. 1.32 in terms of this variable gives us (Dodelson, 2003, p.190)

$$\frac{d^2\Phi}{dy^2} + \frac{21y^2 + 54y + 32}{2y(y+1)(3y+4)}\frac{d\Phi}{dy} + \frac{\Phi}{y(y+1)(3y+4)} = 0. \tag{1.39}$$

An analytic solution to this equation was found by Kodama and Sasaki, 1984, given by

$$\Phi = \frac{\Phi_0}{10}\left[\frac{16\sqrt{y+1} + 9y^3 + 2y^2 - 8y - 16}{y^3}\right]. \tag{1.40}$$

We see from Eq. 1.40 that on super-horizon scales, as we go from the radiation dominated to the matter dominated phase Φ only changes by a factor

$9/10$. Using a similar argument that we used in the previous sections we can show that on super-horizon scales, in the matter dominated phase

$$\delta_\chi = -2\Phi. \tag{1.41}$$

So the main point from this section is that the perturbations on super-horizon scales are essentially frozen in (in the conformal Newtonian gauge). This also makes perfect sense, since there is no causal contact on these scales.

Sub-Horizon Evoluition

On scales much smaller than the horizon ($k\eta \gg 1$) things are much more interesting. In this limit Eq. 1.32 reduces to the Poisson equation

$$k^2\Phi = -4\pi G a^2 \Big[\rho_0^\chi \delta_\chi + \rho_0^\gamma \delta_\gamma\Big], \tag{1.42}$$

If we have $\rho_0^\chi \delta_\chi \ll \rho_0^\gamma \delta_\gamma$ this equation can be combined with Eqs. 1.30 and 1.31 to give the evolution equation for Φ

$$\frac{d^2\Phi}{dz^2} + \frac{4}{z}\frac{d\Phi}{dz} + \Phi = 0, \tag{1.43}$$

where we have defined the variable $z \equiv \eta k/\sqrt{3}$. Since we are in the $z \gg 1$ limit we get

$$\Phi \approx -A\cos(z)/z^2, \tag{1.44}$$

where A is just a constant obtained from matching this solution for Φ onto the previous solution. Using Eq. 1.42 we then get

$$\delta_\gamma \approx 2A\cos(z). \tag{1.45}$$

Combining Eqs. 1.28 and 1.29 we can get the evolution equation for δ_χ as well

$$\frac{d^2\delta_\chi}{dz^2} + \frac{1}{z}\frac{d\delta_\chi}{dz} = -3\Phi, \tag{1.46}$$

The solution of this equation is complicated, but in the limit $z \gg 1$ the growing part of the solution is given by

$$\delta_\chi \approx 3A\ln(z). \tag{1.47}$$

We see from these results that while δ_γ is oscillating, δ_χ is growing, albeit slowly. This means that sooner or later, even while we are still in the radiation dominated universe, we will get $\rho_0^\chi \delta_\chi \gg \rho_0^\gamma \delta_\gamma$. Writing all the equations in terms of y $(= \rho_0^\chi/\rho_0^\gamma)$ in this limit, we get the Meszaros equation (Meszaros, 1974)

$$\frac{d^2\delta_\chi}{dy^2} + \frac{2+3y}{2y(y+1)}\frac{d\delta_\chi}{dy} - \frac{3}{2y(y+1)}\delta_\chi = 0. \tag{1.48}$$

The growing solution of this equation is given by

$$\delta_\chi \propto 1 + \frac{3}{2}y. \tag{1.49}$$

From this result we see that once $\rho_0^\chi \delta_\chi \gg \rho_0^\gamma \delta_\gamma$ the growth of δ_χ essentially stops until the universe starts to become matter dominated, at which point it grows as

$$\delta_\chi \propto a\,. \tag{1.50}$$

It is also interesting to study what will happen in a de Sitter universe, like it looks like our universe is evolving into. In this (almost) de Sitter space we will get

$$\delta_\chi'' + \frac{\delta_\chi'}{\eta} = 4\pi G \rho_0^\chi \delta_\chi, \tag{1.51}$$

with no growing solutions.[5]

As we see from this, aside from a slow (but important) growth during the radiation dominated universe, the matter perturbations can really only grow a lot during the matter dominated phase. In the matter dominated phase the perturbations grow proportional to the scale factor, a, but since a only grows by a factor of $\sim 10^3$ during matter domination, this severely limits the amount of growth possible.

It is also important to note that the perturbations can not start to grow until they enter the horizon, so the growth of the various modes depend crucially on when they enter the cosmological horizon. We should also note that small scales enter the horizon first, and have most time to grow, as can be seen in Fig. 1.1.

1.2.3 Pressure

The matter component that we did not mention is the baryon fluid. The baryons are very strongly coupled to the photons until recombination (about $a = 10^{-3}$), shortly after matter-radiation equality. The pressure in the relativistic fluid keeps the perturbations in the, highly non-relativistic, baryons from growing.

The DM over-densities, however, are growing, and as the baryons begin to fall into the potential wells created by the DM, and then forced out by the photon pressure, the characteristic acoustic oscillations from the CMB power spectrum are created. See Fig. 1.2.

When we modeled the DM fluid in the previous section we completely neglected the pressure ($w = 0$). The equation for a non-relativistic perturbation in a matter dominated universe in general (including pressure), is given by

$$\delta'' + \frac{\delta'}{\eta} + \frac{k^2 c_s^2}{a^2}\delta = 4\pi G \rho_0^\chi \delta_\chi, \tag{1.52}$$

where we have assumed that the dominant contribution to the 1st order Poisson equation comes from $\rho_0^\chi \delta_\chi$. For the DM fluid itself this reduces to

$$\delta_\chi'' + \frac{\delta_\chi'}{\eta} + \omega^2 \delta_\chi = 0, \tag{1.53}$$

[5]Note that this analysis is only valid in the linear regime. Non-linear processes mean that at small scales structures can grow even in a de Sitter background, if they go non-linear already during the matter dominated phase.

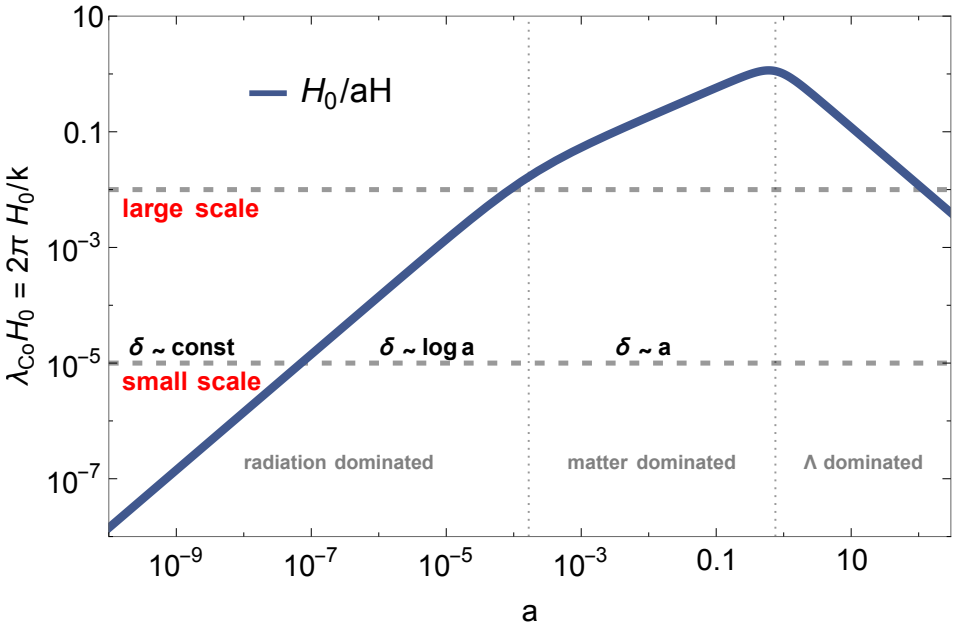

FIGURE 1.1: Overview plot of structure formation. On the y-axis we have comoving length scale, $\lambda_{\rm co}$, and on the x-axis we have the scale factor, a. The thick blue line corresponds to the comoving horizon of the universe. As the matter perturbations, δ, can only start to grow after they enter the horizon ($\lambda_{\rm co} \ll 1/aH$), we see that the perturbations on small scales start to grow first, and have more time to grow. Note that at some point the perturbations, on small scales, become non-linear ($\delta \sim 1$), and the results derived above are not applicable. Perturbations on large scales enter the horizon later and may still be in the linear regime $\delta \ll 1$ today, at $a = 0$. Note also that as the cosmological constant, Λ, starts to dominate, the comoving horizon starts to shrink, and the largest scales move out of the horizon again.

where $\omega^2 \equiv 4\pi G\rho_0^\chi \left(\frac{k^2}{k_J^2} - 1\right)$ and we have defined the Jeans wave-number k_J by

$$k_J \equiv \frac{2\pi}{\lambda_J} = \frac{2\pi a}{c_s}\sqrt{\frac{G\rho_0^\chi}{\pi}}, \tag{1.54}$$

where $c_s^2 \equiv \left(\frac{\partial P}{\partial \rho}\right)_S$ is the adiabatic sound speed. Note here that both k_J and λ_J as defined here are *co-moving* scales (sometimes they are also defined as physical scales).

The Jeans scale represents the equilibrium between gravitational and pressure forces. On scales smaller than the Jeans scale, the pressure forces are largest and we get oscillatory solutions, while on larger scales the gravitational forces are stronger and the perturbations grow.

1.2.4 Free Streaming

Another effect that can dampen the growth of structures is *free streaming*. If a collisionless particle that starts in a potential well, corresponding to an overdensity, has a large enough velocity to escape the well and move to an

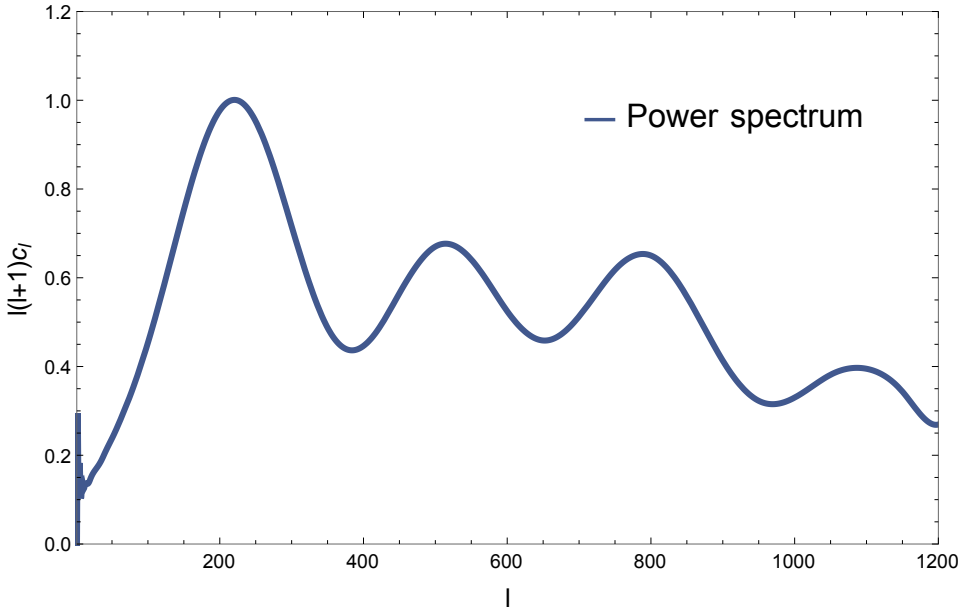

FIGURE 1.2: Power spectrum of the temperature fluctuations in the cosmic microwave background. Based on numerically solving the Einstein-Boltzmann equations for the full ΛCDM model (without neutrinos). The odd peaks (1st, 3rd etc.) corresponds to compression peaks, while even peaks corresponds to decompressions. The first peak represent the modes where the baryons and physics have just had time to compress maximally in the DM potential wells, and the pressure is just about to decompress the fluid. The second peak corresponds to the first complete decompression, where the photon pressure have moved the fluid out of the DM potential wells exactly once. The scale on the y-axis is arbitrary.

underdense region, this will tend to dampen both over- and underdensities. To analyze this it is useful to introduce the (comoving) free-streaming length

$$\lambda_{\text{fs}} \equiv \int_{t_{\text{ls}}}^{t} \frac{v(t')}{a(t')} dt', \tag{1.55}$$

where t_{ls} is the time of last scattering and $v(t)$ is the particle velocity at time t. $\lambda_{\text{fs}}(t)$ is then simply the comoving length traveled by a particle free-streaming from last scattering to the time t.

Roughly we can say that density contrasts gets washed out on smaller scales than λ_{fs}, but remain unsuppressed at larger scales.

If we define a_{ls} as the scale factor at the time of last scattering of DM, we have roughly $v \approx v_{\text{ls}} a_{\text{ls}}/a$. Using this we can estimate the free streaming length during radiation domination

$$\lambda_{\text{fs}} = \int_{a_{\text{ls}}}^{a} \frac{v(a)}{a^2 H(a)} da \approx \sqrt{\frac{3T_{\text{ls}}}{m_\chi}} \frac{a_{\text{ls}}}{H_{\text{eq}} a_{\text{eq}}^2} \ln\left(\frac{a}{a_{\text{ls}}}\right), \tag{1.56}$$

where we have used the fact that $a^2 H \approx a_{\text{eq}}^2 H_{\text{eq}}$ is almost constant during radiation domination, and have introduced the average velocity $v =$

$\sqrt{3T/m_\chi}$. Note that $a_{\rm ls} \neq a_{\rm kd}$ (see Sec. 5), although the two are related. This is because DM also scatters for a short period after KD, but with a rate that is too slow to keep up the DM temperature. The free streaming length quickly becomes constant when we enter matter domination, so it is usually a good order of magnitude estimate to just evaluate the free streaming length at matter-radiation equality.

The free-streaming length of DM then decides the size of the smallest scales where structure formation can go on unsuppressed. Since the free-streaming length increases as the DM mass decreases, this effect allows us, under certain assumptions, to put a lower bound on the DM mass. This effect is discussed briefly is Sec. 5.4 where we compare it to the effect of late KD, which is the main focus of this thesis.

1.2.5 The Power Spectrum

The distribution of the initial perturbations in the various fluids are considered random. It is simply one realization drawn from a general ensemble. Theory clearly cannot predict the exact distribution of perturbations, but it can predict the statistical properties of the ensemble that this realization is taken from. The power spectrum, which denotes the variance of of the various modes is given by

$$P(k,t) \equiv \langle |\delta(k,t)|^2 \rangle = P_i(k) T(k)^2 D(t)^2. \tag{1.57}$$

The initial power spectrum $P_i(k)$ is proportional to the square of the initial value of Φ

$$P_i(k) \propto \langle |\Phi_0(k)|^2 \rangle. \tag{1.58}$$

The transfer function, $T(k)$, is used to take into account the evolution of Φ during the radiation dominated phase. The modes that enter the horizon during radiation domination get severely suppressed, since Φ decays inside the horizon, but is frozen in outside the horizon. The growth function $D(t)$ takes into account the growth of the perturbations during and after the matter dominated phase

$$\delta(k,t) = D(t)\delta_0(k).$$

Note that the density perturbation here is a late-time quantity, defined in and after the matter dominated phase by the Poisson equation

$$\delta(k,t) \equiv -\frac{k^2 \Phi(k,t)}{4\pi G a^2 \rho}, \tag{1.59}$$

and not in general equal to the matter perturbation in the conformal Newtonian gauge at earlier times.

If, as a simple assumption, we assume that the matter perturbations grow logarithmically during all of radiation domination, we get the following expression for the transfer function (Mo, Bosch, and White, 2010, p. 198)

$$T(k) = \begin{cases} 1 & \text{if } k \ll k_{\rm eq}, \\ C(k/k_{\rm eq})^{-2} \ln(k/k_{\rm eq}) & \text{if } k \gg k_{\rm eq}, \end{cases} \tag{1.60}$$

where $k_{\rm eq} \equiv 2\pi/\eta_{\rm eq}$ is the wave mode that enters the horizon exactly at matter radiation equality and C is some constant.

1.2.6 Simulations of Structure Formation

Linear theory is extremely useful, and the fact that it works is the reason that we can extract so precise information out of the cosmic microwave background radiation.

When the perturbations grow and we need to solve the full, non-linear equations, things become a lot harder. We can do much by simulating structure formation using just DM. This works well, at least on large scales, since most of the matter in the universe is dark.

Including baryonic physics, however, is much harder. One of the main reasons this is so much harder, is that baryons have so many important interactions to take into account. Cooling, heating, star formation, feedback mechanisms, radiation and black holes are just some of the interesting but challenging features that need to be taken into account when including baryons to your simulation.

Another important reason baryonic physics is hard to include, is the fact that baryonic physics happens at so many scales at the same time. All the way from stellar scales to reionization of the intergalactic medium, baryonic physics play an important role. You would need practically infinite resolution to incorporate all important effects. This difference in scales necessitates the use of various prescriptions for sub-grid physics, which are very hard to test or verify.

Chapter 2

Thermodynamics and Kinetic Theory in the Expanding Universe

2.1 Thermodynamics in the Expanding Universe

In this section we will review the physics of particles at hight temperatures and in an expanding background. This is certainly the physics describing the SM particles in the early universe, and also in many cases the physics describing the dark sector in this epoch.

It is clear that there is a certain contradiction in talking about thermodynamic equilibrium in a system that is constantly expanding and cooling, however, under certain conditions, the tools of equilibrium statistical mechanics will be both applicable and indeed very useful. As long as the equilibration time, t_{eq}, of the system is much smaller than the characteristic time of expansion (e.g. $t_{\text{eq}} \ll 1/H$), the system will, at any given time t, be in its equilibrium configuration at a common temperature $T(t)$.

Phase Space Density

The phase space density of a particle species in equilibrium at a temperature T is given by the Fermi-Dirac distribution (fermions) or the Bose-Einstein distribution (bosons)

$$f_i(\mathbf{p}, T) = \frac{1}{e^{\frac{E_i(\mathbf{p})-\mu_i}{T}} \pm 1}, \tag{2.1}$$

where $E_i = \sqrt{\mathbf{p}^2 + m_i^2}$ is the energy and μ_i is the chemical potential of species i. T is the temperature. The Fermi-Dirac distribution corresponds to the plus sign, while the Bose-Einstein distribution corresponds to the minus sign. Note that the p that occurs here corresponds to the *physical* momentum.

In general, even when a species is not in equilibrium, we can write the number density, energy density and pressure of a species in terms of the

distribution function

$$n_i(\mathbf{x},t) \equiv g_i \int \frac{d^3p}{(2\pi)^3} f_i(\mathbf{p},\mathbf{x},t), \tag{2.2}$$

$$\rho_i(\mathbf{x},t) \equiv g_i \int \frac{d^3p}{(2\pi)^3} E_i(\mathbf{p}) f_i(\mathbf{p},\mathbf{x},t), \tag{2.3}$$

$$P_i(\mathbf{x},t) \equiv g_i \int \frac{d^3p}{(2\pi)^3} \frac{\mathbf{p}^2}{3E_i(\mathbf{p})} f_i(\mathbf{p},\mathbf{x},t). \tag{2.4}$$

In general we have the energy momentum tensor

$$T_i^{\mu\nu}(\mathbf{x},t) = g_i \int \frac{d^3p}{(2\pi)^3} \frac{P^\mu P^\nu}{E_i(\mathbf{p})} f_i(\mathbf{p},\mathbf{x},t), \tag{2.5}$$

where $P^\mu = m\,\partial x^\mu/\partial\lambda$ is the energy-momentum four vector (not to be confused with the pressure), obeying

$$g_{\mu\nu}P^\mu P^\nu = E^2 - a^2\delta_{ij}P^iP^j = E^2 - p^2 = m^2. \tag{2.6}$$

We can write the thermal average of any quantity $\mathcal{O}(\mathbf{p},\mathbf{x},t)$

$$\big\langle \mathcal{O}_i \big\rangle(\mathbf{x},t) \equiv \frac{g_i}{n_i} \int \frac{d^3p}{(2\pi)^3} \Big(\mathcal{O}(\mathbf{p},\mathbf{x},t)\Big) f_i(\mathbf{p},\mathbf{x},t). \tag{2.7}$$

We see immediately that $\rho_i = n\langle E_i\rangle$ and $P_i = n/3\,\langle|\mathbf{p}|v\rangle = n\langle|\mathbf{p}|^2/3E_i\rangle$.

Equilibrium Values

In equilibrium we can calculate the number density, energy density and pressure analytically in the relativistic and non-relativistic limits.

In the non-relativistic limit we get

$$n_i^{\text{eq}} = g_i \left(\frac{mT}{2\pi}\right)^{3/2} e^{(\mu-m_i)/T}, \tag{2.8}$$

$$\rho_i^{\text{eq}} = n_i m_i + \frac{3}{2} n_i T, \tag{2.9}$$

$$P_i^{\text{eq}} = n_i T. \tag{2.10}$$

While, in the relativistic limit ($m, \mu \ll T$), we get

$$n_i^{\text{eq}} = \begin{cases} \left(\frac{g_i\zeta(3)}{\pi^2}\right) T^3 & \text{Bosons,} \\ \frac{3}{4}\left(\frac{g_i\zeta(3)}{\pi^2}\right) T^3 & \text{Fermions,} \end{cases} \tag{2.11}$$

$$\rho_i^{\text{eq}} = \begin{cases} \left(\frac{g_i\pi^2}{30}\right) T^4 & \text{Bosons,} \\ \frac{7}{8}\left(\frac{g_i\pi^2}{30}\right) T^4 & \text{Fermions,} \end{cases} \tag{2.12}$$

$$P_i^{\text{eq}} = \rho_i^{\text{eq}}/3. \tag{2.13}$$

2.1.1 Chemical Potential

For a species in equilibrium, you need to know the value of the chemical potential, μ_i, in order to calculate the density or pressure. In order to determine μ_i, we can use the fact that, in equilibrium, μ is conserved in all reactions. This means that if we have a scattering process $i+j \to a+b$, then we know that $\mu_i + \mu_j = \mu_a + \mu_b$.

We also know that, since photon number is not conserved, the chemical potential of photons is zero. This means that for any species in equilibrium with photons, the chemical potential of the anti-particles are negative those of the particles. This means that, for particles that have an antiparticle, a non-zero chemical potential signifies an asymmetry between the number of particles and the number of anti-particles. In the relativistic limit, the difference in number densities is given by (Lesgourgues et al., 2013, p. 81)

$$n_i - \bar{n_i} = \frac{g_i}{6} T_i^3 \left[\frac{\mu_i}{T_i} + \frac{1}{\pi^2} \left(\frac{\mu_i}{T_i} \right)^3 \right]. \tag{2.14}$$

Note that this is an exact result, and not a truncated power series in μ_i/T_i.

When the universe cools down to temperatures below the rest mass of a given species, the particles and anti-particles start to annihilate with eachother leaving just this small excess. Even if $\mu = 0$, however, there will be a relic density of particles and anti-particles left over, since they could not find a partner to annihilate with. This is usually what is thought to account for the relic density of DM.

Since the particle/antiparticle asymmetry is very small in the standard model, we can usually just neglect the chemical potentials in the relativistic limit.

2.1.2 Entropy

To calculate the equilibrium entropy of a species, we use the grand potential, $\Omega = -PV$ (Pathria and Beale, 2011, p.283)

$$S_i = -\left.\frac{\partial \Omega}{\partial T}\right|_{\mu,V} = V \left.\frac{\partial P_i}{\partial T}\right|_{\mu}. \tag{2.15}$$

A more useful quantity for us is the specific entropy, s, given by

$$s_i = \frac{S_i}{V} = \left.\frac{\partial P_i}{\partial T}\right|_{\mu} = g_i \int \frac{d^3p}{(2\pi)^3} \frac{p^2}{3E_i(p)} \left.\frac{\partial f_i(p,t)}{\partial T}\right|_{\mu}. \tag{2.16}$$

For a Fermi-Dirac or Bose-Einstein distribution this becomes

$$s_i = g_i \int \frac{d^3p}{(2\pi)^3} \frac{p^2}{3E_i(p)} \frac{E_i - \mu_i}{T^2} \frac{\exp\left(\frac{E_i-\mu_i}{T}\right)}{\left[\exp\left(\frac{E_i-\mu_i}{T}\right) \pm 1\right]^2}. \tag{2.17}$$

We can rewrite this as

$$s_i = -g_i \int \frac{d^3p}{(2\pi)^3} p \frac{E_i - \mu_i}{3T} \left(\frac{\partial}{\partial p} \frac{1}{\exp\left(\frac{E_i-\mu_i}{T}\right) \pm 1} \right), \tag{2.18}$$

which, upon integration by parts, gives simply

$$s_i = \frac{\rho_i - \mu n_i + P_i}{T}. \tag{2.19}$$

For a relativistic boson, with no chemical potential, the entropy density is given by

$$s_i = g_i \frac{2\pi^2}{45} T^3. \tag{2.20}$$

Since the entropy density of relativistic species usually dominate the total entropy, it is useful to define the total entropy in terms of an effective number of relativistic degrees of freedom (for entropy), $g_{*\mathrm{S}}$

$$s_{\mathrm{tot}} = g_{*\mathrm{S}} \frac{2\pi^2}{45} T^3, \tag{2.21}$$

where

$$g_{*\mathrm{S}} = \sum_{\mathrm{bosons}} g_i \left(\frac{T_i}{T}\right)^3 + \frac{7}{8} \sum_{\mathrm{fermions}} g_i \left(\frac{T_i}{T}\right)^3, \tag{2.22}$$

where T is the temperature of the heat bath, and we have allowed for the possibility that some relativistic species have decoupled from the heat bath and have a different temperature, T_i. Note that we have also assumed here that the chemical potentials are negligible. Note also that the sum here is only over relativistic species.

In most cases of interest, the expansion of the universe is adiabatic, meaning that the comoving entropy density is constant in time

$$\frac{\partial}{\partial t}\left(sa^3\right) = 0. \tag{2.23}$$

This means that we can directly relate the temperature, T, and the scale factor, a, which is incredibly useful

$$T = g_{*\mathrm{S}}^{-1/3}(T)/a. \tag{2.24}$$

2.1.3 Hubble Rate during Radiation Domination

During radiation domination the energy density of the universe was given by

$$\rho = g_* \frac{\pi^2}{30} T^4, \tag{2.25}$$

where g_* is the effective number of degrees of freedom for energy

$$g_* \equiv \sum_{\mathrm{bosons}} g_i \left(\frac{T_i}{T}\right)^4 + \frac{7}{8} \sum_{\mathrm{fermions}} g_i \left(\frac{T_i}{T}\right)^4. \tag{2.26}$$

Inserting this energy into the first Friedmann eqn. (1.11), we get (assuming a flat universe)

$$H(T) = \sqrt{\frac{4\pi^3 g_*}{45}} \frac{T^2}{M_{\mathrm{Pl}}}. \tag{2.27}$$

2.1.4 Chemical and Kinetic Equilibrium

It is useful to decompose the full thermodynamic equilibrium into two parts, *chemical equilibrium* and *kinetic equilibrium*.

Chemical equilibrium means that the number density of a species, n_i, is equal to the equilibrium number density of the species, $n_i^{\rm eq}$.

Kinetic equilibrium, however, means that the phase-space distribution is proportional to the equilibrium phase-space distribution, while allowing for a departure from chemical equilibrium

$$f_i = \kappa f_i^{\rm eq}, \tag{2.28}$$

where $\kappa \equiv n_i/n_i^{\rm eq}$. If we think about the temperature as the average kinetic energy of the particles, then kinetic equilibrium basically means that the temperature of a species is equal to the temperature of the heat bath.[1]

2.2 Boltzmann Equation

In this thesis we are studying the departure from equilibrium. When we want to analyze the statistical behavior of a thermodynamic system that is *not* in equilibrium, we can often use the *Boltzmann Equation* (BE). The relativistic BE is given by

$$\frac{df(\mathbf{p},\mathbf{x},t)}{d\lambda} = \left[P^\alpha \frac{\partial}{\partial x^\alpha} - \Gamma^\alpha{}_{\beta\gamma} P^\beta P^\gamma \frac{\partial}{\partial P^\alpha}\right] f(\mathbf{p},\mathbf{x},t) = C[f]. \tag{2.29}$$

In a flat FRW universe, the BE is given by the much simpler

$$E(p)(\partial_t - Hp\,\partial_p) f_i(p,t) = C[f_i], \tag{2.30}$$

where p denotes the physical momenta of the species i. $C[f_i]$ is called the collision term, and takes into account all the interactions that species i can be involved in.

2.2.1 Collision Term

If we restrict ourselves, for simplicity, to processes involving only two particles in the initial and final state, the general form of the collision term is given by (Kolb and Turner, 1990, p. 116-117)

$$\begin{aligned} C[f_i] = \sum_{j,a,b} \frac{1}{2g_i} \int \frac{d^3p_j}{(2\pi)^3 2E_j} \int \frac{d^3p_a}{(2\pi)^3 2E_a} \int \frac{d^3p_b}{(2\pi)^3 2E_b} \\ \times (2\pi)^4 \delta(p + p_j - p_a - p_b) \\ \times \Big[|\mathcal{M}|^2_{i,j\to a,b} f_i(E) f_j(E_j)(1 \mp f_a(E_a))(1 \mp f_b(E_b)) \\ - |\mathcal{M}|^2_{a,b\to i,j} f_a(E_a) f_b(E_b)(1 \mp f_i(E))(1 \mp f_j(E_j)) \Big], \end{aligned} \tag{2.31}$$

[1] Note that these are not the definitions of chemical and kinetic equilibrium, but they the main characteristics of a particle in chemical or kinetic equilibrium. The definitions would involve comparing the relevant interaction rates to the Hubble rate. See Chs. 4 and 5.

where j, a and b can be any species (including species i itself) part of a physically allowed process involving species i. Note that in our convention $|\mathcal{M}|^2$ is summed over all internal degrees of freedom (spins, colors, etc.).

2.2.2 Collisionless Boltzmann Equation

If the collision term is zero,

$$E(p)(\partial_t - Hp\,\partial_p)f(p,t) = 0, \tag{2.32}$$

the BE has a very simple solution. If you know the distribution, $f_0(p)$ at some time t_0 then the distribution at any other time is given by

$$f(p,t) = f_0\left(\frac{a(t)}{a_0}p\right). \tag{2.33}$$

This just reflects the fact that, during expansion, all momenta scale like $p \propto 1/a$. This holds for both relativistic, and non-relativistic particles, leading to $T \propto p \propto 1/a$ for relativistic particles, but $T \propto p^2 \propto 1/a^2$ for non-relativistic particles.

In particular, a relativistic species decoupling from a heat bath at a temperature T_d will follow a thermal distribution.

$$f(p,T) = f_\mathrm{eq}\left(p, \frac{a_\mathrm{d}}{a(T)}T_\mathrm{d}\right) = f_\mathrm{eq}\left(p, \left[\frac{g_{*\mathrm{S}}(T)}{g_{*\mathrm{S}}(T_\mathrm{d})}\right]^{1/3} T\right). \tag{2.34}$$

Equivalently, we can say that the Fermi-Dirac and Bose-Einstein distributions, for relativistic particles, are solutions to the collisionless BE. As an example, this is the reason why the CMB is, still, such a perfect blackbody spectrum today.

If a species decouples[2], instantaneously, while it is completely non-relativistic, it will also follow a thermal-like distribution, but with a temperature dependent chemical potential to ensure that the co-moving number density stays constant.

In the case where a species decouples while it is semi-relativistic, or if it becomes non-relativistic after decoupling, it is not, in general, possible to write it like a thermal distribution. Even in these cases, however, we can simply write down the distribution using Eq. 2.33.

If a species is not ultra-relativistic at decoupling, and we cannot assume instantaneous decoupling, there is no such simple solution for the distribution f.

[2]In these cases, we are often, but not necessarily, talking about KD, assuming CD has already happened.

Part II

Dark Matter

Chapter 3

Dark Matter

3.1 Evidence, Constraints and Candidates

3.1.1 Motivation and Evidence for Dark Matter

We infer the need for an additional matter component to the visible matter on a large range of scales. All the way from Dwarf galaxy scales $M \sim 10^9 M_\odot$, to cosmological scales (Gorenstein and Tucker, 2014).

The first person to give a name to this excess mass was Fritz Zwicky (Zwicky, 1933), who, in 1933 when studying radial velocities in the Coma cluster, discovered a unexpectedly large velocity dispersions, that could not be explained from only visible matter, but needed an extra component of *dark* matter.

Since that time the DM paradigm has been extremely successful, becoming part of the bedrock of modern cosmology. Strong independent lines of evidence for DM comes from:

- **Rotation curves of spinning galaxies:**

  In spinning galaxies, such as our own, we can study the rotational velocity or the stars as a function of the distance from the centre of the galaxy. Using the law of gravity, we can calculate the matter density of the galaxy required to produce this rotation curve. When we do this, we see that neither the amount, nor the distribution, of visible matter can explain the shape of the rotation curve. Hence, we need an additional, dark, matter component (see e.g. Borriello and Salucci, 2001).

- **Velocity dispersion in galaxy clusters:**

  As Zwicky noticed, the velocity dispersions in clusters of galaxies are too large for the system to be gravitationally bound, unless there is a significant DM contribution in addition to the visible matter.[1]

- **Gravitational lensing:**

  Gravitational lensing is a very powerful probe of the matter distribution of various astronomical objects. The presence of any mass bends path of light traveling close to it, resulting in a distorted image of a far away object if the light has passed through a dense matter distribution. This is usually called *weak lensing*. Astronomers can use statistical techniques to recreate the matter distribution from the distortion of the light (see e.g. van Uitert et al., 2012).

[1] For a more modern analysis on the relation between cluster masses and velocity dispersion see e.g. Saro et al., 2013.

In some rare cases, gravitational lensing can be so efficient that it produces multiple images of the same background objects, or even Einstein-rings. This is called *strong lensing* (see e.g. Moustakas and Metcalf, 2003).

Since both strong and weak lensing offer ways to measure the distribution of mass in an object, we can compare it to the mass inferred for just the visible matter. If we do this than we see that in this case as well we need DM.

- **Cosmic microwave background:**

  The CMB has been precisely measured by the Planck satellite, and provides a powerful probe of the linear physics of big bang cosmology. In particular, the shape of the power spectrum is highly dependent on the amount of various energy components in the universe (see Fig. 5.6). The CMB results have confirmed the standard ΛCDM model to great accuracy, meaning that it needs a DM component of about 25 % (Planck Collaboration et al., 2015).

- **Non-linear structure formation:**

  Cosmological simulations of structure formation using CDM only have been extremely successful at reproducing the large scale structure of the universe (see e.g. Boylan-Kolchin et al., 2009).

It is impressive that simply positing a new heavy non-SM particle with small or no interactions with the visible sector can explain such a breath of independent observations.

It is interesting to note, however, that in all the stated cases, DM is inferred from its gravitational effects. This has led some to suggest a modification to gravity to explain these phenomena (see e.g. Milgrom, 2010). It has, however, not been possible to devise a modification of gravity that can explain more than a few of the above lines of evidence for DM at a time.

3.1.2 Constraints on Dark Matter Candidates

The most precise cosmological observable relevant for DM is the relic abundance Ω_{DM}. From different observations this quantity is known with percent accuracy (Planck Collaboration et al., 2015)

$$\Omega_{\mathrm{DM}} h^2 = 0.1188 \pm 0.0010, \tag{3.1}$$

where the dimensionless Hubble parameter $h = 67.74 \pm 0.46$ is defined by Eq. 1.5.

The precision of this value is impressive, especially because all we know about DM is known indirectly, from the gravitational effect DM has on the visible matter.

Although we do not know the precise particle nature of DM, we have a number of strong constraints on its properties:[2]

- **It must be non-luminous:**

[2] A good and more expansive summary of such constraints is given by Taoso, Bertone, and Masiero, 2008.

In practice this means no coupling (or extremely weak) to $U(1)_{em}$ and no coupling to $SU(3)_c$. We know it cannot interact with the strong force because e.g. radiation of gluons would give rise, among other things, to neural pions that decay to photons. Although DM has to be essentially neutral, small values of e.g. the magnetic moment is still allowed (Pospelov and ter Veldhuis, 2000). In general DM can not have any large coupling to any light standard model particle.

- **It must not have too strong self interaction:**

  Many observations on different scales constrain the self interaction of DM. A velocity dependent interaction however could get around the strongest constraints to give a significant self interaction on other scales. Also, the constraint is much weaker for higher DM-masses. Constraints from self interaction will be discussed in detail in Sec. 3.3.

- **It must be cold:**

  DM has to be non-relativistic during structure formation. The free streaming from relativistic, or warm DM tends to suppress structure formation on small scales. This means that DM must have a mass larger than roughly $m_\chi \gtrsim 1$ keV (e.g. Abazajian and Koushiappas, 2006). This constraint is dependent on the DM temperature.

- **It must be stable:**

  If DM had a decay rate comparable to the age of the universe it would affect cosmology significantly, something we do not see. This means that the DM lifetime is constrained to $\tau_\chi \gg 1/H_0$.

3.1.3 Dark Matter Candidates

In this thesis we take a completely phenomenological approach to particle physics models for the dark sector, setting the issue of embedding this sector into a complete and consistent theoretical framework aside. However, we will still give a brief mention of some of the most popular candidates for particle DM.

The most popular class of DM candidates are WIMP DM. WIMPs are motivated, among other things, by the WIMP miracle (see Sec. 4.2.2). In addition the hierarchy problem of the Higgs sector, suggests the need for new physics at the weak scale.

Probably the most studied WIMP candidate is the neutralino, the lightest supersymmetric partner to the neutral bosons of the SM. By the R-parity often introduced to prevent proton decay, the lightest supersymmetric particle (LSP) is automatically stable. If the neutralino is the LSP, then it serves as a natural WIMP candidate.

Kaluza-Klein exitations from universal extra dimensions can also provide a viable WIMP candidate (Hooper and Profumo, 2007), as well as the Little Higgs DM (Birkedal et al., 2006).

Popular non-WIMP candidates are Axions (Preskill, Wise, and Wilczek, 1983), sterile neutrinos (Dodelson and Widrow, 1994 and Bezrukov, Hettmansperger, and Lindner, 2010) and gravitinos (Bolz, Brandenburg, and Buchmüller, 2001).

3.1.4 Going Beyond CDM

Although the standard CDM-paradigm has been extremely successful, there are some small scale problems of the standard ΛCDM model that motivates us to look beyond CDM to consider models where DM is not completely collisionless.

We will list three of the main problems here, the *missing satellites problem* (Klypin et al., 1999; Kravtsov, Gnedin, and Klypin, 2004), the *cusp/core problem* (Dubinski and Carlberg, 1991; Stetson, 1994; Blok, 2010) and the *too big to fail* (Boylan-Kolchin, Bullock, and Kaplinghat, 2011; Jiang and Bosch, 2015) problem.

The missing satellites problem comes from the difference in the number of small DM halos predicted by simulations and the small number of satellite galaxies observed in the Milky-Way and Andromeda galaxies. This problem could potentially be solved by DM having a late kinetic decoupling, since this will create a cutoff in the matter power spectrum on small scales, as discussed in Sec. 5.4.

DM simulations predict *cuspy* galactic density profiles, while the observed profiles in low surface brightness galaxies and dwarf satellites are *cored*, this is called the cusp-core problem. The too big to fail problem is the prediction that heavy satellites should be immune to many of the feedback mechanisms proposed to prevent star formation in smaller satellites. Still we do not observe these heavier satellites. Both these problems could potentially be solved by self interacting DM, possible with the right velocity dependence, as discussed in Sec. 3.3.

3.2 Detection of Dark Matter

There are many different ways of looking for DM, except for just its gravitational effect. Here we will give a brief overview of the main methods used in the field. The things we will discuss here are mostly in the setting of WIMP DM, although some of it is more general.

3.2.1 Direct Detection

Direct detection is based on the idea of a DM particle scattering off some SM particle, usually a heavy nucleus, in our experiment, allowing us to measure the recoil of this scattering. The chance of this happening to any one particle is very small, but if we gather a lot of heavy atoms and try to shield them from all other possible background sources (cosmic rays, radioactive decay etc.), this is a viable strategy for detection.

Since the earth moves through the galactic DM halo the local flux of DM particles can be fairly high. If we assume a local DM density of 0.3 GeV/cm^3(Arneodo, 2013) and a WIMP mass of 100 GeV, the local flux would be of the order $\phi = 10^5/(\text{cm}^2\text{s})$.

The differential recoil rate per unit mass of detector is given by (Gelmini, 2015)

$$\frac{dR}{dE_R} = N_T n_\chi \int_{v>v_{min}} d^3v f_{\text{Earth}}(\vec{v}) v \frac{d\sigma_{\chi T}}{dE_R}, \tag{3.2}$$

where E_R is the recoil energy, N_T is the number of targets per unit mass of detector, v_{min} is the minimum velocity a DM particle needs in order to

give a recoil energy of E_R, n_χ is the local DM number density, $f_{\text{Earth}}(\vec{v})$ is the velocity distribution of DM particles reaching our detector (this distribution is dominated by earths motion through the galaxy) and $\frac{d\sigma_{\chi T}}{dE_R}$ is the differential cross section for DM to scatter with recoil energy E_R.

What cross sections we get is highly dependent on the DM model. If we use nuclei as targets, DM needs to have some interaction with quarks which we can translate into an interaction with whole nuclei. If the interaction is scalar or vector, we get what is called spin-independent (SI) scattering. This is the best case, since DM interacts with each nucleus proportional to the number of nucleons, A, squared e.g. $\sigma \sim A^2$. If the interaction is pseudo-scalar or axial vector we get what is called spin- dependent (SD) scattering. This is highly suppressed, since the interaction is proportional to the total angular momentum of the nuclei (or the spin of the nuclei), e.g. $\sigma \sim J(J+1)$ (Arneodo, 2013). An overview of spin independent bounds are found in figure 3.1.

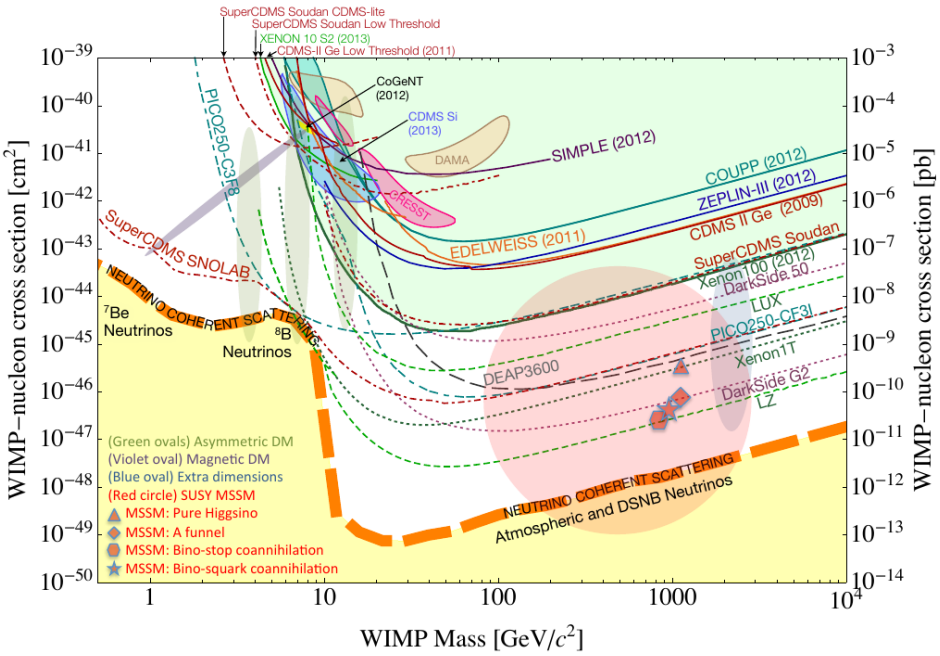

FIGURE 3.1: Summary of current (solid lines) and future direct detection experiments. Bounds on spin-independent WIMP-nucleon scattering cross section. Yellow area corresponds to areas where neutrino backgrounds become significant. Figure taken from (Cushman et al., 2013)

3.2.2 Indirect Detection

Indirect detection is based on observing the annihilation products from DM-annihilation. Even though, if DM is thermally produced, the annihilation rate $\Gamma_{today} \ll H$, this does *not* imply that $\Gamma_{today} = 0$. The nice thing about this method is that we can use our (incomplete) knowledge of the distribution of dark matter in the nearby universe to predict which direction to observe these annihilation products from (Bringmann, 2011).

In order to get a signal that we can actually detect, we need the annihilation products to be able to reach our detectors and we need to be able to distinguish the signal from the background. The four main viable possibilities are(Arneodo, 2013): gamma rays, neutrinos, antiprotons and positrons.

As an example the expected flux expected from DM annihilation to photons in a density distribution $\rho(\vec{r})$ is given by (The Fermi-LAT Collaboration et al., 2013)

$$\phi_i(\Delta\Omega) = \underbrace{\frac{1}{4\pi}\frac{\langle\sigma_{\chi\bar{\chi}\to i}\rangle}{2m_\chi^2}\int_{E_i}\frac{dN_i}{dE_i}dE_i}_{\Phi_{\rm PP}}\underbrace{\int_{\Delta\Omega}\int_{\rm l.o.s.}\rho^2(l)dld\Omega}_{J}, \tag{3.3}$$

where i denotes the relevant annihilation channel to photons and l.o.s. denotes a line of sight integral. Note that this flux divides into to factors, $\Phi_{\rm PP}$ and J. $\Phi_{\rm PP}$ is determined by the particle physics properties of your DM-model, while J contains the astrophysical contents.

The main DM annihilation channels are usually quarks, leptons or W, Z, these again decay into positrons, antiprotons and secondary photons (+ stuff with alot of background). We can then try to detect these final products. One large problem with these channels however is that the backgrounds are usually significant, and to a large extent unknown, and the signal is spread out in energy. Therefore it is often preferable to get direct annihilation to photons (primary photons), even if it is highly suppressed (eg. fig 3.2), since then we would have a clear smoking gun signal at some specific energy corresponding to m_χ.

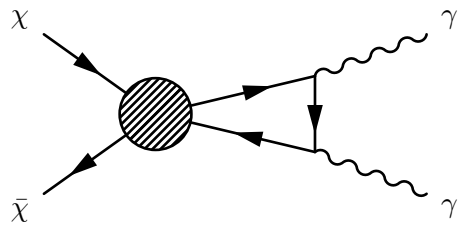

FIGURE 3.2: DM annihilation to photons, fermions (could be W^+W^-) go in loop. This process is loop suppressed, but would give a smoking gun signal at $E_\gamma = m_\chi$.

Using DM simulations of structure formation it was found roughly 20 years ago that the density distribution in DM-halos can be fitted very well by a simple analytical profile for DM halos (Navarro, Frenk, and White, 1996), called the Navarro-Frenk-White (NFW) profile.

$$\rho_{\rm NFW} = \frac{\rho_0}{\frac{r}{r_0}\left(1+\frac{r}{r_0}\right)^2}, \tag{3.4}$$

where ρ_0 and r_0 are parameters that are dependent on the particular halo.

There are two main sources that are interesting to look at for these types of detections, the galactic center, and dwarf spheroidal galaxies (DSG). The galactic center is good because the density of DM is expected to be very high, so we would get a high signal, but the astrophysical background is also very large here. DSG are also interesting because they are totally dominated by their DM content, so we expect low astrophysical backgrounds,

however they are alot smaller and we expect a lot lower signal. Some limits placed on the annihilation cross section derived from DSG by the Fermi large area telescope are shown in figure 3.3 (The Fermi-LAT Collaboration et al., 2013).

3.2.3 Dark Matter searches at Large Hadron Collider

The goal of DM searches at Large Hadron Collider (LHC) is to create DM and to be able to recognize it. We cannot expect to detect any of the potential DM particles that are produced directly, but we can try to infer their existence from the other particles involved in the collision. In a collision DM would show up as missing momentum. We would see a set of visible particles, but their momenta would not add up to zero, hence we would know that something else had to be there. This is entirely analogous to what is the case for neutrinos at the LHC.

The most straightforward way to create DM would be a collision between a quark-antiquark pair that created a DM particle-antiparticle pair, like the left part of figure 3.4. The problem with this process is that although there is missing momentum, since the interaction COM is not equal to the lab COM, the missing momentum is in the longitudinal direction, and is not picked up in the detectors. Therefore we need processes where we get at least one visible particle out of the collision, like a gluon (middle part of figure 3.4), a quark, a photon, W or Z. These processes are suppressed by an extra factor of α, but this is not too bad, since e.g. $\alpha_s \sim 0.1$ at these energies. The missing momentum that we can then find is the missing *transverse* momentum, often called missing transverse energy, $\not{E}_T$.

$$\not{E}_T \equiv -\sum \vec{p}_{T(\text{visible})}. \tag{3.5}$$

One of the main problems with this approach is that neutrinos have exactly the same signature as DM, see e.g. right part of figure 3.4. This means that in order to get a detection of DM, we must be very sure about the rate of the processes that involve neutrinos. Another problem is that even if we actually detect another particle due to missing transverse energy, we have no way of knowing whether or not this is *the* DM, or just another unknown particle.

To try to get model independent constraints on DM properties, we can parametrize different potential higher energy theories involving DM using an effective field theory approach, analogous to the Fermi theory of electro-weak interactions. We can collect the lowest order operators possibly producing DM into a table, see table 3.1 (Askew et al., 2014). The different operators clearly arise from a high energy theory, e.g. the vector operator $\frac{1}{\Lambda^2}\bar{\chi}\gamma^\mu\chi\bar{q}\gamma_\mu q$ is just the low energy operator from a theory with a vector boson, with mass $m_V^2 = \Lambda^2/(g_\chi g_q)$, that couples both to χ and q with couplings g_χ and g_q respectively.

Various limits on DM properties from monojet + $\not{E}_T$ events at LHC, for the different operators, are given in figure 3.5.

A potential problem with the effective field theory approach mentioned above is that it assumes that all the mediator particles have a very high mass. If this is not the case, then the effective field theory approach really does not make sense. What we can then do is to include the mediator into

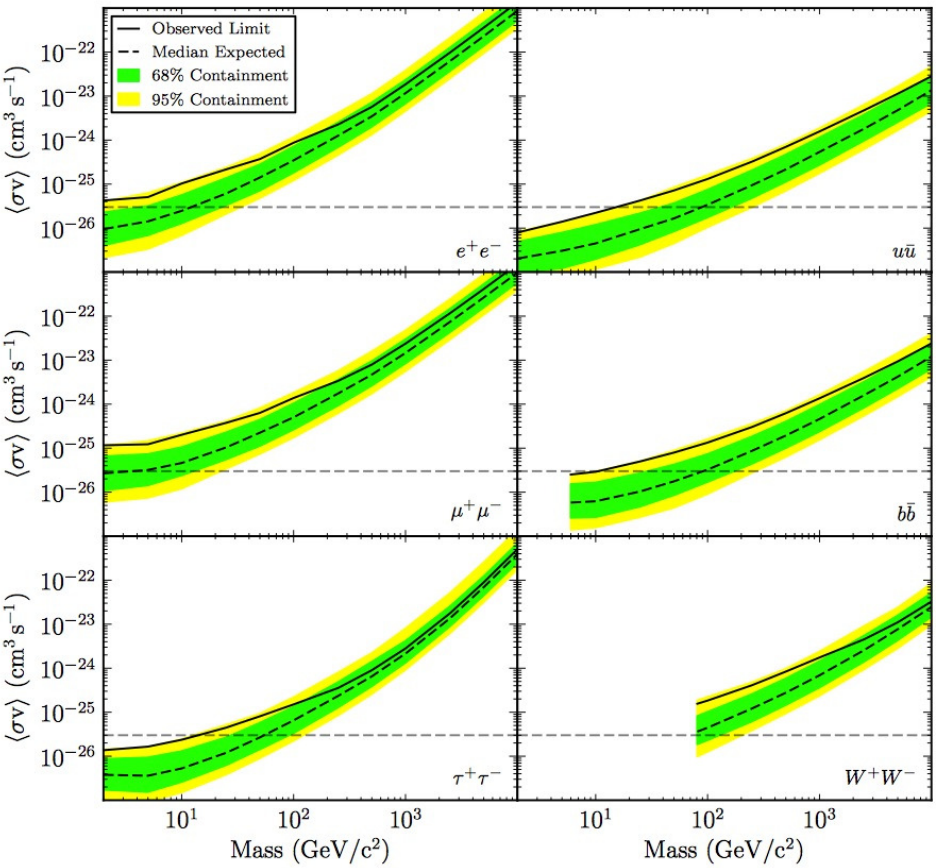

FIGURE 3.3: Upper limits on the annihilation cross section from 15 DSG found by FermiLAT. The limits are assuming DM decays exclusively in each channel. Horizontal dashed line represents thermal relic annihilation cross section. Note that in indirect detection, while sensitivity typically increases with energy (or m_χ), the limits are usually weaker, since rates rapidly decrease with energy because of the lower number densities of DM, as can be seen in equation 3.3. Figure taken from (The Fermi-LAT Collaboration et al., 2013).

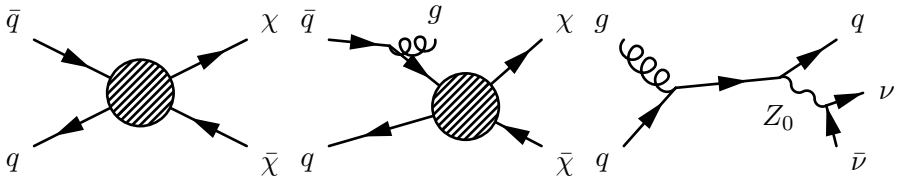

FIGURE 3.4: Left: $q\bar{q} \to \chi\bar{\chi}$, missing momentum in the longitudinal direction. This is not picked up in any detector. Middle: $q\bar{q} \to g\chi\bar{\chi}$, missing transverse momentum. "Mono-jet" process. Right: Background "Mono-jet" + $\not{E}_T$ process associated with neutrinos.

Name	Operator	Type	SI/SD
D1	$\frac{m_q}{\Lambda^3}\bar{\chi}\chi\bar{q}q$	Scalar	SI
D5	$\frac{1}{\Lambda^2}\bar{\chi}\gamma^\mu\chi\bar{q}\gamma_\mu q$	Vector	SI
D8	$\frac{1}{\Lambda^2}\bar{\chi}\gamma^\mu\gamma^5\chi\bar{q}\gamma_\mu\gamma^5 q$	Ps.-vector	SD
D9	$\frac{1}{\Lambda^2}\bar{\chi}\sigma^{\mu\nu}\chi\bar{q}\sigma_{\mu\nu}q$	Tensor	SD
D11	$\frac{\alpha_s}{\Lambda^3}\bar{\chi}\chi G^{\mu\nu a}G^a_{\mu\nu}$	Gluon	SI

Name	Operator	Type	SI/SD
C1	$\frac{m_q}{\Lambda^2}\phi^\dagger\phi\bar{q}q$	Scalar	SI
C3	$\frac{1}{\Lambda^2}\phi^\dagger\overleftrightarrow{\partial^\mu}\phi\bar{q}\gamma_\mu q$	Vector	SI
C5	$\frac{\alpha_s}{\Lambda^2}\phi^\dagger\phi G^{\mu\nu a}G^a_{\mu\nu}$	Gluon	SI

TABLE 3.1: Table of effective operators for Dirac fermion DM (top), and complex scalar DM (bottom). Λ represents some heavy mass of the high energy theory. SI and SD denote spin-independent and spin-dependent interactions respectively. Note that the scalar interaction is assumed to be proportional to the quark mass.

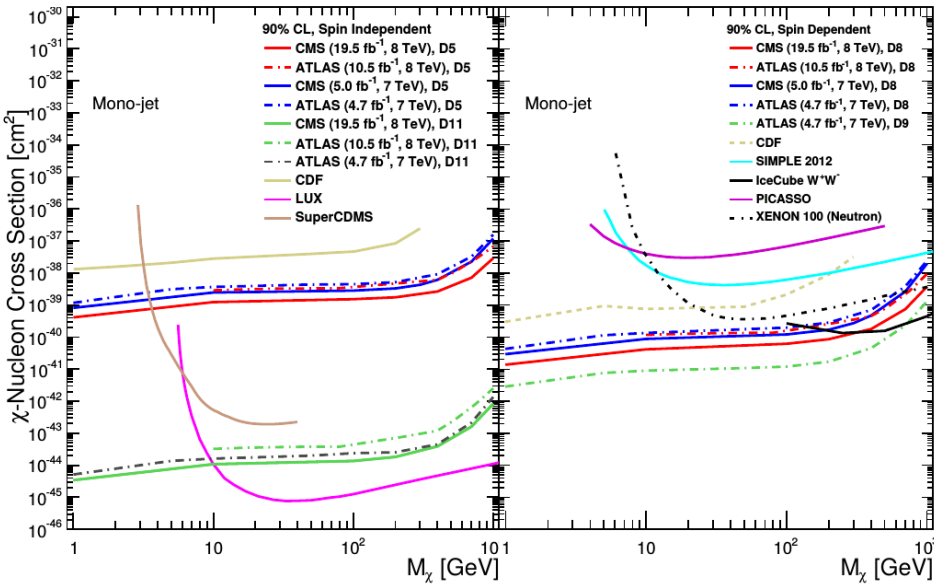

FIGURE 3.5: Note that LHC measurements are much more competitive for SD processes than for the SI processes when compared to the direct detection experiments. Figure taken from (Askew et al., 2014).

the analysis, and try to find joint limits on mediator properties as well. We suddenly have more parameters to look at, since we need to include the different couplings, widths etc, but this is doable. Some results for models including the mediator properties are found in figure 3.6.

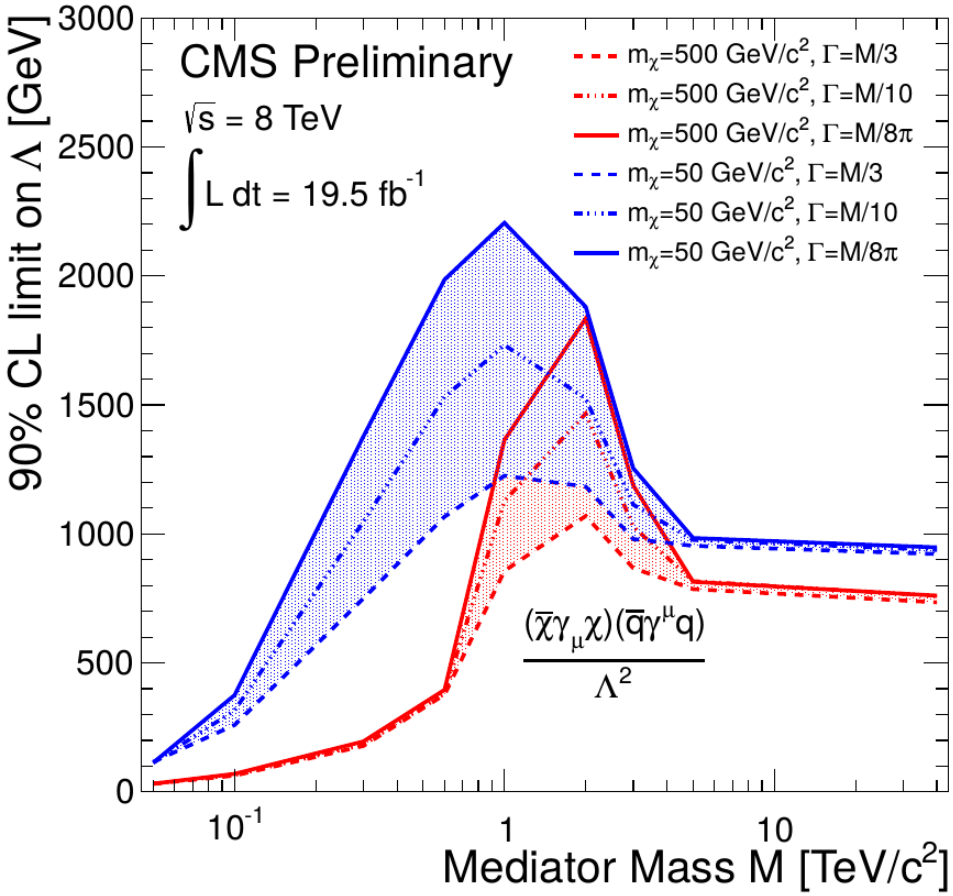

FIGURE 3.6: Analysis of model with vector mediator for two different DM masses, and three different mediator widths. Figure taken from (Askew et al., 2014).

3.3 Dark Matter Self-Interaction

Self interacting DM is a large field of study in itself, and we will only scratch the surface in this section. In many cases, models that give rise to late KD, also, naturally, leads to a significant self-interaction. This is great, because, since self-interaction of DM is severely constrained by observations and simulations, we get strong bounds on model parameters, and it severely restricts the landscape of viable models for late KD of DM.

In addition, since self-interacting DM has the potential to solve several small-scale problems, like the *cusp/core* and *too big to fail* problems (Loeb and Weiner, 2011; Vogelsberger, Zavala, and Loeb, 2012), if a model can obtain both late KD and a significant self-interaction, then this is a very attractive feature.

In order to address the small-scale issues we need a transfer cross section of at least the order (Tulin, Yu, and Zurek, 2013)

$$\frac{\sigma_T}{m_\chi} \gtrsim 0.1 \, \frac{\text{cm}^2}{\text{g}} \approx 2 \cdot 10^{-25} \, \frac{\text{cm}^2}{\text{GeV}}, \tag{3.6}$$

at dwarf galaxy scales. Meaning that a value lower than this is likely to be indistinguishable from cold DM.

3.3.1 Constraints on Self-Interaction Cross Section

Upper bounds on the cross-section are dependent on the scale. The strongest constraints on σ_T/m_χ come from the observed X-ray cluster ellipticity (Loeb and Weiner, 2011, Fig. 2), these scales correspond roughly to $v \sim 10^3$ km/s and limit $\sigma_T/m_\chi \lesssim 0.02$ cm^2/g. These bounds are somewhat controversial, and more recent analysis suggests that they may be too strong Tulin, Yu, and Zurek, 2013, Zavala, Vogelsberger, and Walker, 2013 and Rocha et al., 2013. An upper bound of order $\sigma_T/m_\chi \lesssim 0.1$ cm^2/g at these scales, however, seems to be a reasonable consensus.

At dwarf galaxy scales, $v \sim 10$ km/s, where the small scale issues are potentially addressed, the constraints are significantly weaker. Here the constraint is approximately $\sigma_T/m_\chi \lesssim 35$ cm^2/g and comes from the *gravothermal catastrophe* (Balberg, Shapiro, and Inagaki, 2002).

Since at a given scale, there will be a significant spread in the velocities of DM particles, it is usually more meaningful to talk about a velocity averaged transfer cross section as the quantity that is constrained by observational bounds (Cyr-Racine et al., 2015)

$$\langle \sigma_T \rangle_{v_0} \equiv \int \frac{d^3 v}{(2\pi v_0^2)^{3/2}} e^{\frac{1}{2} v^2 / v_0^2} \sigma_T(v), \tag{3.7}$$

where $v = |\mathbf{v_1} - \mathbf{v_2}|$ is the relative velocity, and v_0 is the most probable (single particle) velocity, usually given in km/s.

3.3.2 Constant Cross Section

In this context, a constant Cross section is one that is independent of DM velocity. As we see from the previous discussion, explaining the cusp/core and too big to fail problems with a constant self-interaction cross section is hard, and may already be ruled out, depending on how much you trust the various constraints.

For such a model to work, it must have a cross section in the narrow range (Zavala, Vogelsberger, and Walker, 2013) $\sigma_T/m_\chi \simeq 0.1 - 1$ cm^2/g.

3.3.3 Yukawa Potential

If (non-relativistic) DM is coupled to a light bosonic particle, this sets up an effective Yukawa potential for DM-DM scattering. This scattering partner could be the $\tilde{\gamma}$ that leads to late KD, or it could be some other particle that couples to DM. For generality we will denote this mediator particle by ϕ, and DM by χ in this section.

The mass of the mediator, m_ϕ, decides the range of the potential, given by

$$V(r) = \pm\frac{\alpha}{r}e^{-m_\phi r}. \tag{3.8}$$

If ϕ is a scalar, then the interaction is always attractive (-), while if ϕ is a vector particle, the interaction can be both attractive or repulsive depending on whether DM is scattering with an anti-particle or not (entirely analogous to Coulomb scattering between electrons and positrons).

Calculating the interaction cross section for a Yukawa potential is in general not that easy, but we have analytical formulas for the transfer cross section σ_T that are valid in different regions.

Born Limit

In the perturbative limit, $\alpha\, m_\chi/m_\phi \ll 1$, we can use the Born approximation to calculate the transfer cross section (Tulin, Yu, and Zurek, 2013)

$$\sigma_T^{\text{Born}} = \frac{8\pi\alpha^2}{m_\chi^2 v^4}\left(\ln\left[1+\frac{m_\chi^2 v^2}{m_\phi^2}\right] - \frac{m_\chi^2 v^2}{m_\phi^2 + m_\chi^2 v^2}\right), \tag{3.9}$$

here v is the relative velocity. Note that this result is the same for both attractive and repulsive potentials.

Classical Limit

In the classical limit $m_\chi v/m_\phi \gg 1$ it is also possible to obtain parametric expressions for the transfer cross section (Cyr-Racine et al., 2015)

$$\sigma_T^{-,\,\text{class}} = \begin{cases} \frac{2\pi}{m_\phi^2}\beta^2\ln(1+1/\beta^2) & \beta \lesssim 10^{-2}, \\ \frac{7\pi}{m_\phi^2}\frac{\beta^{1.8}+280(\beta/10)^{10.3}}{1+1.4\beta+0.006\beta^4+160(\beta/10)^{10}} & 10^{-2} \lesssim \beta \lesssim 10^2, \\ \frac{0.81\pi}{m_\phi^2}\left(1+\ln\beta-(2\ln\beta)^{-1}\right)^2 & \beta \gtrsim 10^2, \end{cases} \tag{3.10}$$

$$\sigma_T^{+,\,\text{class}} = \begin{cases} \frac{2\pi}{m_\phi^2}\beta^2\ln(1+1/\beta^2) & \beta \lesssim 10^{-2}, \\ \frac{8\pi}{m_\phi^2}\frac{\beta^{1.8}}{1+5\beta^{0.9}+0.85\beta^{1.6}} & 10^{-2} \lesssim \beta \lesssim 10^2, \\ \frac{\pi}{m_\phi^2}\left(\ln 2\beta - \ln\ln 2\beta\right)^2 & \beta \gtrsim 10^2, \end{cases} \tag{3.11}$$

where $\beta \equiv 2\alpha m_\chi/(m_\chi v^2)$. Here $(-)$ corresponds to an attractive potential, while $(+)$ corresponds to a repulsive.

Resonant Regime

Outside the perturbative and the classical regime, the two expressions we have discussed are not applicable. However, exact non-perturbative results have been obtained for the Hulthén potential, which provides an excellent approximation for the Yukawa potential (Tulin, Yu, and Zurek, 2013).

$$V_{\text{Hulthén}}(r) = \pm\frac{\alpha\delta e^{-\delta r}}{1-e^{-\delta r}}, \tag{3.12}$$

where $\delta = \kappa m_\phi$ and $\kappa = \sqrt{2\zeta(3)} \approx 1.55$.

Outside the classical region ($m_\chi v/m_\phi \lesssim 1$) we often expect the scattering to be dominated by the s-wave. The s-wave contribution to the transfer cross section for the Hulthén potential is given by (Tulin, Yu, and Zurek, 2013)

$$\sigma_T^{\text{Hulthén}} = \frac{16\pi}{m_\chi v^2} \sin^2 \delta_0, \tag{3.13}$$

where the phase shift δ_0 is given by

$$\delta_0 = \arg\left(\frac{i\Gamma\left(\frac{im_\chi v}{\kappa m_\phi}\right)}{\Gamma(\lambda_+)\Gamma(\lambda_-)}\right), \quad \lambda_\pm \equiv \begin{cases} 1 + \frac{im_\chi v}{2\kappa m_\phi} \pm \sqrt{\frac{\alpha m_\chi}{\kappa m_\phi} - \frac{m_\chi^2 v^2}{4\kappa^2 m_\phi^2}} & \text{attractive,} \\ 1 + \frac{im_\chi v}{2\kappa m_\phi} \pm i\sqrt{\frac{\alpha m_\chi}{\kappa m_\phi} + \frac{m_\chi^2 v^2}{4\kappa^2 m_\phi^2}} & \text{repulsive.} \end{cases} \tag{3.14}$$

In the attractive case, this potential gives rise to resonant behavior both complicating the picture, and making it more interesting. An example of this behavior is shown in Fig. 3.7.

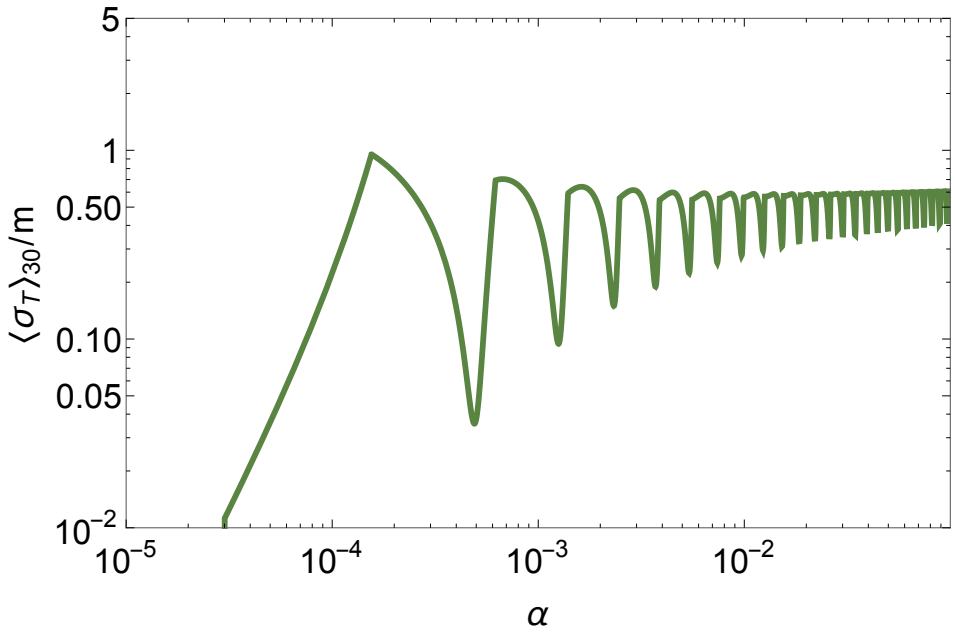

FIGURE 3.7: Example of the resonant behavior of the self interaction in the non-classical regime. These results were calculated using the Hulthén cross section, $\sigma_T^{\text{Hulthén}}$. Here $m_\chi = 100$ GeV, $m_\phi = 10$ MeV.

Constraint on $\chi\chi\tilde{\gamma}$ Coupling for Bosonic $\tilde{\gamma}$

If a dark radiation particle $\tilde{\gamma}$ is bosonic, a $\chi\chi\tilde{\gamma}$ coupling will induce a Yukawa potential, and hence usually lead to a substantial self interaction for χ. If we want the scattering with $\tilde{\gamma}$ to be responsible for keV-scale KD of χ (see Pt. III), then this requires $m_{\tilde{\gamma}} \lesssim$ keV. Since long range forces between DM are so heavily constrained, this leads to serious bounds on the other parameters of the model, see Fig. 3.8 (Bringmann et al., 2016).

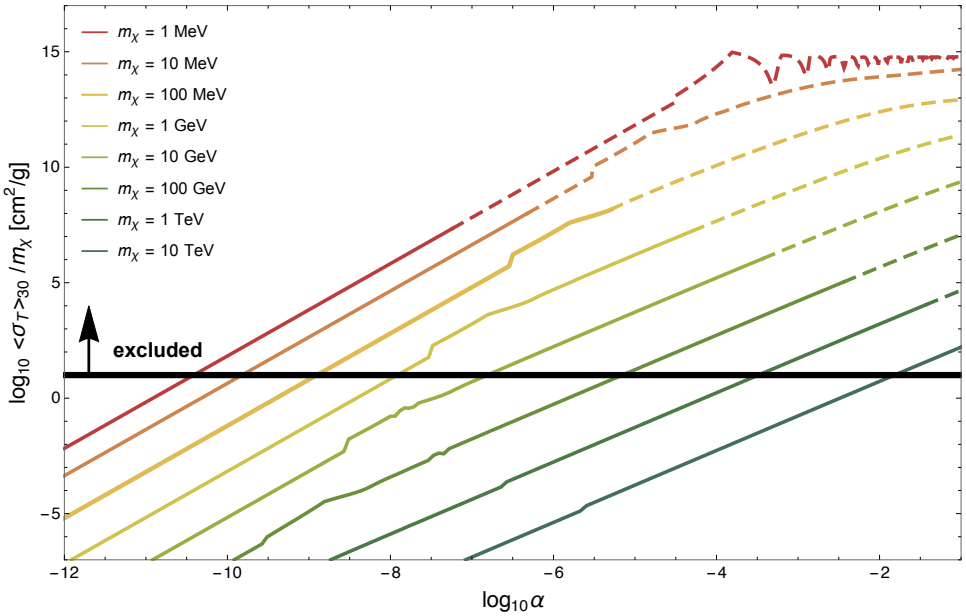

FIGURE 3.8: DM self interaction from Yukawa potential generated by $\chi\chi\tilde{\gamma}$ interaction. The cross section $\langle\sigma_T\rangle_{30}$ is plotted against the coupling, $\alpha = g^2/4\pi$, for many different DM masses, m_χ. The velocity averaging has been done around $v_0 = 30$ km/s, a scale relevant for dwarf galaxies. Here $m_{\tilde{\gamma}} = 100$ eV. Lighter masses lead to stronger self-interaction. The horizontal black line roughly corresponds roughly to what is excluded from observations at this scale. The dashed lines corresponds to areas of parameter space that are ruled out because the strong coupling would deplete the relic density below the one required for DM. Note that, for all these models, the bounds from self-interactions are stronger than the ones from relic density considerations.
Figure taken from Bringmann et al., 2016.

Chapter 4

Chemical Decoupling

Chemical decoupling of DM is a very important area of study, because it is the process that decides the density of DM in the later evolution of the universe. As the DM density is a quantity that is determined from cosmological observations, calculating the relic density from first principle particle physics provides a direct link between particle properties of DM models and cosmology.

As we will see, for most WIMP models, relic density constraints usually fixes, roughly, the ratio between the coupling and the DM mass α/m_χ. That means that for heavy DM particles, we need a large coupling, while we need a small coupling for light DM particles.

When talking about "Chemical decoupling" we have already implicitly assumed that at some time DM was in thermal (or at least chemical) equilibrium with some heat bath. As we see from Fig. 4.1 this need not be the case. In any case, however, the results from this section will still be useful, in the sense that they will give an upper bound on the couplings. This is because if the annihilation cross section is larger than the one required to get the correct relic density, annihilations would still deplete the DM density below the required value.

4.1 Boltzmann Equation for Chemical Decoupling

The BE in a flat FRW universe is given, as discussed in section 2.2 by:

$$E(p)(\partial_t - Hp\,\partial_p)f(p) = C[f], \tag{4.1}$$

where $f(p)$ is the phase space distribution function of the dark matter particles.

Integrating this equation over p we get the BE for the DM number density, n

$$\frac{1}{a^3}\frac{d\left(na^3\right)}{dt} = 2g_\chi \int \frac{d^3p}{(2\pi)^3 2E} C[f]. \tag{4.2}$$

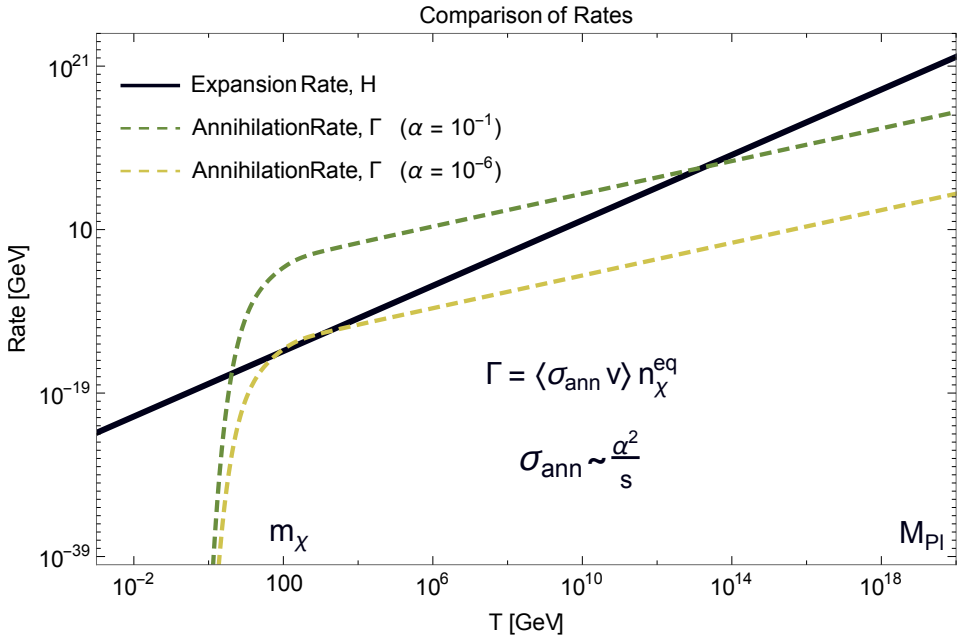

FIGURE 4.1: Comparison of the equilibrium interaction rate and the expansion rate in the early universe. We have chosen a DM mass of 100 GeV as an example. Note that as long as DM is relativisitic it tends towards equilibrium, but as it becomes non-relativistic it goes out of equilibrium. So the values of α and m_χ, as well as initial conditions, determine whether DM ever goes into equilibrium or not.

Massaging the Collision Terms

The only parts of $C[f]$ that survive the integration over p are those that change the DM number density. The RHS, from Eq. 2.31, is then given by

$$\begin{aligned} 2g_\chi \int \frac{d^3p}{(2\pi)^3 2E} C[f] = &- \sum_{\tilde{\gamma}} \int \frac{d^3p}{(2\pi)^3 2E} \int \frac{d^3\tilde{p}}{(2\pi)^3 2\tilde{E}} \int \frac{d^3k}{(2\pi)^3 2\omega} \int \frac{d^3\tilde{k}}{(2\pi)^3 2\tilde{\omega}} \\ &\times (2\pi)^4 \delta(p + \tilde{p} - k - \tilde{k}) \\ &\times \Big[|\mathcal{M}|^2_{\bar{\chi}\chi \to \tilde{\gamma}\tilde{\gamma}} f(E) f(\tilde{E}) (1 \pm g(\omega))(1 \pm g(\tilde{\omega})) \\ &- |\mathcal{M}|^2_{\tilde{\gamma}\tilde{\gamma} \to \bar{\chi}\chi} g(\omega) g(\tilde{\omega}) (1 \pm f(E))(1 \pm f(\tilde{E})) \Big] \qquad (4.3) \\ \simeq\ & g_\chi^2 \sum_{\tilde{\gamma}} \int \frac{d^3p}{(2\pi)^3} \int \frac{d^3\tilde{p}}{(2\pi)^3} v \sigma_{\bar{\chi}\chi \to \tilde{\gamma}\tilde{\gamma}} \\ &\times \Big[f_{\rm eq}(E) f_{\rm eq}(\tilde{E}) - f(E) f(\tilde{E}) \Big] , \qquad (4.4) \end{aligned}$$

where $k = (\omega, \mathbf{k})$ and $\tilde{k} = (\tilde{\omega}, \tilde{\mathbf{k}})$ are the momenta of the outgoing heat bath particles, $p = (E, \mathbf{p})$, $\tilde{p} = (\tilde{E}, \tilde{\mathbf{p}})$ are the momenta of the two incoming DM particles, and where $v = v_{\rm Møl} \equiv (E\tilde{E})^{-1} \sqrt{(p \cdot \tilde{p})^2 - m_\chi^4}$ is the Møller velocity. $g(\omega) = (e^{\omega/T_{\tilde{\gamma}}} \pm 1)^{-1}$ is the distribution of the heat bath particles, assumed to be in equilibrium. In our convention $|\mathcal{M}|$ is summed over all internal degrees of freedom (spins, colors etc.) both initial and final, and the sum $\sum_{\tilde{\gamma}}$ is a sum over all heat bath particles (SM or DR).

To get from Eq. 4.3 to 4.4 we need to make a few assumptions, as well as a few observations. First of all, we use Maxwell-Boltzmann statistics instead of Bose-Einstein or Fermi-Dirac. If there is no Bose-Einstein condensate or degenerate fermions, this is a fairly good approximation, and in this case we can also neglect the stimulated emission and Pauli-suppression factors in 4.3 (Kolb and Turner, 1990, p. 118). In the non-relativistic limit Maxwell-Boltzmann statistics becomes exactly correct.

We can also observe that since we are in equilibrium, by *detailed balance*, the rate for production and annihilation of DM must be equal. We must have[1]

$$|\mathcal{M}|^2_{\bar{\chi}\chi\to\tilde{\gamma}\tilde{\gamma}} f_{\text{eq}}(E) f_{\text{eq}}(\tilde{E}) = |\mathcal{M}|^2_{\tilde{\gamma}\tilde{\gamma}\to\bar{\chi}\chi} g(\omega) g(\tilde{\omega}).$$

However, by invariance under time reversal (or CP) we also have

$$|\mathcal{M}|^2_{\tilde{\gamma}\tilde{\gamma}\to\bar{\chi}\chi} = |\mathcal{M}|^2_{\bar{\chi}\chi\to\tilde{\gamma}\tilde{\gamma}}.$$

We also use the definition of the scattering cross section (Peskin and Schroeder, 1995, p. 106)

$$\sigma_{\bar{\chi}\chi\to\tilde{\gamma}\tilde{\gamma}} = \frac{1}{4E\tilde{E}v} \int \frac{d^3k}{(2\pi)^3 2\omega} \int \frac{d^3\tilde{k}}{(2\pi)^3 2\tilde{\omega}} (2\pi)^4 \delta(p + \tilde{p} - k - \tilde{k}) \overline{|\mathcal{M}|}^2_{\bar{\chi}\chi\to\tilde{\gamma}\tilde{\gamma}}.$$

Here we need to remember that in our convention $|\mathcal{M}|^2$ is summed over all internal degrees of freedom, while the standard $\overline{|\mathcal{M}|}^2$ (from Peskin and Schroeder) is averaged over the initial and summed over the final internal degrees of freedom. This means that

$$|\mathcal{M}|^2 = g_\chi^2 \overline{|\mathcal{M}|}^2,$$

giving us the last piece we needed to go from Eq. 4.3 to 4.4.

In order to go on, we can note that as long as DM is in kinetic equilibrium, which is usually the case until much later than chemical decoupling, we have

$$\frac{f_{\text{eq}}}{f} = \frac{n_{\text{eq}}}{n}.$$

Using this we can rewrite the factor

$$\left[f_{\text{eq}}(E) f_{\text{eq}}(\tilde{E}) - f(E) f(\tilde{E}) \right] = \frac{f(E) f(\tilde{E})}{n^2} \left(n_{\text{eq}}^2 - n^2 \right).$$

Defining

$$\langle \sigma v \rangle \equiv \sum_{\tilde{\gamma}} \langle \sigma_{\bar{\chi}\chi\to\tilde{\gamma}\tilde{\gamma}} v \rangle = \sum_{\tilde{\gamma}} \frac{g_\chi^2}{n^2} \int \frac{d^3p}{(2\pi)^3} \int \frac{d^3\tilde{p}}{(2\pi)^3} v \sigma_{\bar{\chi}\chi\to\tilde{\gamma}\tilde{\gamma}} f(E) f(\tilde{E}),$$

we can rewrite the complete BE in the simple form

$$\frac{1}{a^3} \frac{d\left(na^3\right)}{dt} = \langle \sigma v \rangle \left(n_{\text{eq}}^2 - n^2 \right).$$

[1] Note that this argument could be made even if we had not used MB statistics.

Changing Coordinates

It is useful to introduce the dimensionless variables

$$x \equiv m_\chi / T, \tag{4.5}$$
$$Y \equiv n / s_v, \tag{4.6}$$

where $s_v(T) = g^v_{*S}(T)\frac{2\pi^2}{45}T^3$ is the entropy of all the particles in the SM heat bath before CD of DM. This is meaningful since if the dark and visible sectors are already decoupled, entropy will be conserved separately in each of the sectors, so we can use either. Note also that we use the photon temperature T, which is not necessarily the same as the temperature of the heat bath DM is interacting with, $T_{\tilde{\gamma}}$.

Using these coordinates we can rewrite the BE on the form van den Aarssen, Bringmann, and Goedecke, 2012

$$\frac{x}{Y}\frac{dY}{dx} = -\left(1 - \frac{x}{3g^v_{*S}}\frac{dg^v_{*S}}{dx}\right)\frac{\Gamma_{\text{ann}}}{H}\left(1 - \frac{Y^2_{\text{eq}}}{Y^2}\right), \tag{4.7}$$

where $\Gamma_{\text{ann}} \equiv \langle\sigma v\rangle n$ is the annihilation rate of DM and $Y_{\text{eq}} \equiv n_{\text{eq}}/s_v$.

4.2 Solving the Boltzmann Equation

When we talk about CD of DM, then "solving the BE" typically means finding the relic density of DM. From cosmological observations we know that the relic density of DM is given by (Planck Collaboration et al., 2015)

$$\Omega_{\text{DM}}h^2 = 0.1188 \pm 0.0010. \tag{4.8}$$

At late times, when the RHS of Eq. 4.7 becomes negligible, that is when $H \gg \Gamma_{\text{ann}}$, the solution to the BE equation is just $Y = \text{constant} = Y_\infty$. Y is equal to the number of DM particles per entropy, so, as long as entropy is conserved, a constant value of Y means that the comoving number density of DM is also constant. So our goal, in solving the BE, is to end up with the right amount of DM left over, after all the DM annihilations have stopped. This means we want to end up at the right value of Y_∞.

The "Right" Amount of Dark Matter

In order to find out what is the "right" value of Y_∞ we need to relate it to the current DM abundance Ω_{DM}.

The dark matter density today is given by

$$\rho_\chi = m_\chi n_0 = m_\chi Y_\infty s_0 = m_\chi Y_\infty g^v_{*S}(T_0)\frac{2\pi^2}{45}T_0^3, \tag{4.9}$$

where the subscript "$_0$" denotes quantities today. $\Omega_{\rm DM}$ is then given by[2]

$$\Omega_{\rm DM} = \frac{\rho_\chi}{\rho_{\rm c0}} = \frac{16\pi^3 G m_\chi Y_\infty g^v_{*S}(T_0) T_0^3}{135 H_0^2} \tag{4.10}$$

4.2.1 Relativistic Decoupling

If DM decouples when it is still relativistic we do not need to solve the BE at all to find Y_∞, unless $g^v_{*S}(T)$ changes during the period of decoupling[3]. This is because for a relativistic species, $Y_{\rm eq}$ is a constant. This means that

$$Y^{\rm rel}_\infty = Y_{\rm eq}(T_{\rm cd}) = \frac{g^{\rm eff}_\chi 45\zeta(3)\xi^3(T_{\rm cd})}{g^v_{*S}(T_{\rm cd}) 2\pi^4}, \tag{4.11}$$

where $g^{\rm eff}_\chi \equiv g_\chi$ for bosons and $g^{\rm eff}_\chi \equiv 3g_\chi/4$ for fermions.

Inserting this into Eq. 4.10, we get

$$\Omega_{\rm DM} = \frac{8 g^{\rm eff}_\chi G m_\chi \zeta(3)\xi^3(T_{\rm cd}) T_0^3}{3\pi H_0^2} \frac{g^v_{*S}(T_0)}{g^v_{*S}(T_{\rm cd})}. \tag{4.12}$$

Inserting current values $T_0 = 2.346 \cdot 10^{-4}$ eV and $g^v_{*S}(T_0) = 2 + 7/8 \cdot 2 \cdot 3\,(4/11) \approx 3.91$, we get

$$m_\chi = 1.56 \text{ eV} \left(\frac{g^v_{*S}(T_{\rm cd})}{g^{\rm eff}_\chi}\right) \xi^{-3}(T_{\rm cd}) \left(\frac{\Omega_{\rm DM} h^2}{0.1188}\right). \tag{4.13}$$

We see that for DM to decouple while it is relativistic while not producing too large relic density requires that DM is very light. This observation can also be though of as a lower bound on the DM mass[4], that is, if DM is lighter than this, it cannot have a large enough relic density to make up the DM that we know exists today. We should note that for DM, this bound is mostly of theoretical interest, since the bounds from structure formation already restricts $m_{\rm WDM} \gtrsim$ keV.[5]

A species that undergoes CD while relativistic, typically also undergoes KD at the same time. Since, in this thesis, we are studying models with late KD, relativistic decoupling of DM is not a very interesting possibility for us.

The same situation, however, shows up when we are looking at models with a finite DR mass. In that case, these considerations will be a very useful constraint for us (see Ch. 9).

[2]This assumes that χ is its own antiparticle, as we will do for the rest of this section. If not there is an extra factor of two since we get $\Omega_{\rm DM} = (\rho_\chi + \rho_{\bar\chi})/\rho_{\rm c0}$. A more complicated case is the one of asymmetric DM, where the relic density is set by an asymmetry between DM and anti-DM, similar to what is the case for baryonic matter (for a nice review of this class of models se Petraki and Volkas, 2013).

[3]Interestingly, for the particles in the universe that we know decoupled while they were relativsitic, namely neutrinos, $g^v_{*S}(T)$ actually does change slightly since electrons and positrons start annihilating during neutrino decoupling, as is discussed in Sec. 6.3.

[4]In the context of neutrino decoupling, this is referred to as the Cowsik-McClelland bound (Cowsik and McClelland, 1972), but is then an upper bound on the neutrino mass, since we know that it decoupled while relativistic.

[5]Note that these bounds hold for thermally produced DM, as long as the free-streaming velocity is small, the mass of DM can be much smaller than keV.

4.2.2 Non-Relativistic Decoupling

In the non-relativistic case we actually need to solve the BE. We can always do this numerically, of course, but it is useful also to derive an approximate analytic expression for us to look at, in order to understand the important features of the solution[6].

In Fig. 4.2 we show the evolution of the co-moving number density of DM during CD. We can see clearly that the amount of DM left over is tightly linked to the value of $\langle \sigma v \rangle$. In general a larger annihilation cross section leads to lower relic density, and a smaller cross section leads to high relic density.

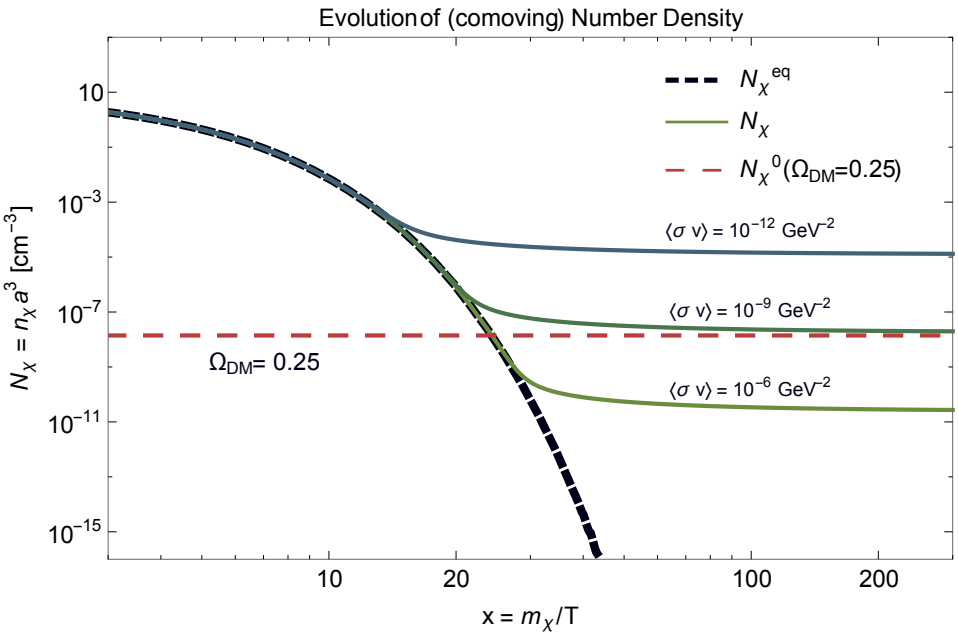

FIGURE 4.2: Co-moving number density of DM during CD. The number density (solid lines) follows the equilibrium number density (thick dashed line) until the annihilation rate can not keep up with the expansion rate any more. The annihilations stop fairly quickly and the relic density of DM is fixed from then on. The annihilation rate can keep the number density in equilibrium longer if the cross section for annihilation is larger, leading to a lower relic density. Here we have chosen $m_\chi = 100$ GeV. Changing this mass will change the numbers on the y-axis, but the shape of the curves would be roughly the same.

[6]This will be a fairly standard derivation of the relic density for DM in the non-relativistic limit following Kolb and Turner, 1990 and Gondolo and Gelmini, 1991. The main new feature is that we allow for the possibility that the dark sector has a different temperature than the visible sector.

Annihilation Cross Section in the Non-Relativistic Limit

We want to solve Eq. 4.7 in the non-relativistic limit. First, let us look at how the thermal averaged cross section behaves in this limit

$$\langle \sigma v \rangle = \frac{g_\chi^2}{n^2} \int \frac{d^3p}{(2\pi)^3} \int \frac{d^3\tilde{p}}{(2\pi)^3} v \sigma_{\bar{\chi}\chi \to \tilde{\gamma}\tilde{\gamma}} f(E) f(\tilde{E}) \tag{4.14}$$

$$\simeq \sum_{\tilde{\gamma}} \frac{4(x/\xi)^{3/2}}{\sqrt{\pi}} \int_0^1 v_\chi^2 dv_\chi (\sigma v) e^{-v_\chi^2 x/\xi}, \tag{4.15}$$

where v_χ is the velocity of one of the DM-particles in the COM frame, and where the last approximation is valid in the extreme non-relativistic limit ($x/\xi \gtrsim 10$) (van den Aarssen, Bringmann, and Goedecke, 2012).

Often, in the non-relativistic limit, we can approximate σv with a power law

$$\sigma v \approx \sigma_0 v_\chi^{2n}.$$

If this is the case we can evaluate the integral in Eq. 4.15, giving us

$$\langle \sigma v \rangle \simeq \frac{2\sigma_0}{\sqrt{\pi}} \Gamma\left(n + \frac{3}{2}\right) \left(\frac{x}{\xi}\right)^{-n} \equiv \tilde{\sigma}_0 \left(\frac{x}{\xi}\right)^{-n}. \tag{4.16}$$

In the radiation dominated era, we have $H = \sqrt{g_*(x)/g_*(m_\chi)} H(m_\chi) x^{-2}$ and $s_v = g_{*S}^v(x)/g_{*S}^v(m_\chi) s(m_\chi) x^{-3}$. We can then write Eq. 4.7 in the following form

$$\frac{dY}{dx} = -\frac{\lambda}{x^{2+n}} \left(Y^2 - Y_{\text{eq}}^2\right), \tag{4.17}$$

where

$$\lambda(x) = \left(1 - \frac{x}{3 g_{*S}^v(x)} \frac{d g_{*S}^v(x)}{dx}\right) \frac{\sqrt{g_*(x)} g_{*S}^v(x) \xi^n(x) s(m_\chi) \tilde{\sigma}_0}{\sqrt{g_*(m_\chi)} g_{*S}^v(m_\chi) H(m_\chi)}, \tag{4.18}$$

and

$$Y_{\text{eq}}(x) = \frac{45\xi^{3/2}}{2\pi^4} \left(\frac{\pi}{8}\right)^{1/2} \frac{g_\chi}{g_{*S}^v} x^{3/2} e^{-x/\xi}. \tag{4.19}$$

Since we are looking for a simple analytic approximation, we will make the simplifying assumption that g_* and g_{*S}^v do not change appreciably during CD, which is usually a good approximation. If this is true than $\lambda(x) \approx \frac{\xi^n(x) s(m_\chi) \tilde{\sigma}_0}{H(m_\chi)}$, and all the x-dependence of λ comes from the change in the relative temperature of the dark and visible sectors. If $\tilde{\gamma}$ is the photon, or another SM particle, or if the dark sector has not decoupled from the visible sector yet, then of course $\xi = 1$, but if the dark sector is already decoupled then we need to take this change into account.

Evolution of ξ at Chemical Decoupling

Let us look closer at the function $\xi(x)$ close to CD, for a decoupled dark sector. We will assume, as is the case in many of the types of models considered in this thesis, that the dark sector consists of just the DM particle χ and a relativistic heat bath particle $\tilde{\gamma}$. Let us also, for simplicity assume that they have an equal number of degrees of freedom.

When χ becomes non-relativistic it will start to annihilate, heating up the dark heat bath relative to the SM heat bath. Since CD also happens shortly after DM becomes non-relativistic, we may need to take this effect into account.

Assuming that almost all χ particles annihilate (which is equivalent to the assumption that χ is extremely non-relativistic at CD), we can calculate the total temperature change

$$\xi_{\text{after}} = \left(\frac{g_{*S}^{\tilde{\gamma}} + g_{*S}^{\chi}}{g_{*S}^{\tilde{\gamma}}} \right)^{1/3} \xi_{\text{before}} \approx 1.26\, \xi_{\text{before}}. \tag{4.20}$$

We see that to get a precise calculation of the relic density we would need to take this change into account.

As long as we are in the non-relativistic limit, however, most of the temperature change has already happened, so ξ is fairly constant, and equal to the final value of ξ, during the actual decoupling. From Fig. 4.3 we see that this is a reasonable approximation if $x_{\text{cd}}/\xi \gtrsim 5$.

For the rest of this discussion we will use the value $\xi \approx \text{constant} = \xi_{\text{after}}$, to make things simple.

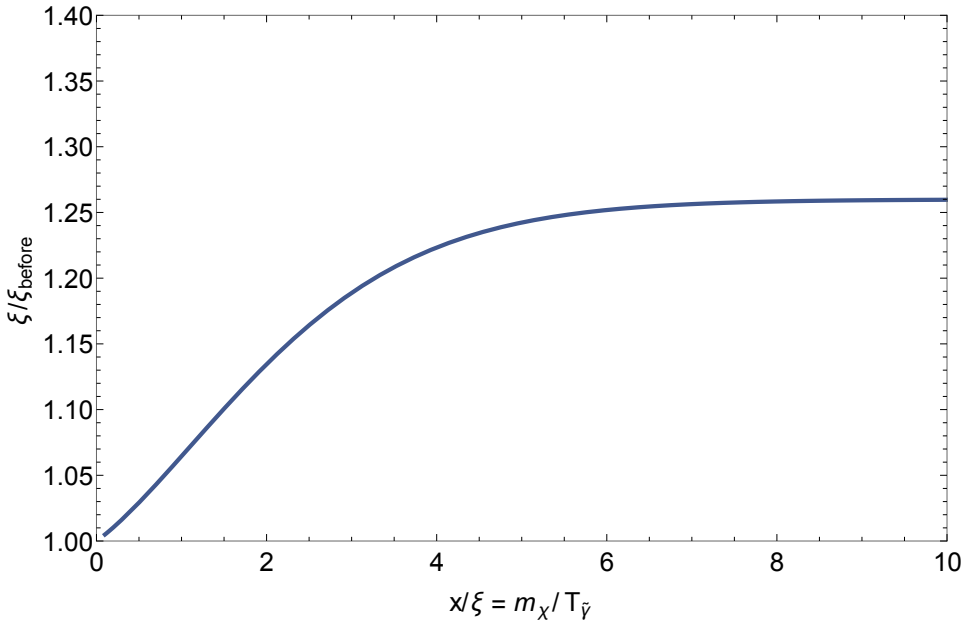

FIGURE 4.3: Plot of how the relative temperatures of the dark and visible sectors change as χ becomes non-relativisitc and annihilates heating the dark heat bath. Note how the curve flattens out as almost all the χ particles annihilate before $T_{\tilde{\gamma}} \sim m_{\chi}/5$. Here we have assumed that $g_{*S}^{\tilde{\gamma}} = g_{*S}^{\chi}$.

Calculating Y_∞

If we can, as we have argued is an acceptable approximation in the non-relativistic limit, treat λ as a constant, then Eq. 4.17 is much easier to solve. In order to get a simple analytic expression however, we will still have to make a few more approximations.

When χ starts to go out of chemical equilibrium, Y very quickly becomes much larger than $Y_{\rm eq}$. To quantify this departure we introduce the departure from equilibrium, $\Delta \equiv Y - Y_{\rm eq}$. We can now write Eq. 4.17 in temrms of Δ

$$\frac{d\Delta}{dx} = -\frac{dY_{\rm eq}}{dx} - \frac{\lambda}{x^{2+n}}\Delta(2Y_{\rm eq} + \Delta). \tag{4.21}$$

At early times, before decoupling, Δ and $|d\Delta/dx|$ are both small. In this region we get the solution

$$\Delta \simeq x^{n+2}/2\lambda.$$

At late times, after decoupling, however, $\Delta \approx Y \gg Y_{\rm eq}$ and Eq. 4.21 becomes

$$\frac{d\Delta}{dx} = -\frac{\lambda}{x^{2+n}}\Delta^2 \qquad (Y \gg Y_{\rm eq}). \tag{4.22}$$

Integrating this function from $x_{\rm cd}$ to ∞ we get

$$Y_\infty = \frac{(n+1)x_{\rm cd}^{n+1}}{\lambda}, \tag{4.23}$$

leaving us only with the task to determine $x_{\rm cd}$.

Determining $x_{\rm cd}$

The only thing left to do is to determine the value of $x = m_\chi/T$ at decoupling. If $\xi = 1$ then this is equivalent to deciding how non-relativistic χ is at CD. In general, however, it is the quantity $m_\chi/T_{\tilde{\gamma}} = x/\xi$ that is the measure of how non-relativistic χ is. This should lead us to expect that as a first approximation (for $x_{\rm cd}/\xi \gg 1$)

$$x_{\rm cd}(\xi)/\xi \approx x^*_{\rm cd},$$

where $x^*_{\rm cd} \equiv x_{\rm cd}(\xi = 1)$, and we will see that this behavior does show up.

CD denotes the time when Y goes out of equilibrium, this turnover happens when $\Delta \sim Y_{\rm eq}$. Using this, we will define $x_{\rm cd}$ by the equation [7]

$$\Delta(x_{\rm cd}) = cY_{\rm eq}(x_{\rm cd}), \tag{4.24}$$

where c is some order one constant that should be decided by solving the equations numerically and using the values of c that reproduce the numerical results best. If we now plug $x_{\rm cd}$ into the early time solution $\Delta(x_{\rm cd}) \simeq x^{n+2}/(2+c)\lambda$ we can solve the equation to find $x_{\rm cd}$.

Organizing the terms

$$\begin{aligned}\frac{cY_{\rm eq}(x_{\rm cd})}{\Delta(x_{\rm cd})} &= \frac{c\frac{45\xi^{3/2}}{2\pi^4}\left(\frac{\pi}{8}\right)^{1/2}\frac{g_\chi}{g^v_{*S}}x_{\rm cd}^{3/2}e^{-x_{\rm cd}/\xi}}{x_{\rm cd}^{n+2}/[(2+c)\lambda]} \\ &= \underbrace{\left(\frac{45}{2\pi^4}\left(\frac{\pi}{8}\right)^{1/2}\frac{g_\chi}{g^v_{*S}}c(c+2)\lambda\right)}_{\equiv\, \mathsf{a}}\xi^{3/2}x_{\rm cd}^{-(1-2n)/2}e^{-x_{\rm cd}/\xi},\end{aligned} \tag{4.25}$$

[7] Following Kolb and Turner, 1990 here.

gives us

$$e^{x_{\rm cd}/\xi} = a\xi^{3/2} x_{\rm cd}^{-(1+2n)/2}, \tag{4.26}$$

where $a\xi^{3/2} \gg 1$ since $x_{\rm cd}/\xi \gg 1$.

Such an equation can be solved iteratively giving us a good approximation when $a\xi^{3/2} \gg 1$. We then get

$$\begin{aligned} x_{\rm cd} = \xi \ln[a] + \frac{3}{2}\xi \ln[\xi] - \frac{1+2n}{2} \ln[\ln[a]] - \frac{1+2n}{2}\xi \ln[\xi] \\ + \mathcal{O}\Big(\ln[\ln[\ln[a]]], \ln[\ln[\xi]] \Big). \end{aligned} \tag{4.27}$$

As we expected we get

$$x_{\rm cd} = \xi x_{\rm cd}^* - (1-n)\xi \ln[1/\xi] + \mathcal{O}\Big(\ln[\ln[\xi]] \Big), \tag{4.28}$$

where

$$x_{\rm cd}^* = \ln[a] - \frac{1+2n}{2} \ln[\ln[a]] + \mathcal{O}\Big(\ln[\ln[\ln[a]]] \Big).$$

Relic density

We are now ready to plug our value of Y_∞ into Eq. 4.10

$$\begin{aligned} \Omega_{\rm DM} &= \frac{m_\chi (n+1) x_{\rm cd}^{n+1} s_0}{\rho_{\rm c0} \lambda} \\ &= \sqrt{\frac{4\pi^2}{45}} \frac{g_{*S0}^v}{g_{*S}^v(m_\chi)} \frac{(n+1)\xi \Big[x_{\rm cd}^* - (1-n)\ln[1/\xi] \Big]^{(n+1)}}{\rho_{\rm c0}} \frac{g_*^{1/2}(m_\chi) T_0^3}{m_{\rm Pl} \tilde{\sigma}_0}. \end{aligned} \tag{4.29}$$

In many cases the annihilation cross section is dominated by the s-wave ($n = 0$). In that case $\tilde{\sigma}_0 = \sigma_0 = \langle \sigma v \rangle$ and we get

$$\langle \sigma v \rangle = 1.0 \cdot 10^{-9} \text{GeV}^{-2} \xi \left(\frac{g_{*S}^v(m_\chi)}{100} \right)^{-1} \left(\frac{g_*(m_\chi)}{100} \right)^{1/2} \left(\frac{x_{\rm cd}^*}{25} \right) \left(\frac{\Omega_{\rm DM} h^2}{0.1188} \right)^{-1}. \tag{4.30}$$

where, for simplicity, we have made the approximation $x_{\rm cd} \approx \xi x_{\rm cd}^*$.

The most striking and important general feature of Eq. 4.29 and 4.30 is that the value of $\langle \sigma v \rangle$ needed to obtain the correct relic density is (almost) independent of m_χ. There is of course an implicit dependence on m_χ through $x_{\rm cd}^*$, g_{*S}^v and g_* but this is only a very weak dependence.

Since the cross section usually scales like

$$\langle \sigma v \rangle \propto \frac{\alpha^2}{m_\chi^2},$$

the requirement of obtaining the correct relic density usually corresponds roughly to fixing the ratio between α and m_χ.

It is also interesting to note that since

$$\frac{\alpha_W^2}{64\pi (100\,\text{GeV})^2} \sim 5 \cdot 10^{-10}\,\text{GeV}^{-2},$$

a new particle with weak-scale mass, charged under the weak force, will, almost automatically, get a relic density of about the right order of magnitude. This is often referred to as the "*WIMP miracle*".

The precise number in Eq. 4.30 should not be taken too seriously, since we made a lot of approximations in our analysis. A more careful analytical or numerical analysis (Steigman, Dasgupta, and Beacom, 2012) leads to the requirement (for $\xi = 1$)

$$\langle \sigma v \rangle \simeq 2.2 \cdot 10^{-26} \mathrm{cm}^3 \mathrm{s}^{-1} \simeq 1.9 \cdot 10^{-9}\ \mathrm{GeV}^{-2} \quad (10\ \mathrm{GeV} \lesssim m_\chi \lesssim 10\ \mathrm{TeV}), \tag{4.31}$$

and

$$\langle \sigma v \rangle \simeq 5 \cdot 10^{-26} \mathrm{cm}^3 \mathrm{s}^{-1} \simeq 4 \cdot 10^{-9}\ \mathrm{GeV}^{-2} \quad (100\ \mathrm{MeV} \lesssim m_\chi \lesssim 5\ \mathrm{GeV}), \tag{4.32}$$

in order to obtain the correct relic density.

Chapter 5

Kinetic Decoupling

Kinetic equilibrium refers to the situation where the momentum of a species follows a thermal distribution, while we allow for the possibility that the species is out of chemical equilibrium. In terms of the phase space distribution function, we can say that a species, i, is in kinetic equilibrium as long as

$$f_i(\mathbf{x}, \mathbf{p}) = \kappa f_i^{\mathrm{eq}}(\mathbf{x}, \mathbf{p}),$$

where $\kappa = n_i(\mathbf{x})/n_i^{\mathrm{eq}}(\mathbf{x})$.

Kinetic equilibrium is upheld by elastic scattering, as is shown in Fig. 5.1, with some heat bath particle, which we will denote by $\tilde{\gamma}$.

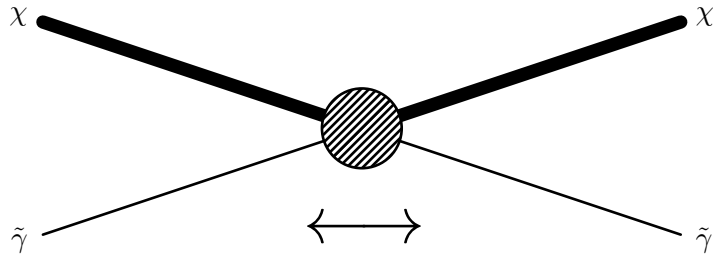

FIGURE 5.1: Processes that maintain kinetic equilibrium. Thick line corresponds to a heavy particle.

For typical DM models, which undergo CD while non-relativistic, kinetic equilibrium is usually maintained until well after CD. This means that we can usually assume kinetic equilibrium during CD and that we can assume a constant co-moving number density of DM during KD. In general, however, it is not always possible to treat these processes separately, and we must treat a set of coupled differential equations for departure from both chemical and kinetic equilibrium, as is discussed in van den Aarssen, Bringmann, and Goedecke, 2012. In this section we will assume that we can treat KD separately, and that χ is highly non-relativistic.

5.1 Boltzmann Equation for Kinetic Decoupling

In order to study the process of KD in more detail we need the BE for the DM temperature. The temperature is a good variable by which to analyze KD, since the scaling of the temperature changes as DM decouples from the relativistic heat bath. The temperature of the heat bath scales like $T_{\tilde{\gamma}} \sim 1/a$, while the temperature of the decoupled non-relativistic DM scales like $T_\chi \sim 1/a^2$, see Fig. 5.2. Therefore, we only need to find the the temperature at which the scaling changes, and this will be the kinetic decoupling temperature, T_{kd}.

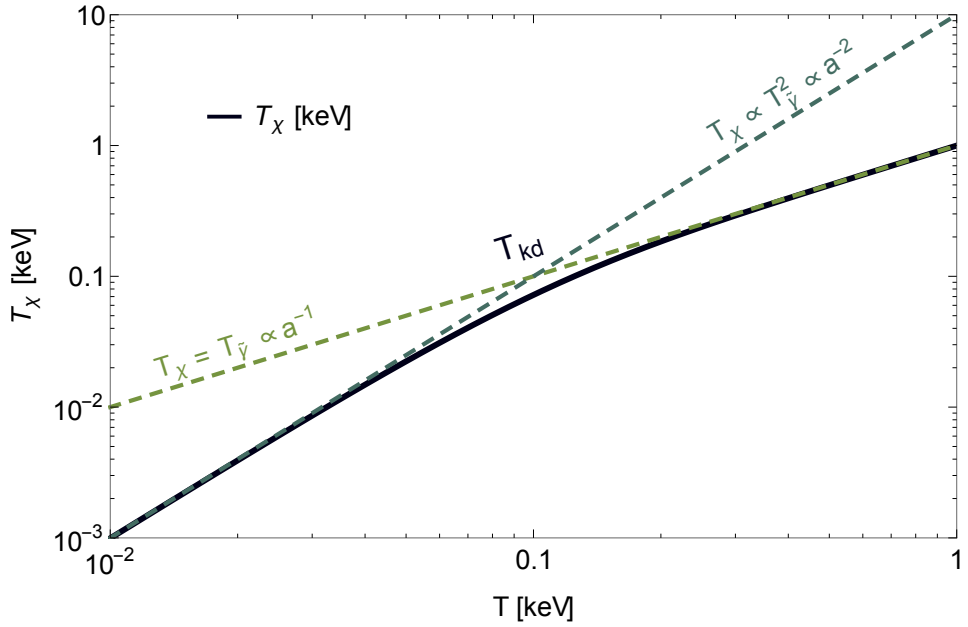

FIGURE 5.2: Plot of the DM temperature during kinetic decoupling. At high temperatures T_χ follows the heat bath temperature $T_{\tilde\gamma}$, while at low temperatures, after KD, it scales like $T_\chi \sim 1/a^2$. We define the kinetic decoupling temperature, $T_{\rm kd}$, to be the temperature at which the two asymptotic curves meet.

The collision term (Eq. 2.30) relevant for kinetic decoupling is the one that involves elastic scattering between, χ and $\tilde\gamma$. The general term is given by

$$\begin{aligned} C[f] = &\sum_{\tilde\gamma} \frac{1}{2g_\chi} \int \frac{d^3k}{(2\pi)^3 2\omega} \int \frac{d^3\tilde k}{(2\pi)^3 2\tilde\omega} \int \frac{d^3\tilde p}{(2\pi)^3 2\tilde E} \\ &\times (2\pi)^4 \delta^{(4)}(\tilde p + \tilde k - p - k)\, |\mathcal{M}|^2_{\chi\tilde\gamma \leftrightarrow \chi\tilde\gamma} \\ &\times \Big[f(\tilde{\mathbf{p}}) g^{\pm}(\tilde\omega)(1 \mp f(\mathbf{p}))(1 \mp g^{\pm}(\omega)) \\ &- f(\mathbf{p}) g^{\pm}(\omega)(1 \mp g^{\pm}(\tilde\omega))\,(1 \mp f(\tilde{\mathbf{p}})) \Big]. \end{aligned} \tag{5.1}$$

We should note here that we consider particles and antiparticles together. So if χ is a Dirac fermion $g_\chi = 4$ and we consider both processes with particles and processes with antiparticles in $|\mathcal{M}|^2$. This differs from our convention in Sec. 4, where we considered particles and antiparticles separately.

Since DM is not in full thermal equilibrium, it is not entirely clear what we mean when we talk about the DM temperature. It is natural, however, to define it by the average kinetic energy in a thermal distribution

$$\frac{3}{2} T_\chi \equiv \left\langle \frac{p^2}{2m_\chi} \right\rangle = \frac{g_\chi}{n} \int \frac{d^3p}{(2\pi)^3} \left(\frac{p^2}{2m_\chi} \right) f(E). \tag{5.2}$$

It is also useful to introduce the dimensionless variables

$$y \equiv \frac{m_\chi T_\chi}{s_v^{2/3}}, \tag{5.3}$$

$$x \equiv \frac{m_\chi}{T}. \tag{5.4}$$

In order to get a BE for the temperature we need to multiply Eq. 2.30 by p^2 and integrate over d^3p. Keeping only leading terms in p^2/m_χ^2 gives us (van den Aarssen, Bringmann, and Goedecke, 2012)

$$\frac{x}{y}\frac{dy}{dx} = \left(1 - \frac{x}{3g_{*S}^v}\frac{dg_{*S}^v}{dx}\right)\frac{\gamma(T_{\tilde{\gamma}})}{H(T)}\left(\frac{y_{\rm eq}}{y} - 1\right), \tag{5.5}$$

where $y_{\rm eq} \equiv m_\chi T_{\tilde{\gamma}}/s_v^{2/3}$, where

$$\gamma(T_{\tilde{\gamma}}) \equiv \frac{1}{48 g_\chi \pi^3 T_{\tilde{\gamma}} m_\chi^3}\int d\omega\, k^4 \left(1 \mp g^{\pm}(\omega)\right) g^{\pm}(\omega) \left\langle |\mathcal{M}|^2 \right\rangle_t, \tag{5.6}$$

is called the *momentum transfer rate*, and where

$$\left\langle |\mathcal{M}|^2 \right\rangle_t \equiv \frac{1}{8k^4}\int_{-4k^2}^{0} dt(-t)\, |\mathcal{M}|^2 . \tag{5.7}$$

As we are primarily interested in kinetic decoupling at the keV scale, the electrons and positrons are long since done annihilating. This means that g_{*S}^v will be a constant throughout the whole process of KD. As long as this is the case, Eq. 5.5 simplifies, and we get

$$\frac{dT_\chi}{dT} - 2\frac{T_\chi}{T} = \frac{\gamma(T_{\tilde{\gamma}})}{H(T)}\left(\frac{T_\chi}{T} - \xi(T)\right), \tag{5.8}$$

where, as we have indicated, ξ is still, in principle, a function of T.

From Eq. 5.8 we can see clearly that it is the ratio $\gamma(T_{\tilde{\gamma}})/H(T)$ which governs the transition between the two regions with different scaling of T_χ. At early times, when $\gamma(T_{\tilde{\gamma}}) \gg H(T)$ we see that the ratio T_χ/T is forced to be equal to ξ, or equivalently T_χ is forced to be equal to $T_{\tilde{\gamma}}$. At low temperatures, however, when $\gamma(T_{\tilde{\gamma}}) \ll H(T)$, the RHS can be completely neglected, and the change in T_χ is governed by the $2T_\chi/T$ term, leading to $T_\chi \sim T^2 \sim 1/a^2$. We define the temperature of KD, $T_{\rm kd}$, as the temperature where these two asymptotes meet, i.e.

$$T_\chi(T) = \begin{cases} T_{\tilde{\gamma}}(T) & \text{for } T \gtrsim T_{\rm kd}, \\ \xi T_{\rm kd}\left(\frac{a(T_{\rm kd})}{a(T)}\right)^2 & \text{for } T \lesssim T_{\rm kd}. \end{cases} \tag{5.9}$$

This analysis requires that $\gamma(T_{\tilde{\gamma}}) \propto T^{n+4}$, with $n > -2$ (or an even stronger dependence on T) in order for γ to dominate at high temperatures and H to dominate at low temperatures. If this is not the case, it is not clear that KD will ever happen. We will return to this point later when we look at the solutions of the BE.

5.2 Analytic Solution of the Kinetic Decoupling Equation

In general, the BE for KD must be solved numerically. Under a few more assumptions, however, we can find an exact analytic solution to the equation.

First, we assume that ξ is constant during KD. Second, we assume that the momentum transfer rate scales like a power law e.g.

$$\gamma(T_{\tilde{\gamma}}) \propto \left(\frac{T}{m_\chi}\right)^{4+n}, \tag{5.10}$$

where $n > -1$. These assumptions are actually very good in a wide range of models that we will be considering.

We will now solve the BE analytically under the stated assumptions. In solving Eq. (5.8) it is useful to first consider the homogeneous equation

$$\frac{dT_\chi}{dT} = \frac{T_\chi}{T}\left[2 + a_n\left(\frac{T}{m_\chi}\right)^{n+2}\right], \tag{5.11}$$

where

$$a_n \equiv \frac{\gamma(T_{\tilde{\gamma}})}{H(T)}\left(\frac{m_\chi}{T}\right)^{n+2},$$

is a constant if $H(T) \propto T^2$ as it is in the radiation dominated phase ($T \gtrsim$ eV).

This equation is separable and the solution is given by

$$T_\chi^{\text{hom}} = c_1\left(\frac{T}{m_\chi}\right)^2 e^{k_n}, \tag{5.12}$$

where $k_n = \frac{a_n}{n+2}\left(\frac{T}{m_\chi}\right)^{n+2}$.

We now need to find a particular solution T_χ^p to the full Eq. (5.8), following (Bringmann and Hofmann, 2007) we try the ansatz $T_\chi^p = \lambda(T)T_\chi^{\text{hom}}$. Inserting this into Eq. (5.8) we derive the following equation for $\lambda(T)$

$$T_\chi^{\text{hom}}\frac{d\lambda}{dT} = a_n\xi\left(\frac{T}{m_\chi}\right)^{n+2}. \tag{5.13}$$

This equation can be solved to find the complete solution $T_\chi = T_\chi^p + AT_\chi^{\text{hom}}$

$$T_\chi = \xi T\left[1 - \frac{k_n^{1/(n+2)}e^{k_n}}{n+2}\Gamma(-1/(n+2), k_n)\right] + AT_\chi^{\text{hom}}. \tag{5.14}$$

We want to match this general solution onto the asymptotic behavior we expect

$$T_\chi \overset{T\to\infty}{=} \xi T, \tag{5.15}$$

$$T_\chi \overset{T\to 0}{=} \xi T_{\text{kd}}\left(\frac{T}{T_{\text{kd}}}\right)^2. \tag{5.16}$$

To do this we also need to look at the expansion of the incomplete gamma function in these limits

$$\Gamma(-1/(n+2), k_n) \overset{k_n \to \infty}{=} k_n^{-1/(n+2)} e^{-k_n}/k_n, \tag{5.17}$$

$$\Gamma(-1/(n+2), k_n) \overset{k_n \to 0}{=} (n+2)\left[k_n^{-1/(n+2)} - \Gamma\left(\frac{n+1}{n+2}\right)\right]. \tag{5.18}$$

Let us look at the $T \to \infty$ limit first

$$T_\chi \overset{T \to \infty}{=} \xi T\left[1 - \frac{1}{k_n(n+2)}\right] + A T_\chi^{\text{hom}} = \xi T + A T_\chi^{\text{hom}}. \tag{5.19}$$

From this we see that $A = 0$. Looking at the $T \to 0$ limit now lets us solve for the kinetic decoupling temperature T_{kd} in terms of the model parameters

$$T_\chi \overset{T \to 0}{=} \xi T k_n^{1/(n+2)} \Gamma\left(\frac{n+1}{n+2}\right) = \xi \left(\frac{a_n}{n+2}\right)^{\frac{1}{n+2}} \frac{T^2}{m_\chi} \tag{5.20}$$

giving

$$\frac{T_{\text{kd}}}{m_\chi} = \left[\left(\frac{a_n}{n+2}\right)^{\frac{1}{n+2}} \Gamma\left(\frac{n+1}{n+2}\right)\right]^{-1}. \tag{5.21}$$

5.3 Momentum Transfer Rate, $\gamma(T_{\tilde{\gamma}})$

When looking at Eq. 5.8 (at least almost) all the interesting physics is in the momentum transfer rate, $\gamma(T_{\tilde{\gamma}})$. Let us now look a bit closer at this function. First we can do a little trick using integration by parts.

Using the following mathematical identity

$$g^\pm(1 \mp g^\pm) = -T_{\tilde{\gamma}} \partial_\omega g^\pm,$$

we can use partial integration to rewrite Eq. 5.6 as

$$\gamma(T_{\tilde{\gamma}}) = \frac{1}{48 g_\chi \pi^3 m_\chi^3} \int_{m_{\tilde{\gamma}}}^\infty d\omega g^\pm \partial_\omega \left[k^4 \left\langle |\mathcal{M}|^2 \right\rangle_t\right], \tag{5.22}$$

where we have only assumed that

$$\lim_{k \to 0}\left[k^4 \left\langle |\mathcal{M}|^2 \right\rangle_t\right] = 0.$$

We have also included the limits on the integral over ω to avoid any confusion.

In general, this is as far as we get, and we have to solve Eq. 5.8 numerically. We should try to examine, however, under what circumstances $\gamma(T_{\tilde{\gamma}})$ scales like a power law in temperature, since in these cases we have an exact analytic solution.

If we assume that $\tilde{\gamma}$ is ultra-relativistic, this means $k \approx \omega$ and Eq. 5.22 simplifies. If we further assume that the leading term in the t-averaged scattering matrix element squared scales like a power law

$$\left\langle |\mathcal{M}|^2 \right\rangle_t \approx c_n \left(\frac{\omega}{m_\chi}\right)^n, \tag{5.23}$$

we can rewrite Eq. 5.22 in the following simple form

$$\gamma(T_{\tilde{\gamma}}) = \frac{c_n}{48 g_\chi \pi^3 m_\chi^{n+3}}(n+4)\int_0^\infty d\omega g^{\pm}\left[\omega^{n+3}\right]. \tag{5.24}$$

This integral can be solved analytically, giving us

$$\gamma(T_{\tilde{\gamma}}) = \frac{c_n \xi^{n+4} m_\chi}{48 g_\chi \pi^3} N^{\pm}_{n+3}\left(\frac{T}{m_\chi}\right)^{n+4}, \tag{5.25}$$

where

$$N^{-}_{n+3} \equiv \zeta(n+4)(n+4)!\,, \tag{5.26}$$

$$N^{+}_{n+3} \equiv (1-2^{-(n+3)})N^{-}_{n+3}\,. \tag{5.27}$$

In Figs. 5.3 and 5.4 we see the evolution of the momentum transfer rate, $\gamma(T_{\tilde{\gamma}})$, compared to the expansion rate, $H(T)$. For the cases in Fig. 5.3 ($n \geq 0$) we can

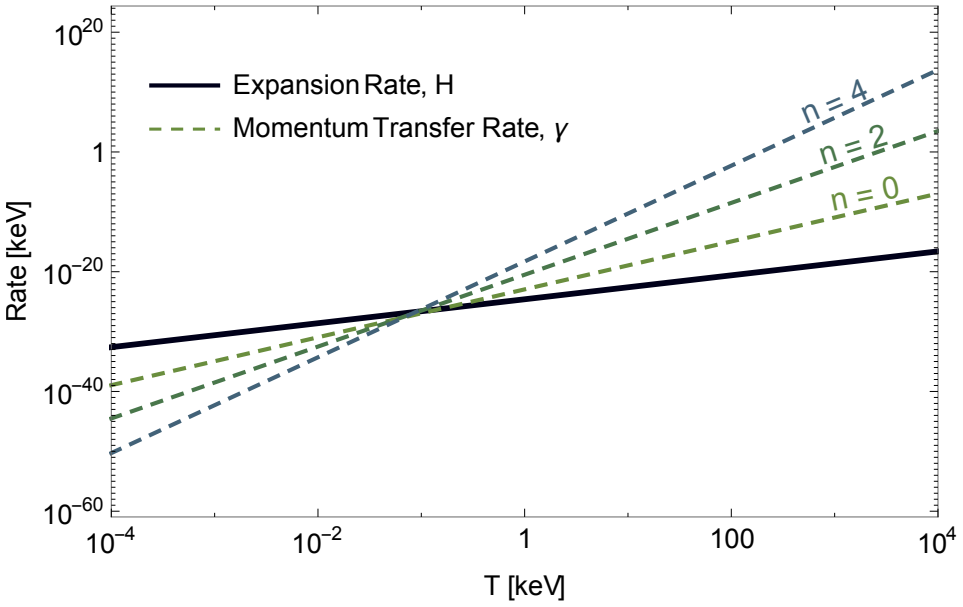

FIGURE 5.3: Plot of the momentum transfer rate, $\gamma(T_{\tilde{\gamma}})$ (dashed lines), compared to the expansion rate, $H(T)$ (solid line). The different lines correspond to different power law scalings of the t-averaged squared matrix element, $\langle|\mathcal{M}|^2\rangle_t \sim c_n(\omega/m_\chi)^n$. We see that i all cases we have kinetic equilibrium at high temperatures, and then we go out of kinetic equilibrium at low temperatures. The values of c_n have been adjusted to result in kinetic decoupling at 100 eV.

We can now put this result into the analytical solution. Using $H^2 = (4\pi^3 G/45)g_* T^4$ we get the following expression for a_n

$$a_n = \sqrt{\frac{5}{2(2\pi)^9 g_*}} N^{\pm}_{n+3}\,\xi^{n+4}\frac{c_n}{g_\chi}\frac{m_{\rm Pl}}{m_\chi}. \tag{5.28}$$

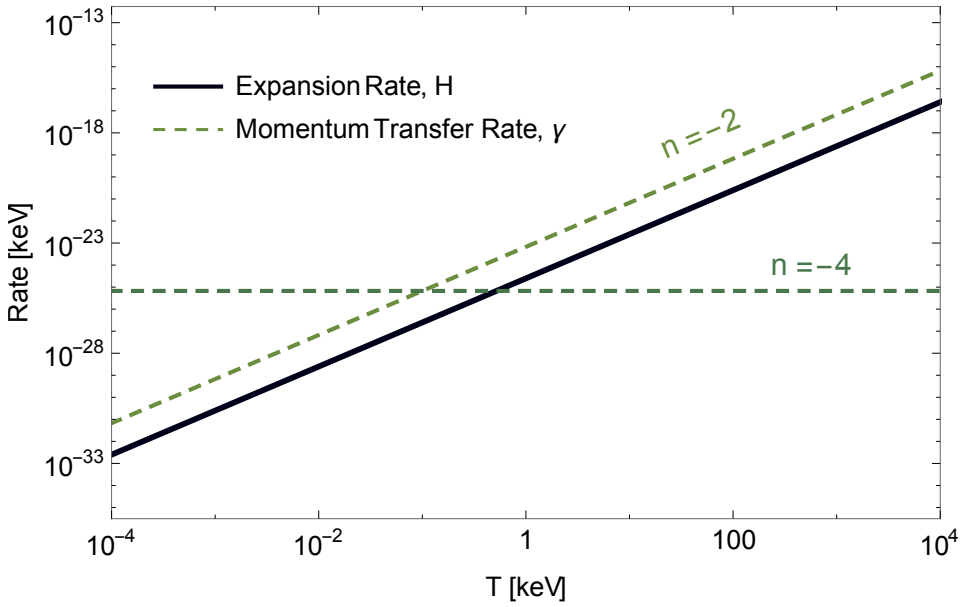

FIGURE 5.4: Plot of the momentum transfer rate, $\gamma(T_{\tilde{\gamma}})$ (dashed lines), compared to the expansion rate, $H(T)$ (solid line). The different lines correspond to different power law scalings of the t-averaged squared matrix element, $\langle|\mathcal{M}|^2\rangle_t \sim c_n(\omega/m_\chi)^n$. These are cases where it is impossible to achieve kinetic decoupling (under the assumptions that we have made in Eq. 5.25). For the $n = -2$ case, the momentum transfer rate scales in exactly the same way as the Hubble rate, meaning that you are either always in equilibrium, or never in equilibrium. The $n = -4$ case, however, corresponds to a case where you are out of equilibrium at early times, but then go into equilibrium at some time (*kinetic recoupling*?). After it has gone into kinetic equilibrium, it will stay there (at least until matter domination).

5.4 Suppressing Structure Formation on Small Scales

As long as the DM particles interact with a relativistic heat bath, the pressure of the heat bath leads to acoustic oscillations that wash out the overdensities that starts growing in the DM fluid, leading to a suppression of structure on all scales (within the horizon). See Fig. 5.5 for a description.

KD corresponds (at least roughly) to the time at which the interactions between the DM fluid and the heat bath become negligible. This means that only modes on a larger scale than the horizon at KD remain unsuppressed. So we should see a cutoff in the linear matter power spectrum at the scale of roughly the size of the cosmological horizon at KD.

The cutoff in the linear matter power spectrum corresponds to a cutoff mass, given, as a first approximation, by the mass (in DM) within the horizon at KD

$$M_{\text{cut}} \equiv \frac{4\pi}{3}\frac{\rho_{\text{DM}}(T_{\text{kd}})}{H^3(T_{\text{kd}})} = \frac{4\pi}{3}\left[\frac{4\pi^3}{45 g_{\text{eff}}}\right]^{-3/2}\frac{\Omega_{\text{DM}}\rho_{\text{c0}} m_{\text{Pl}}^3}{T_{\text{kd}}^3 T_0^3}, \tag{5.29}$$

where T_0 is the CMB temperature today, and we have assumed that $g_{*\text{S}}^v$ does not change between KD and today. This is clearly just a rough estimate, and

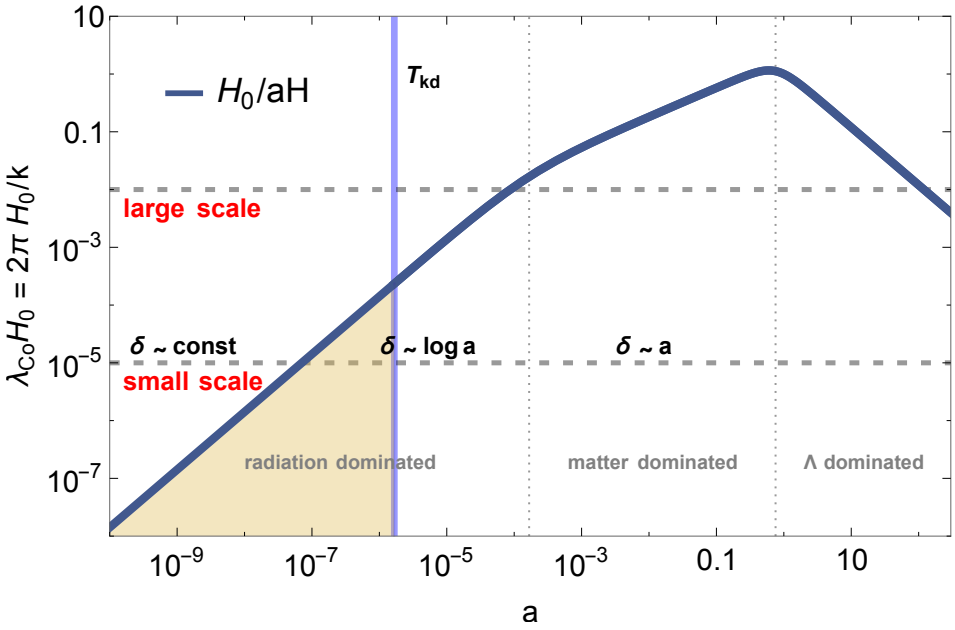

FIGURE 5.5: Overview plot of structure formation. On the y-axis we have comoving length scale, $\lambda_{\rm co}$, and on the x-axis we have the scale factor, a. See Fig. 1.1 for more details. The shaded area before $T_{\rm kd}$ corresponds to scales and times where acoustic oscillations from elastic scattering of χ and $\tilde{\gamma}$, suppress the growth of the perturbations in the DM-fluid. The first scale that enters the horizon after KD is the smallest unsuppressed scale, and corresponds to the smallest DM structures today.

recent numerical estimates of the cutoff gives a value of (Vogelsberger et al., 2015)

$$M_{\rm cut} = 5 \cdot 10^{10} \left(\frac{T_{\rm kd}}{100\,{\rm eV}} \right)^{-3} h^{-1}\, M_\odot \,. \tag{5.30}$$

In WDM models, a similar cutoff in the power spectrum arises from the free-streaming of light DM particles (see Sec. 1.2.4). The corresponding numerical estimate for this effect is given by (Vogelsberger et al., 2015)

$$M_{\rm cut,WDM} = 10^{11} \left(\frac{m_{\rm WDM}}{\rm keV} \right)^{-4} h^{-1}\, M_\odot \,. \tag{5.31}$$

Clearly, the largest of these cutoff masses is the one that is relevant. This will have to be estimated on a model by model basis. For models where a (highly) non-relativistic DM candidate undergoes KD at the keV-scale, which is what we are mainly considering in this thesis, the cutoff from KD is much larger. In Fig. 5.6 we can see a comparison of the linear matter power spectrum in models with late KD and WDM models.

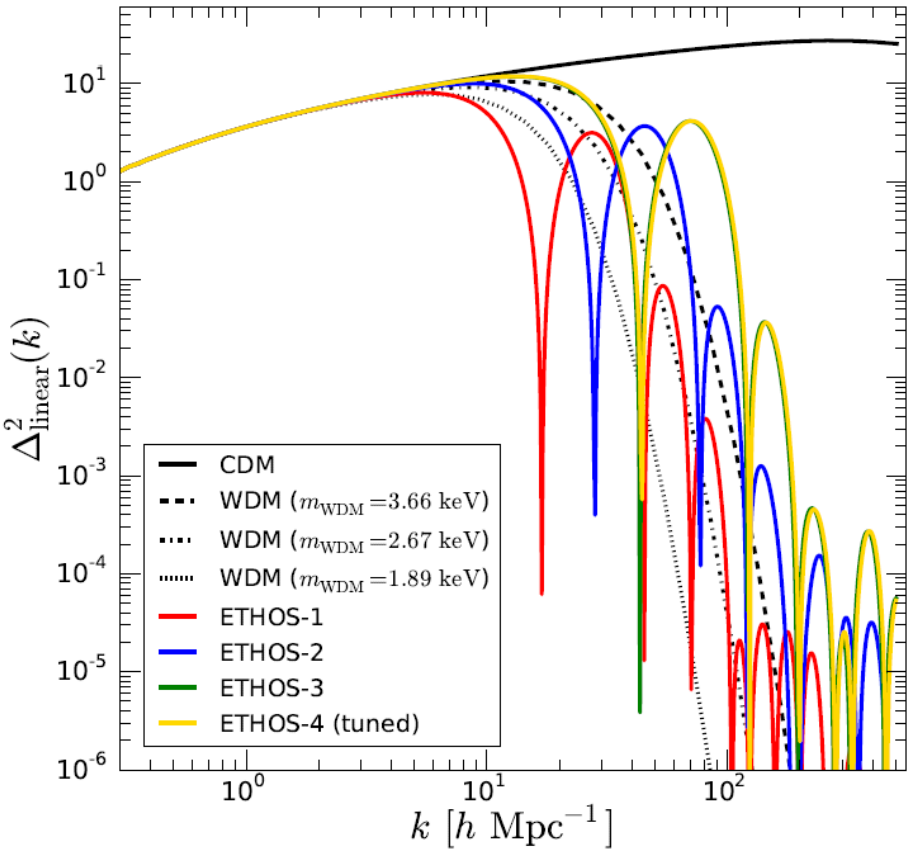

FIGURE 5.6: Plot of the linear matter power spectrum, $\Delta^2_{\rm linear}(k) \equiv k^3 P_{\rm linear}(k)/2\pi^2$, in different DM models. Figure taken from Vogelsberger et al., 2015. The solid black line corresponds to regular CDM cosmology. The dotted and dashed black curves correspond to different WDM models, while the colored lines corresponds to models with late KD. The exponential cutoff in the power spectrum arising from WDM and late KD are similar, although the exact shape is different, the acoustic oscillations taking place in models with late KD is entirely absent in WDM models, but this difference is hard to see in the non-linear matter power spectrum.

Part III

Late Kinetic Decoupling of Dark Matter

Chapter 6

General Considerations

6.1 Late Kinetic decoupling

In typical WIMP - models kinetic decoupling happens far too early to possibly address the missing satellite problem. For e.g. neutralino DM we get kinetic decoupling temperatures in the range $T_{\rm kd} \sim$ MeV - GeV, leading to cutoff masses of the order $M_{\rm cut} \sim 10^{-11} - 10^{-3} M_\odot$, far below the $M_{\rm cut} \sim 10^{10} M_\odot$ relevant for dwarf galaxy scales (Bringmann, 2009). This means that we typically need to do something special in order to get $T_{\rm kd} \sim$ keV, like we need.

6.1.1 Scattering Partner $\tilde{\gamma}$

The reason for the cutoff in the matter power spectrum is the pressure resulting from the interaction between DM particles, χ, and some heat bath particle, $\tilde{\gamma}$. This particle has to be relativistic, or at least very light. The main reason for this is that, since the number density, $n_{\tilde{\gamma}}$, of a non-relativistic particle is exponentially suppressed, the interaction rate for elastic scattering, $\Gamma \sim \sigma v n_{\tilde{\gamma}}$, is reduced correspondingly.

You can try to get around this by stipulating that $\tilde{\gamma}$ has decoupled from the SM (or other) heat bath while relativistic, so that its comoving number density is constant, like a relativistic particle. Another problem that arises is then that the temperature, $T_{\tilde{\gamma}} \sim a^{-2}$, quickly drops as $\tilde{\gamma}$ becomes non relativistic, leading to a negligible pressure.

The observant reader will know that there is still a further possibility. $\tilde{\gamma}$ could be in kinetic equilibrium with a relativistic particle, but still have a large constant comoving number density, perhaps arising from some conserved charge or quantum number possessed by $\tilde{\gamma}$. This is possible, but there is still a very strong constraint from the relic density of $\tilde{\gamma}$ (see Eq. 4.13), making it very hard to avoid $m_{\tilde{\gamma}}/\xi \lesssim T_{\rm kd}$.[1]

6.1.2 General Requirements for Late Kinetic Decoupling

If we want some general expressions relating the kinetic decoupling temperature to the other parameters we need to make some more assumptions. We will first assume that $\tilde{\gamma}$ is ultra relativistic, second we will assume that the amplitude is given by

$$\left\langle |\mathcal{M}|^2 \right\rangle_t \approx c_n \left(\frac{\omega}{m_\chi} \right)^n , \tag{6.1}$$

[1] In Sec. 9.2.2 we see a model where we push the limits of exactly these assumptions.

where ω is the energy of the heat bath particle $\tilde{\gamma}$. We showed in Sec. 5.2 that using these assumptions we can solve the BE for KD analytically for the temperature of KD, $T_{\rm kd}$. Using Eqs. 5.21 and 5.28 this we get [2]

$$\frac{c_n}{g_\chi} = A_n^{\pm}\xi^{-(n+4)}\left(\frac{m_\chi}{\rm GeV}\right)^{n+3}\left(\frac{T_{\rm kd}}{100\,\rm eV}\right)^{-(n+2)}, \tag{6.2}$$

where

$$A_n^- = \sqrt{\frac{2(2\pi)^9 g_*}{5}}\frac{n+2}{(n+4)!\zeta(n+4)}\left[\frac{1}{\Gamma\left(\frac{n+1}{n+2}\right)}\right]\frac{\rm GeV}{M_{\rm Pl}}\left(\frac{\rm GeV}{100\,\rm eV}\right)^{n+2}, \tag{6.3}$$

and

$$A_n^+ = \frac{A_n^-}{1-2^{-(n+3)}}. \tag{6.4}$$

To get a handle on this let us look at a couple of values of A_n^-

$$A_0^- = 1.8\cdot 10^{-3}, \tag{6.5}$$
$$A_2^- = 5.7\cdot 10^{11}, \tag{6.6}$$
$$A_4^- = 2.1\cdot 10^{26}. \tag{6.7}$$

We see that for $n > 0$ we need a significant enhancement of the "rest" of the matrix element c_n.

In general we see that reducing n makes it easier to achieve late kinetic decoupling, and for $n = 0$ we can achieve it simply with $c_n \sim 0.1$ and $m_\chi \sim$ GeV.

Another thing we can always do to achieve later kinetic decoupling is to reduce m_χ, there are, however, limits to how light DM can be. The free streaming effects from warm DM become relevant when m_χ approaches the keV-scale (see Eq. 5.31), so this is a lower limit on the mass.[3]

6.1.3 Thermal Production

If we assume that DM was thermally produced in the early universe, then this typically means that the ratio α/m_χ is fixed.

The coupling, α, that is fixed by requiring the correct relic density, is not necessarily the same as the coupling(-s) involved in the elastic scattering process relevant for KD. However, since in many cases the two couplings are the same, it is useful to study this possibility in more detail.

Let us assume that the DM annihilation process is dominated by the s-wave and that the scattering cross section is given by $\langle\sigma v\rangle = \pi\alpha^2/2m_\chi^2$. If we then use the canonical value for the WIMP annihilation cross section, $\langle\sigma v\rangle = 3\cdot 10^{-26}\,\rm cm^3/s \sim 2\cdot 10^{-9}\,GeV^{-2}$ we get $\alpha \sim 6\cdot 10^{-5}\,m_\chi/\rm GeV$.

[2] Note that this solution is only valid for $n > -1$. If this is not the case then, under our definition, KD actually never happens, which is why we cannot get an expression for it. In reality it means that KD does not happen under the assumptions we have made. KD *can* happen if the assumptions are broken, for example when $\tilde{\gamma}$ becomes non-relativistic.

[3] It is unclear how the free-streaming effects change for $\xi \ll 1$. Since the effects come from the velocity of the DM-particles, it seems clear that there should be an effect there, but we have not found any work in the literature addressing this issue specifically.

Introducing the ratio $r \equiv c_n/g_\chi\alpha^2$ we can rewrite Eq. 6.2 to get

$$r \sim 3 \cdot 10^8 A_n^{\pm} \xi^{-(n+4)} \left(\frac{m_\chi}{\text{GeV}}\right)^{n+1} \left(\frac{T_{\text{kd}}}{100\,\text{eV}}\right)^{-(n+2)}. \tag{6.8}$$

We see that in this case it is significantly harder to achieve late KD. Also, reducing the mass does not help nearly as much. This means that if the coupling α is responsible for both CD and KD, we need a huge value for r, or we need enormously light DM (or some combination thereof).

6.1.4 Enhancing the Elastic Scattering

As we see from the above discussion, in most cases we need a significant enhancement of the matrix element ($c_n \gg \alpha^2$) in order to obtain late KD. As long as we are in the perturbative regime (meaning that the leading term in the expansion of the S-matrix dominates the scattering amplitude), we can only create such an enhancement if we put a propagator almost on-shell. At tree-level the scattering can occur in the s-, t- and u-channels. We will look at these in turn.

t-channel Enhancement

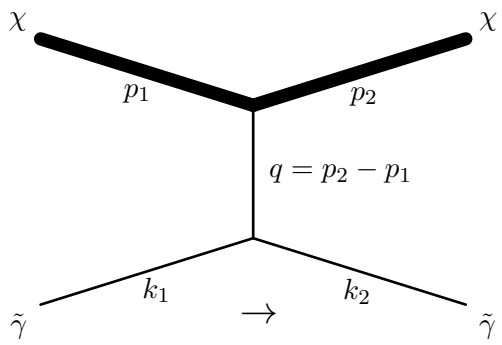

FIGURE 6.1: Feynman diagram for generic t-channel elastic scattering ($\chi\tilde{\gamma} \to \chi\tilde{\gamma}$). Since the kinematics forces t to be small, if we want an enhancement from the propagator, we need to have a light mediator ($m_{\text{mediator}} \ll m_\chi$).

We have made the assumption that $m_\chi \gg \omega$. This ensures that kinematics of the elastic scattering in the t-channel forces $t \equiv (p_1 - p_2)^2$ to be very small ($t \sim \omega^2 \ll m_\chi$), meaning that we need a light mediator mass ($m_{\text{mediator}} \ll m_\chi$) in order to get an enhancement from the propagator (see Fig. 6.1).

We expect the leading term in the squared amplitude to be of the form

$$|\mathcal{M}|^2 \sim \alpha_\chi \alpha_{\tilde{\gamma}} \frac{m_\chi^4}{(t - m_{\text{mediator}}^2)^2} \left(\frac{\omega}{m_\chi}\right)^n, \tag{6.9}$$

where α_χ and $\alpha_{\tilde{\gamma}}$ are the couplings between the mediator, χ and $\tilde{\gamma}$ respectively.

If $m_{\text{mediator}} \gg \omega$ then we get

$$c_n \sim \alpha_\chi \alpha_{\tilde{\gamma}} \left(\frac{m_\chi}{m_{\text{mediator}}} \right)^4 \left(\frac{\omega}{m_\chi} \right)^n, \tag{6.10}$$

which can lead to a huge enhancement if $m_\chi \gg m_{\text{mediator}}$.

If the mediator is massless, then there is a pole in the amplitude at $t = 0$. In any real (finite temperature) system, however, this divergence will (at least) be regulated by the thermal mass of the mediator (e.g Arnold and Yaffe, 1995).

If we cannot make the assumption $m_{\text{mediator}} \gg \omega$ then the t-averaging integral (see Eq. 5.7) also plays a major role in determining the form of the solution.

s- and u-channel Enhancement

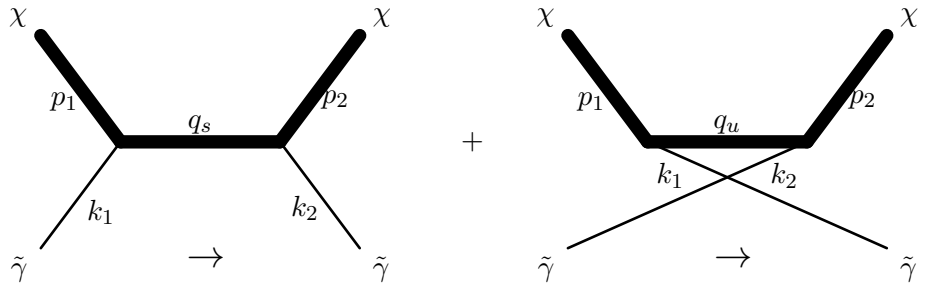

FIGURE 6.2: Feynman diagram for generic s/u-channel elastic scattering ($\chi\tilde{\gamma} \to \chi\tilde{\gamma}$). Since the $s \sim u \sim m_\chi^2$, if we want an enhancement from the propagator, we need to have a heavy mediator ($m_{\text{mediator}} \sim m_\chi$).

As long as $m_\chi \gg \omega$ then s and u are both dominated by the DM momentum p. To first order in ω they are given by

$$s \approx m_\chi^2 + 2m_\chi\omega, \tag{6.11}$$

$$u \approx m_\chi^2 - 2m_\chi\omega. \tag{6.12}$$

We see that in order to get an enhancement from the propagator, we need $m_{\text{mediator}} \sim m_\chi$.

If $\Delta m \equiv m_{\text{mediator}} - m_\chi \gg \omega$, then we expect a squared amplitude of the form

$$|\mathcal{M}|^2 \sim \alpha^2 \frac{m_\chi^2}{\Delta m^2} \left(\frac{\omega}{m_\chi} \right)^n, \tag{6.13}$$

which can be enhanced if $|\Delta m| \ll m_\chi$.

However, if $\Delta m \ll \omega$, something more interesting can happen. In this case the leading terms in the denominators are given by

$$s - m_{\text{mediator}}^2 \approx 2m_\chi\omega, \tag{6.14}$$

$$u - m_{\text{mediator}}^2 \approx -2m_\chi\omega. \tag{6.15}$$

meaning that we typically get a contribution m_χ^2/ω^2 from the propagator. When combining the results from the s- and u-channels, however (which we need to do in most cases), the difference in sign can mean that the leading terms from the two channels exactly cancel. This will depend on the exact amplitudes in question.

6.1.5 Fermionic $\tilde{\gamma}$

We cannot say that much about the scattering matrix elements in general, without specifying the particle physics model. We can, however, make an observation about the case of fermionic $\tilde{\gamma}$. Any elastic scattering amplitude involving fermionic $\tilde{\gamma}$ will need to contain two spinors $u(k)$ and $\bar{u}(k)$ (or v and $\bar{v}$).

Since these spinors are dimensionful and only depend on the momentum, k, and mass, $m_{\tilde{\gamma}}$, of $\tilde{\gamma}$, this has to mean that the amplitude gets a contribution of either ω or $m_{\tilde{\gamma}}$ in the numerator. In the limit where we neglect the mass of $\tilde{\gamma}$ this means that we get $n \geq 2$ (or, if the amplitude is proportional to $m_{\tilde{\gamma}}$, we get nothing) for any process that involves fermionic $\tilde{\gamma}$.[4]

The only exception to this argument is if the denominator is enhanced by the same (or higher) power of ω. In both cases, however, fermionic $\tilde{\gamma}$ reduces the maximally possible enhancement.

A similar argument can be made for scalar $\tilde{\gamma}$ interacting only via a gauge boson, since then the vertices will always include one power of k^μ.

6.2 Evolution of the Dark Radiation Temperature

In cases where the dark sector, that is DM, DR and possibly other particles part of the DR heat bath, is entirely decoupled from the visible sector it is important to keep track of the relative temperature by introducing the temperature fraction ξ

$$T_{\tilde{\gamma}} = \xi T.$$

In general ξ is a function of time (or temperature), and in the limit where entropy is conserved, which is usually a very good approximation, we can calculate this time dependence by following the number of relativistic degrees of freedom in both the visible and dark sector.

Let us denote the total entropy density in the dark and visible sectors by s_d and s_v respectively. We then define the effective numbers of relativistic degrees of freedom in the dark and visible sectors, g_{*S}^d and g_{*S}^v, by the following expressions

$$s_d(T_{\tilde{\gamma}}) = g_{*S}^d \frac{2\pi^2}{45} T_{\tilde{\gamma}}^3, \tag{6.16}$$

$$s_v(T) = g_{*S}^v \frac{2\pi^2}{45} T^3. \tag{6.17}$$

As discussed in Ch. 2, since the entropy is dominated by the contribution from relativistic species, we can approximate the effective relativistic

[4] Note that we here rely on the assumption that the amplitude can be written as a power law in ω.

degrees of freedom in the same way

$$g^d_{*S} = \sum_{\text{bosons}}^{\text{dark}} g_i \left(\frac{T_i}{T_{\tilde{\gamma}}}\right)^3 + \frac{7}{8} \sum_{\text{fermions}}^{\text{dark}} g_i \left(\frac{T_i}{T_{\tilde{\gamma}}}\right)^3,$$
$$g^v_{*S} = \sum_{\text{bosons}}^{\text{visible}} g_i \left(\frac{T_i}{T}\right)^3 + \frac{7}{8} \sum_{\text{fermions}}^{\text{visible}} g_i \left(\frac{T_i}{T}\right)^3.$$

Entropy conservation implies $\frac{\partial}{\partial t}(sa^3) = 0$. After the the two sectors are decoupled this conservation should apply separately in each of the sectors (and of course on the total entropy as well). This means that the expressions

$$g^d_{*S} T^3_{\tilde{\gamma}} a^3$$

and

$$g^v_{*S} T^3 a^3$$

are constants in time.

If the two sectors were in thermal equilibrium in the early universe, and then decoupled at a time corresponding to a temperature T_{dc}, we can find a simple expression for ξ

$$T_{\tilde{\gamma}} = \left(\frac{g^d_{*S}(T_{\text{dc}}) g^v_{*S}(T)}{g^d_{*S}(T_{\tilde{\gamma}}) g^v_{*S}(T_{\text{dc}})}\right)^{1/3} T. \tag{6.18}$$

Even if you do not know when the sectors decoupled, or even know if they were ever in equilibrium at all, but you know the relation between the temperatures at some initial time t_I

$$T_{\tilde{\gamma} I} = \xi_I T_I,$$

you can still use this approach to follow the subsequent evolution of the temperatures

$$T_{\tilde{\gamma}} = \xi_I \left(\frac{g^d_{*S}(T_{\tilde{\gamma} I}) g^v_{*S}(T)}{g^d_{*S}(T_{\tilde{\gamma}}) g^v_{*S}(T_I)}\right)^{1/3} T. \tag{6.19}$$

Let us here just note briefly that although they are fairly simple, Eqs. 6.18 and 6.19 are only implicit equations for $T_{\tilde{\gamma}}$, since the r.h.s. also depends on $T_{\tilde{\gamma}}$, which will need to be taken into account when solving the equation.

What is happening here, physically, is that as the particle species in one of the heat baths become non relativistic (thus reducing the effective number of relativistic degrees of freedom) they start to annihilate, this heats the corresponding heat bath as compared to the other, changing the relative temperature.

An example of this from the standard model is the case of neutrinos. Neutrinos decouple from the SM heat bath at a temperature of a few MeV, this is right before the electrons and positrons become non-relativistic and

start to annihilate. Thus the photon bath gets heated compared to the neutrinos by the electron positron annihilations, leading to a permanent difference in temperature at later times, given by (using Eq. (6.18))

$$T_\nu = \left(\frac{2}{2 + 7/8 \cdot 4}\right)^{1/3} T.$$

It is interesting to take a look at possible values for ξ can take. Let us consider the case where the dark and visible sector are at equilibrium at some high temperature. In this case ξ is entirely decided from the number of relativistic species in the different sectors.

To look at the most extreme case let us consider the case where the dark matter becomes non-relativistic before the two sectors decouple, and there are no other species that annihilate in the dark sector after decoupling. ξ is then determined by the number of degrees of freedom available in the visible sector at the time of decoupling

$$\xi = \left(\frac{2 + 7/8 \cdot 2 \cdot 3\,(4/11)}{g^v_{*S}(T_{\text{dc}})}\right)^{1/3}.$$

For a simple case we can consider all the SM degrees of freedom

$$\xi^{\text{SM}}_{\text{min}} = \left(\frac{2 + 7/8 \cdot 2 \cdot 3\,(4/11)}{28 + 7/8 \cdot 90}\right)^{1/3} \approx 0.33. \tag{6.20}$$

We see that for the most extreme case, even with all the SM particles we cannot even reduce ξ below 0.3. Even if we have 10^3 degrees of freedom we will not go lower that $\xi \sim 0.15$. So if entropy is conserved, it is hard to get a very small value for ξ.

However, if we consider processes that do not conserve entropy, or allow for models where the visible and dark sector are never in thermal equilibrium, there is, in general, no lower bound on ξ. There will, however, always be an upper bound coming from N_{eff} that will be discussed in section 6.3.

6.3 Effective Number of Neutrino Species, N_{eff}

Adding DR into the mix in cosmology changes the energy density in radiation affecting the cosmological evolution. These effects are usually parametrized by introducing the effective number of neutrino species, N_{eff}. At late times the radiation density of the universe is given by

$$\rho_{\text{R}} = \rho_\gamma + 3\rho_\nu + \rho_{\text{DR}}. \tag{6.21}$$

In section 6.2 we showed that the neutrino temperature, at late times, is given by

$$T_\nu = \left(\frac{4}{11}\right)^{1/3} T.$$

This however is only an approximation, it is what you would get in the limit of instantaneous decoupling of massless neutrinos at a temperature $T^{\text{dc}}_\nu \gg m_e$. The actual neutrino temperature will deviate slightly from this.

We define N_{eff} by the following equation (Lesgourgues et al., 2013, p. 103)

$$\rho_{\text{R}} = \rho_\gamma + N_{\text{eff}}\rho_\nu^0, \tag{6.22}$$

where

$$\rho_\nu^0 \equiv \frac{7}{8}\left(\frac{4}{11}\right)^{4/3}\rho_\gamma.$$

In the simplest approximation, then, and in a universe with no DR, we get $N_{\text{eff}} = 3$. In the "standard model", that is, only SM particles and ΛCDM cosmology, however, we get a slightly different result, coming from the fact that the neutrino decoupling is not instantaneous and that $m_e/T_\nu^{\text{dc}} \sim 0.2$. We get (Nollett and Steigman, 2015)

$$N_{\text{eff}}^{\text{SM}} = 3\frac{\rho_\nu}{\rho_\nu^0} \approx 3.046.$$

When considering models with some DR, it is common to introduce the parameter ΔN_{eff}. For us it is natural to define it in a way so that $\Delta N_{\text{eff}} = 0$ corresponds to cosmology with no DR. Following Nollett and Steigman, 2015 we will define it by the relation[5]

$$\rho_{\text{R}} = \rho_\gamma + (3 + \Delta N_{\text{eff}})\rho_\nu. \tag{6.23}$$

Note that with this definition $N_{\text{eff}} \neq (3 + \Delta N_{\text{eff}})$, although this equality holds in the simple approximation discussed earlier. In general we have

$$N_{\text{eff}} = \frac{\rho_\nu}{\rho_\nu^0}(3 + \Delta N_{\text{eff}}) = \left(\frac{T_\nu/T}{(4/11)^{1/3}}\right)^4 (3 + \Delta N_{\text{eff}}) \approx 3.046(1 + \Delta N_{\text{eff}}/3). \tag{6.24}$$

We have already mentioned that N_{eff} is a quantity that is defined at "late times", but now let us be more clear what we mean by that. The standard approach is to define N_{eff} at a temperature $m_\nu \ll T \ll m_e$, but we want to allow for the possibility that some DR becomes non-relativistic and only contributes to the radiation density for a time. Therefore we will adopt a temperature dependent ΔN_{eff} by the simple approximation

$$\Delta N_{\text{eff}}(T) = \frac{\rho_{\text{DR}}(T)}{\rho_\nu(T)},$$

where we assume $\rho_\nu(T)$ evolves like the neutrino density would in a cosmology without any DR. This approach is not perfect, but it allows us to fairly easily translate the bounds on N_{eff}, to rough bounds on our dark sector models. A more careful treatment of this subject is simply beyond the scope of this thesis.

N_{eff} is a severely constrained parameter. The strongest bounds come from analysis of the CMB. The Planck data, combined with data from other experiments (Planck Collaboration et al., 2015) have the following bounds

$$N_{\text{eff}} = 3.04 \pm 0.18. \tag{6.25}$$

[5]The literature, although it seems to agree on the definition of N_{eff}, does not seem to be consistent in the definition of ΔN_{eff}. I have, as an example, seen both $\Delta N_{\text{eff}} = N_{\text{eff}} - 3$ and $\Delta N_{\text{eff}} = N_{\text{eff}} - 3.046$ in addition to the one used here.

If we want to translate this 1σ bound into an upper bound on $\rho_{\rm DR}$ at the time of recombination $T \lesssim$ eV, we get the following bound

$$\frac{\rho_{\rm DR}}{\rho_\nu^0} \lesssim 0.17.$$

We can now translate all this into an upper bound on ξ (or $T_{\tilde{\gamma}}/T$) for dark radiation in the late universe. The general bound is given by

$$\xi \lesssim \left(\frac{7}{4}\frac{0.17}{g_*^{\rm DR}}\right)^{1/4}\left(\frac{4}{11}\right)^{1/3} \approx 0.53\,(g_*^{\rm DR})^{-1/4}, \tag{6.26}$$

where

$$g_*^{\rm DR} \equiv \sum_{\rm bosons}^{\rm DR} g_i\left(\frac{T_i}{T_{\tilde{\gamma}}}\right)^4 + \frac{7}{8}\sum_{\rm fermions}^{\rm DR} g_i\left(\frac{T_i}{T_{\tilde{\gamma}}}\right)^4.$$

This means that if we for example have one real scalar as DR, $\xi_{\rm RS} \lesssim 0.53$, while if we have one Dirac fermion we get $\xi_{\rm DF} \lesssim 0.39$. Keep in mind, however, that these are just the 1σ bounds from CMB. The main point is that ξ is severely constrained from above.

With the next release from Planck, we expect that the limits on $N_{\rm eff}$ will become even stronger.[6] It will then be interesting to see if the confidence interval is still centered around the standard figure of $N_{\rm eff} = 3.046$ or if it will favor some small amount of DR. If $\Delta N_{\rm eff}$ gets even more constrained, then, based on the discussions in this section and those in Sec. 6.2, it may simply rule out the possibility of thermally produced DR (without violating entropy conservation).

The other main constraint on $N_{\rm eff}$ comes from BBN. These are given by (Nollett and Steigman, 2015)

$$N_{\rm eff} = 3.56 \pm 0.23. \tag{6.27}$$

Interestingly, this constraint actually favors some amount of DR, in mild conflict with the CMB results. However, it is important to note that the two sets of data constrain the radiation content of the universe at different temperatures, so they are not directly comparable.

The apparent conflict between the CMB and BBN measurements of $N_{\rm eff}$ also suggests the possibility for DR that becomes non-relativistic after BBN but before recombination. This is an possibility that can be relevant for models where kinetic decoupling of DM is associated with DR becoming non-relativistic.

For a nice review of the constraints on neutrinos and DR see Riemer-Sorensen, Parkinson, and Davis, 2013.

[6] This is partly based on private conversation with members of the Planck team.

Chapter 7

Summary of Previous Work

In this chapter we will summarize the work that has been done on late KD in the literature. We will mostly focus on the work we did in Bringmann et al., 2016 trying to classify all (the simplest) possible phenomenological particle models for DM that can lead to late KD, but we will try to discuss how other work fits into this classification as well.

In Bringmann et al., 2016 we use a completely phenomenological approach to classifying particle models. First we classify them after the number of particles involved in the model. As we argued is Sec. 6.1.1 (with some stated reservations), in order to obtain late KD, we need the DM particle, χ, to scatter elastically off a relativistic heat bath particle, $\tilde{\gamma}$. This means that the "simplest" models are those models that just contain χ and $\tilde{\gamma}$, we call these *2-particle models*. Models involving another particle in addition to χ and $\tilde{\gamma}$ are called *3-particle models*.

In addition to the classification according to the number of particle in the model, we classify the models according to the spins of χ and $\tilde{\gamma}$. This gives a large multiplicity of possible models, which we look at in turn.

On top of this classification we can classify models according to the topology of the main interaction (t-channel, s/u-channel etc.), giving us a further multiplicity of models.

We work only with renormalizable interactions and we impose a Z_2 symmetry for χ, in order to ensure stability. This means that multitude of possible models gets narrowed down significantly. We also only consider spin-1 particles that are gauge bosons, allowing, however, for the gauge symmetry to be broken by giving the gauge bosons a mass.

7.1 2-Particle Models

The Z_2 symmetry imposed on χ means that it is impossible to have fermionic $\tilde{\gamma}$ or gauge boson χ. So χ is a fermion or scalar, interacting with a bosonic $\tilde{\gamma}$. As we discussed in Sec. 3.3.3, considering the self interaction of χ sets severe limits on a $\chi\chi\tilde{\gamma}$ coupling for bosonic $\tilde{\gamma}$. This means that either, the coupling α has to be extremely small, or we need the mass of χ to be really large, and the mass of $\tilde{\gamma}$ not too small (see Fig. 3.8). As we see from Fig. 3.8, it also means that it is (almost) impossible to have annihilation to $\tilde{\gamma}$ be the process that gives the correct relic density of χ.

The self-interaction constraint leads to models with large m_χ and (or) small α. This combination means that it is hard to achieve late KD, particularly, we need a large value for $r = c_n/(g_\chi \alpha^2)$ i.e. a large enhancement from the propagator. Because of the cancellation between the contributions of the s- and u-channels discussed in Sec. 6.1.4, this enhancement really only

	χ	**Scalar**			**Fermion**		
$\tilde{\gamma}$	TOP	LKD	TP	σ_T	LKD	TP	σ_T
Scalar	$4p$	$m_\chi \lesssim$ MeV	Yes	Constant	(dim > 4)		
	t	$m_{\tilde{\gamma}} \sim 1\,\text{keV}$ $m_\chi \gtrsim 100\alpha_\chi^{3/5}$ TeV	$\langle\sigma_T\rangle_{30}$ (for $m_\chi \gtrsim 1$ MeV)	Yukawa	$m_{\tilde{\gamma}} \sim 1\,\text{keV}$ $m_\chi \gtrsim 100\alpha_\chi^{3/5}$ TeV	$\langle\sigma_T\rangle_{30}$ (for $m_\chi \gtrsim 1$ MeV)	Yukawa
	s/u	$\langle\sigma_T\rangle_{30}$			$\langle\sigma_T\rangle_{30}$		
Fermion		Z_2			(dim > 4)		
Vector	s/u	$\langle\sigma_T\rangle_{30}$			$\langle\sigma_T\rangle_{30}$		
	$SU(N)$	$m_{\tilde{\gamma}} \sim 1\,\text{keV}$ $m_\chi \gtrsim 10\alpha_\chi^{3/5}$ TeV	$\langle\sigma_T\rangle_{30}$ (for $m_\chi \gtrsim 1$ MeV)	Yukawa	$m_{\tilde{\gamma}} \sim 1\,\text{keV}$ $m_\chi \gtrsim 10\alpha_\chi^{3/5}$ TeV	$\langle\sigma_T\rangle_{30}$ (for $m_\chi \gtrsim 1$ MeV)	Yukawa

TABLE 7.1: Overview of results for late KD in the 2-particle models from Bringmann et al., 2016. The different rows indicates the topology (TOP) of the (dominant) $\chi - \tilde{\gamma}$ scattering diagram. LKD indicates if the given model can achieve late kinetic decoupling e.g. $T_{\text{kd}} \sim 100$ eV, TP indicates if the annihilation process $\chi\chi \to \tilde{\gamma}\tilde{\gamma}$ can be responsible for the thermal production of DM and σ_T indicates what kind of self interactions are present in this model (if the model is viable). If a cell is white that means that the the model works (i.e. it can obtain the corresponding property, like thermal production (TP).), and for what model parameters. A gray cell means that the model does not work (i.e. it is impossible, ruled out or violates our assumptions). The reason that the model does not work is indicated in the gray cells. For more details see Bringmann et al., 2016.

happens in the t-channel. One of the models with elastic scattering dominated by the t-channel contribution is the $SU(N)$ model discussed in detail in Ch. 9.

The one exception to the strong self-interaction constraint is the model with scalar χ and scalar $\tilde{\gamma}$ interacting through a direct 4-point interaction. This model will be discussed in detail in Ch. 8.

The results obtained in Bringmann et al., 2016 for the 2-particle models is summarized in Tab. 7.1.

7.2 3-Particle Models

For the 3-particle models we add another particle, in addition to χ and $\tilde{\gamma}$, to mediate a force between them. In accordance with the discussion in Sec. 6.1.4, we add a heavy particle χ' slightly heavier than χ in the s/u-channels and we add a light particle $\tilde{\gamma}'$ in the t-channel, in order to get a large enhancement of the amplitudes.

The s/u-channel models are viable for a range of different model parameters if $\Delta m \equiv m_{\chi'} - m_{\chi} \ll m_{\chi}$. Models that are suppressed by the energy of $\tilde{\gamma}$ (i.e. $n > 0$) must have smaller m_{χ} in order to lead to late KD. These models are also generally compatible with thermal production of χ through the annihilation process $\chi\chi \to \tilde{\gamma}\tilde{\gamma}$, although the self interaction at dwarf scales from these models is negligible.

The t-channel models are very interesting. If $\tilde{\gamma}'$ is heavier than $\tilde{\gamma}$ ($m_{\tilde{\gamma}'} \sim$ MeV), then the self interaction resulting from the $\chi\chi\tilde{\gamma}'$ vertex is weaker than the corresponding one for $\chi\chi\tilde{\gamma}$ that we met in the 2-particle models. This allows for arranging both thermal production and an interesting self-interaction at dwarf galaxy scales simultaneously (see Fig. 7.1), as well as ensuring late KD. This triad of properties makes this class of models very attractive.

7.3 Other Works

In Aarssen, Bringmann, and Pfrommer, 2012; Bringmann, Hasenkamp, and Kersten, 2014; Dasgupta and Kopp, 2014; Ko and Tang, 2014; Binder et al., 2016 the autors all look at models where fermionic DM obtains late KD and self-interactions from coupling to MeV scale mediators and with sterile or SM neutrinos as relativistic heat bath particles. These would correspond to our 3-particle models in the t-channel.

Tang, 2016 looks at a similar model to some of our 2-particle models, with fermionic DM and with scalar heat bath particles, but does not seem to take into account the self interaction of DM that would arise from such models.

Chu and Dasgupta, 2014 consider an interesting 3-particle model in the s/u-channels with Majorana fermion DM and with a pseudoscalar heat bath particle.

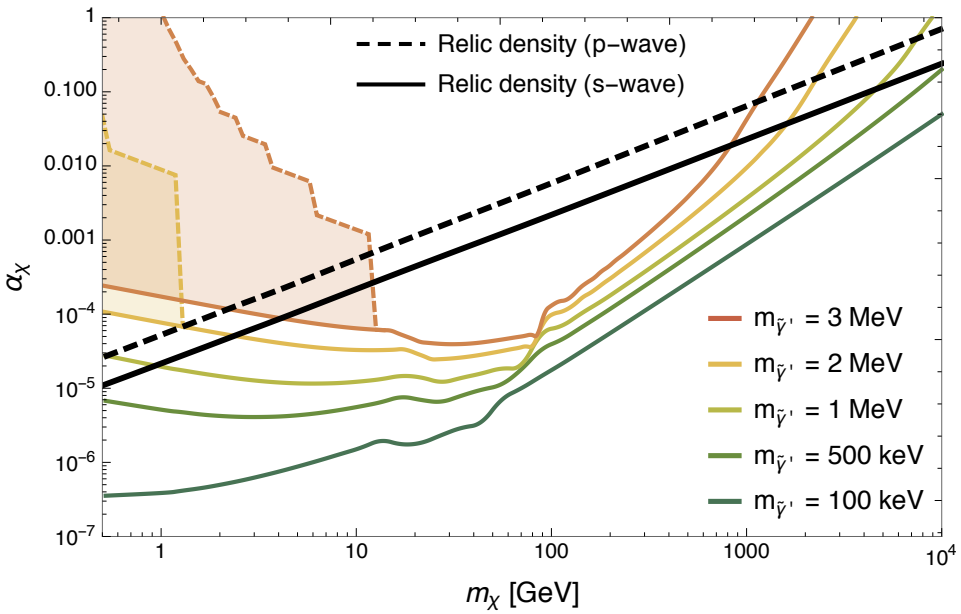

FIGURE 7.1: Plot of parameters needed to obtain the correct relic density and an interesting self interaction at dwarf galaxy scales for 3-particle models in the t-channel. On the y-axis we have the coupling α_χ, corresponding to the $\chi\chi\tilde{\gamma}'$ vertex, while the DM mass m_χ is plotted on the x-axis. The black lines correspond to parameters that will give the correct relic density from the process $\chi\chi \to \tilde{\gamma}'\tilde{\gamma}'$, for s-wave and p-wave annihilation respectively. Clearly these are approximate values, and will depend slightly on the models. The colored lines correspond to parameters needed to give a self interaction of $\langle\sigma_T\rangle_{30} = 1\,\mathrm{g/cm^2}$ for different values of the mediator mass, $m_{\tilde{\gamma}'}$. Anything significantly above the colored lines are ruled out. Note that for high masses $m_\chi \gtrsim 1$ TeV, and for low masses $m_\chi \lesssim 10$ GeV, we can get both thermal production and an interesting self interaction in the same model. For more details see Bringmann et al., 2016.

Chapter 8

Scalar 4-Point Coupling

The simplest possible model for $\chi\tilde{\gamma} \to \chi\tilde{\gamma}$ scattering is simply a 4-point scalar interaction. Given by the Lagranigian

$$\mathcal{L}_{\text{int}} = \frac{\lambda}{4}\phi_\chi^2\phi_{\tilde{\gamma}}^2, \tag{8.1}$$

where ϕ_χ and $\phi_{\tilde{\gamma}}$ are real scalars representing DM and DR respectively.

In addition to being the simplest possible model, the results we get will be essentially the same as for an effective higher dimensional operator, with $m_\chi^2/\Lambda^2 \sim \lambda$, where Λ is the cutoff-mass for the effective theory. This analogy is valid as long as the scattering does not have a dependence on the DR energy ω. This means that the analysis of the simple model, is relevant for a larger class of models.

8.1 Kinetic Decoupling

To calculate the kinetic decoupling temperature in such a model is fairly straightforward, since there is no energy dependence ($n = 0$). We simply have $\langle|\mathcal{M}|^2\rangle_t = \lambda^2$. This means that we can use the analytic solution in Eq. 5.21, giving us

$$\lambda^2 = 6.4 \cdot 10^{-4}\xi^{-4}\left(\frac{m_\chi}{\text{GeV}}\right)^3\left(\frac{T_{\text{kd}}}{100\text{eV}}\right)^{-2}. \tag{8.2}$$

As far as KD is concerned, as long as χ is non-relativistic at KD, this is the whole story.

For the sake of concreteness, let us, in the rest of this chapter, aim for $T_{\text{kd}} = 100$ eV.

8.2 Reconciling Late Kinetic Decoupling with Thermal Production

In order to obtain the correct relic density from thermal production, we want the thermal averaged cross section to be (Steigman, Dasgupta, and Beacom, 2012)

$$\langle\sigma v\rangle \simeq 4 \cdot 10^{-9}\,\text{GeV}^{-2}. \tag{8.3}$$

In the non-relativistic limit, we have

$$\langle\sigma_{\chi\chi\to\tilde{\gamma}\tilde{\gamma}}v\rangle = \frac{\lambda^2}{32\pi m_\chi^2}, \tag{8.4}$$

giving us

$$\lambda^2 \simeq 4 \cdot 10^{-7} \xi \left(\frac{m_\chi}{\text{GeV}} \right)^2 . \tag{8.5}$$

Combining this with Eq. 8.2 we get the combination

$$\lambda \simeq 4 \cdot 10^{-7} \, \xi^{11/2}, \tag{8.6}$$

$$m_\chi \simeq 0.6 \, \text{MeV} \, \xi^5. \tag{8.7}$$

This is a significant result. We see that we need a fairly small m_χ in order to have a small enough annihilation rate. The problem with this is that we go outside the range of validity for the estimate in Steigman, Dasgupta, and Beacom, 2012 for the annihilation cross-section. Also, for lighter DM, the assumption that they are extremely non-relativistic at CD is no longer necessarily valid. This means that we will have to look into the approximations that go into the expression in Eq. 8.3 in more detail.

8.3 Chemical Decoupling for Semi-Relativistic Dark Matter

8.3.1 Approximations

Naively applying Eq. 8.3 to find λ is equivalent to doing many approximations that may or may not be valid for masses ranging from keV to MeV. In particular we will look into 6 such approximations

1. We assume Maxwell-Boltzmann statistics for χ.
2. We neglect Pauli-blocking and stimulated emission factors in the BE.
3. We use the non-relativistic expression for (σv).
4. We assume $x_f \propto \xi$.
5. We neglect the change in ξ during CD.
6. We neglect the changes in $g^{\text{v}}_{*\text{S}}$.

We want to develop an estimate that we can actually trust, this means that if any of the approximations mentioned introduce errors of the order of a few percent, then we need to take it into account. If the error is less than a few percent then we will let the approximation stand.

8.3.2 Maxwell-Boltzmann Statistics and Quantum Factors

First we want to analyze how large the error we get from using Maxwell-Boltzmann statistics and neglecting the quantum factors is.

As the thermal averaging integral would be over the χ distribution and the quantum factors over the $\tilde{\gamma}$ distribution (evaluated at something like the χ energy) we can use the following integral as a good measure for how

the dependence on the distribution enters[1]

$$I_{\text{BE + QF}}(T) \equiv \frac{g_\chi}{n_{\text{eq}}^{\text{BE}}(T)} \int \frac{d^3p}{(2\pi)^3} \frac{1}{e^{E(p)/T}-1} \left(1 + \frac{1}{e^{E(p)/T}-1}\right), \tag{8.8}$$

$$I_{\text{FD + QF}}(T) \equiv \frac{g_\chi}{n_{\text{eq}}^{\text{FD}}(T)} \int \frac{d^3p}{(2\pi)^3} \frac{1}{e^{E(p)/T}+1} \left(1 - \frac{1}{e^{E(p)/T}+1}\right). \tag{8.9}$$

Defining also the different number densities

$$n_{\text{eq}}^{\text{BE}}(T) \equiv g_\chi \int \frac{d^3p}{(2\pi)^3} \frac{1}{e^{E(p)/T}-1}, \tag{8.10}$$

$$n_{\text{eq}}^{\text{MB}}(T) \equiv g_\chi \int \frac{d^3p}{(2\pi)^3} e^{-E(p)/T}, \tag{8.11}$$

$$n_{\text{eq}}^{\text{NR}}(T) \equiv g_\chi \left(\frac{m_\chi T}{2\pi}\right)^{3/2} e^{-m_\chi/T}, \tag{8.12}$$

where $E(p) = \sqrt{p^2 + m_\chi^2}$, we now want to compare the different distributions in the not-so-non-relativistic range.

In Fig. 8.1 we have plotted the relative error in neglecting the quantum factor for the Bose-Einstein distribution. We also include the Fermi-Dirac distribution for comparison. We also see that if we use the Bose-Einstein distribution, but neglect the quantum factor, we incur a relative error of $\lesssim 1.5$ % for $x/\xi \gtrsim 3$. This is what we will chose in the following.

Comparing Maxwell-Boltzmann statistics to Fermi-Dirac or Bose-Einstein statistics give very similar results, with small deviations for $x/\xi \gtrsim 4$. See Fig. 8.2.

8.3.3 Thermal Averaged Cross Section

In section 4.2.2 we used the following approximation for the cross section

$$\langle \sigma v \rangle_{\text{NR}} = (\sigma v)_{\text{NR}} = \frac{\lambda^2}{32\pi m_\chi^2}, \tag{8.13}$$

Since the cross section is independent of energy, the thermal averaging does nothing.

This approximation is valid in the extreme non-relativistic limit, but in the range we are now considering, we need to do better. The full expression is given by

$$\langle \sigma v \rangle = \frac{g_\chi^2}{(n_{\text{eq}}^{\text{BE}})^2} \int \frac{d^3p_1}{(2\pi)^3} \int \frac{d^3p_2}{(2\pi)^3} \frac{1}{e^{E_1/T}-1} \frac{1}{e^{E_2/T}-1} \left(\frac{\lambda^2}{32\pi E_1 E_2}\right), \tag{8.14}$$

[1]Clearly we should also add the p-dependence of whatever we are taking the thermal average over, in our case (σv). But since in our case this is fairly constant, we will not take that into account here. This way we also keep our analysis general, and not just for this specific model.

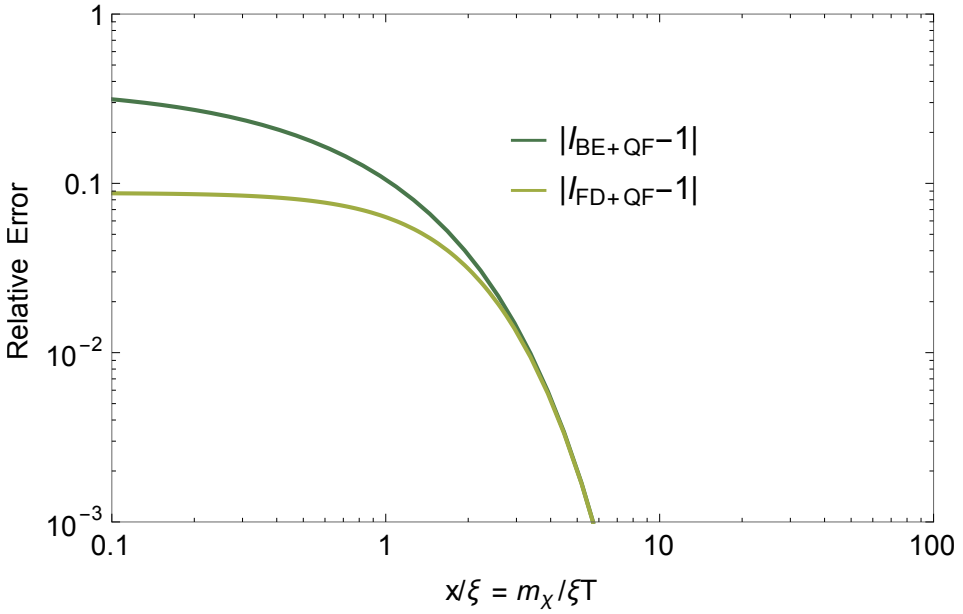

FIGURE 8.1: Plot of the relative error when neglecting the quantum factors when doing the thermal average. We see that we get a relative error of less than 1.5 % for $x/\xi \gtrsim 3$.

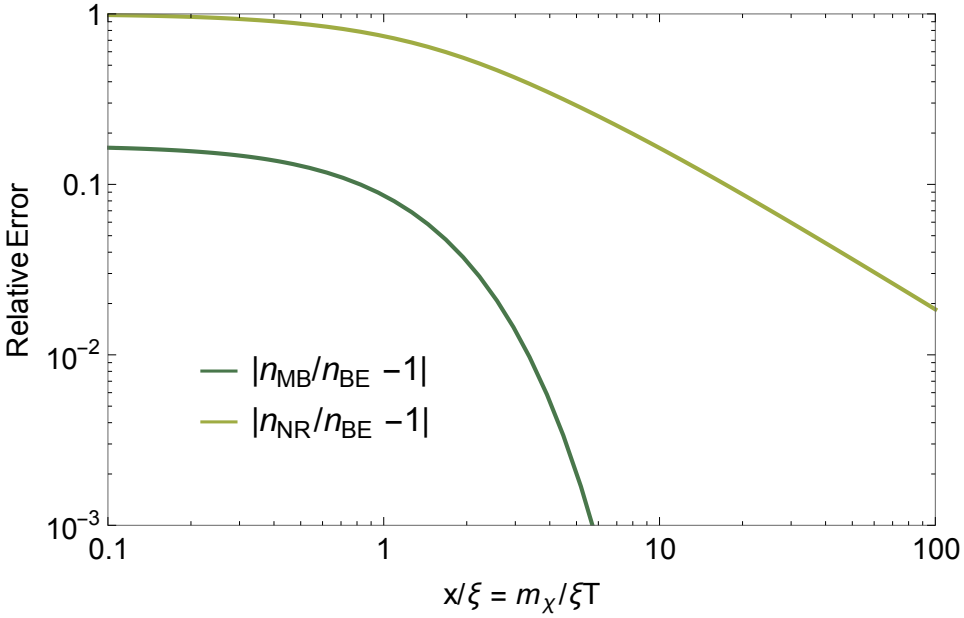

FIGURE 8.2: Plot of the relative error when using Maxwell-Boltzmann statistics to calculate the number density, or using the non-relativistic expression for the number density. We see that for $x/\xi \gtrsim 4$ we get very small relative errors ($\lesssim 2\%$) even when simply using Maxwell-Boltzmann statistics. The non-relativistic expression for the number density, $n = g_\chi \left(\frac{m_\chi T}{2\pi}\right)^{3/2} e^{-m_\chi/T}$, however, is not a good approximation. Even at $x/\xi \sim 10$ there is still an error of about 15 %.

which can be rewritten

$$\langle \sigma v \rangle = \frac{\lambda^2}{128\pi^5} \frac{g_\chi^2}{(n_{\text{eq}}^{\text{BE}})^2} \int dE_1 dE_2 \sqrt{E_1^2 - m_\chi^2} \sqrt{E_2^2 - m_\chi^2} \frac{1}{e^{E_1/T} - 1} \frac{1}{e^{E_2/T} - 1}. \tag{8.15}$$

This gives us a significantly different result, as is shown in Fig. 8.3. We see that the non-relativistic approximation severely overestimates the actual scattering cross section. We also see that even at $x/\xi \sim 10$ the error is still around 30 %. This means that if we want precision in our estimate we need to use the full expression.

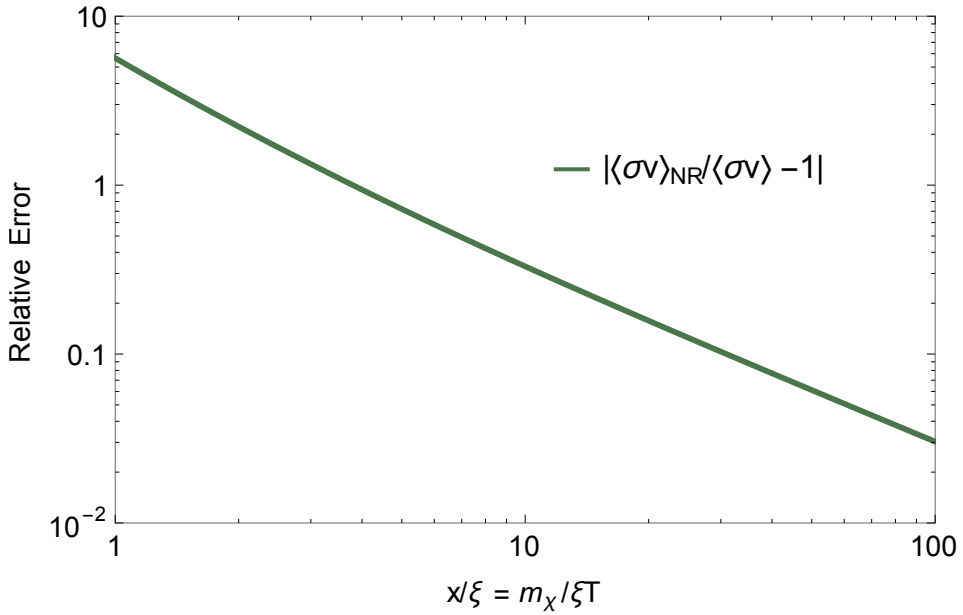

FIGURE 8.3: The non-relativistic expression for the annihilation cross section, $\langle\sigma v\rangle_{\rm NR} = \frac{\lambda^2}{32\pi m_\chi^2}$ overestimates the actual cross section at high temperatures. At $x/\xi \sim 10$ the error is still about 30 %, meaning that we need to use the full energy dependent expression for the cross section, and then take the thermal average, if we want a result with any accuracy.

8.3.4 Evolution of Temperatures

Our back of the envelope calculation (Eq. 8.6), suggested that the DM masses ended up in the MeV scale. As this is at the same scale as electrons and positrons annihilating, this needs to be taken into account, in addition to the effect of DM annihilation.

Visible Sector

In the visible sector, we need to keep track of the effective number of degrees of freedom for entropy $g_{*\rm S}^{\rm v}$. For simplicity we will assume that the neutrinos decouple before electron-positron annihilation starts heating the photon bath.

The full expression for $g_{*\rm S}^{\rm v}$ is then given by

$$g_{*\rm S}^{\rm v} = \frac{s_v}{\frac{2\pi^2}{45}T^3} = 2 + 2\frac{s_e}{\frac{2\pi^2}{45}T^3} + 3\cdot 2\left(\frac{T_\nu}{T}\right)^3, \tag{8.16}$$

where

$$T_\nu = \left(\frac{2 + 2 s_e/(2\pi^2 T^3/45)}{2 + 2 \cdot 2 \cdot 7/8} \right)^{1/3}, \tag{8.17}$$

and where

$$s_e = \frac{\rho_e - \mu_e n_e + p_e}{T}. \tag{8.18}$$

The evolution of $g^{\mathrm{v}}_{*\mathrm{S}}$ is shown in Fig. 8.4.

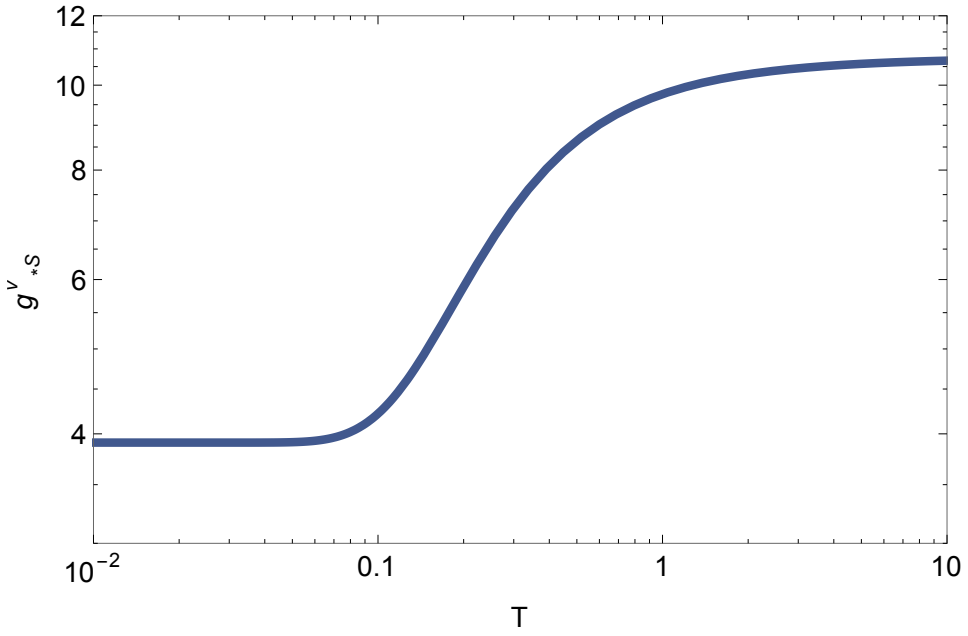

FIGURE 8.4: Change in the effective number of degrees of freedom for entropy in the visible sector, $g^{\mathrm{v}}_{*\mathrm{S}}$, during the heating of the photon bath from electron positron annihilations. Note that $g^{\mathrm{v}}_{*\mathrm{S}}$ decreases for two reasons. First, the electrons and positrons (almost) all annihilate and thus do not contribute to the entropy. The second effect comes because the relative temperature of the neutrinos compared to the photons decreases, reducing the entropy contribution from neutrinos (compared to that of the photons).

Dark Sector

The dark sector consists of two real scalars, ϕ_χ and $\phi_{\tilde{\gamma}}$. We assume that the dark sector has already decoupled from the visible sector, and that its temperature is given by $T_{\tilde{\gamma}} = \xi_I T$ at around $T \simeq 10$ MeV. In this case the evolution of the temperature is given by Eq. 6.19, which becomes

$$T_{\tilde{\gamma}} = \xi_I \left(\frac{2}{1 + s_\chi/(2\pi^2 T^3/45)} \frac{2 + 2 s_e/(2\pi^2 T^3/45)}{2 + 2 \cdot 2 \cdot 7/8} \right)^{1/3} T. \tag{8.19}$$

We see that at late times, if we can assume that s_χ and s_e are negligible, this reduces to

$$T^{\text{late times}}_{\tilde{\gamma}} = \xi_I \left(\frac{8}{11} \right)^{1/3} T \approx 0.90\, \xi_I\, T. \tag{8.20}$$

If we use the equilibrium distribution for the electron and DM species we can calculate the evolution the dark temperature parameter ξ, for different m_χ/ξ_I. The result is shown in Fig. 8.5.

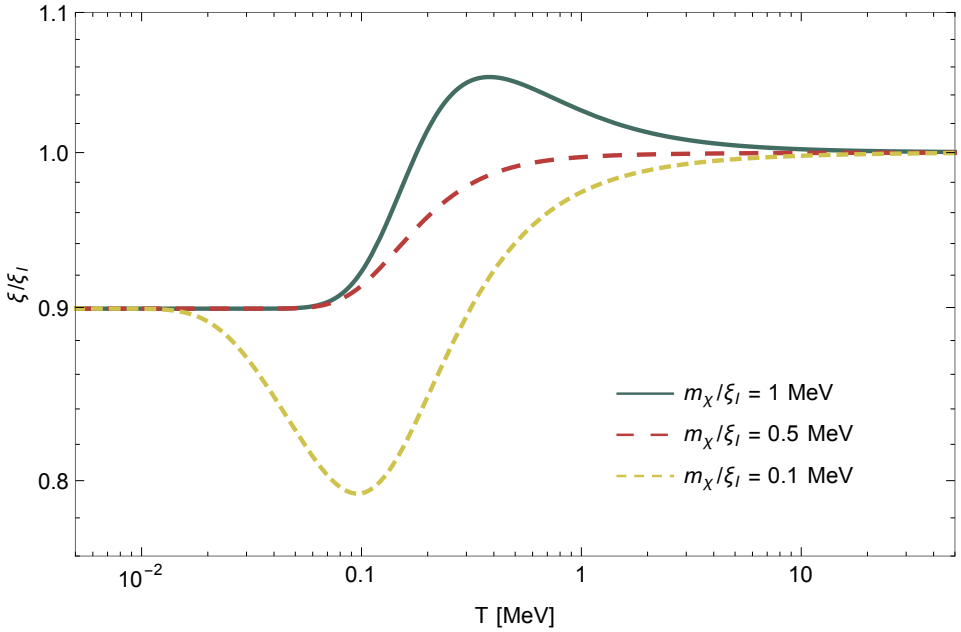

FIGURE 8.5: Evolution of the temperature of the dark sector relative to the visible sector for different m_χ/ξ_I (assuming equilibrium distributions for all species). Note that $T_{\tilde{\gamma}} = \xi T$ and $\xi_I \equiv \xi(T \simeq 10\text{MeV})$ is the initial temperature fraction. There are two events that change the relative temperature of the dark and visible sector (in this temperature range). One is the heating of the photon bath from electron-positron annihilations. The other is the heating of the dark radiation $\tilde{\gamma}$ by the annihilating DM particles. These events occur around the time that the corresponding species become non-relativistic. This means that the order of the events can change depending on m_χ/ξ_I. If $m_\chi/\xi_I > m_e \sim 0.5$ (solid line) MeV the DM annihilates first leading to an increase in ξ first at around $T \simeq m_\chi/\xi$, followed by a decrease in ξ at about $T \sim m_e$. If $m_\chi/\xi_I < m_e$ (small dashes), then ξ first decreases before it increases again at $T \simeq m_\chi/\xi$. If $m_\chi/\xi_I \approx m_e$ then the two effects partly cancel each other out, but since the effect from the electrons and positrons are larger, ξ decreases slightly. Note that in all cases end up at the same value $\xi \approx 0.9$.

All this assumes, however, that χ follows the equilibrium distribution, but we want to allow for the possibility that CD happens when the amount of χ left over is not completely negligible. We also want to follow the detailed evolution of ξ during the CD process. To do this simply we need to relate the entropy of χ, s_χ, to the corresponding number density n_χ. If we have such a relation between s_χ and n_χ then, as we solve the BE for n_χ, we can always keep track of the corresponding entropy s_χ.[2]

[2]There clearly is no such relation in general, since s is dependent on the energy of the particles, while n has no such information. We are only talking about an approximate relation.

What we will do is to use the relation between n and s in equilibrium as an approximation for the general relationship. The equilibrium entropy is given by

$$s = \frac{\rho + P}{T}, \tag{8.21}$$

in the non relativistic limit $s/n \sim m/T$ blows up (as long as we can neglect the chemical potential), but not as fast as the exponential suppression of both s and n. In the relativistic limit we get

$$s = \frac{\frac{4\pi^2/30}{3\zeta(3)/\pi^2}\left(1+\frac{1}{3}\right)Tn}{T} \approx 3.6\, n. \tag{8.22}$$

8.3.5 Solution of Boltzmann Equation

Now that we have listed and analyzed the different approximations, and which ones are appropriate, we can go on to solve the full BE (Eq. 4.7) numerically. If we fix λ by the requirement that $T_{\rm kd} = 100$ eV, then we can find the relation between m_χ and ξ that will result in the correct relic density. This relation is given in Fig. 8.6.

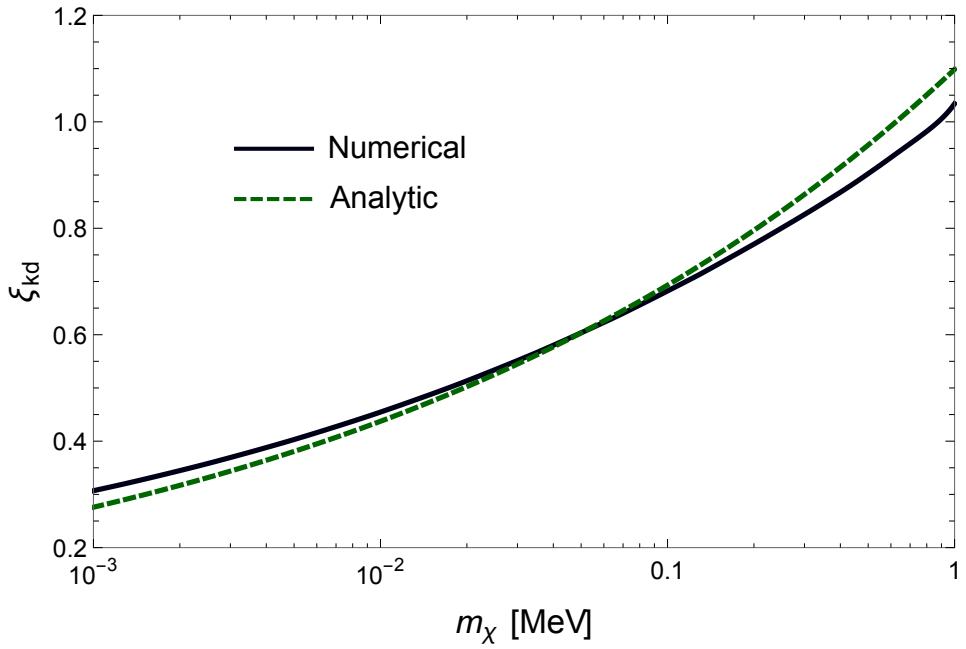

FIGURE 8.6: Parameters that ensures the relic density $\Omega_{\rm DM}h^2 = 0.12$ based on numerically solving the BE for CD. The coupling, $\lambda^2 = 6.4 \cdot 10^{-4}\xi^{-4}\left(\frac{m_\chi}{\rm GeV}\right)^3$, has been fixed in terms of ξ and m_χ by requiring that we get $T_{\rm kd} = 100$ eV. The analytic expression $m_\chi \simeq 0.6$ MeV ξ^5, is based on extrapolating the canonical WIMP expression, including the leading $x_{\rm cd} \propto \xi$ dependence we derived in Sec. 4.2.2, down to MeV-scales. The fact that the analytic approximation actually fits so well with the numerical results appears to be somewhat of a coincidence. It clearly gets the scaling in ξ wrong, and it actually fits worse for higher masses and $\xi \sim 1$, which is opposite of what we would expect.

8.4 Summary

In summary it seems that the simple model with a constant interaction actually can give both late KD and the correct relic density if $m_\chi \sim$ keV - MeV. This is a fairly significant result, since this solution represents a broad class of models for DM and DR.

CD in this mass range is somewhat different from the standard RD calculation for WIMP's. We looked at 6 approximations that are commonly used for CD of non-relativistic DM. 1. was using Maxwell-Boltzmann statistics, 2. was neglecting the quantum factors, 3. was using the non-relativistic expression for (σv), 4. was assuming $x_{\text{cd}} \propto \xi$, 5. was neglecting the change in ξ and 6. was neglecting the change in g_{*S}^{v}.

After looking carefully at the various approximations and assumptions made, we can conclude that 3 and 4 are the two most problematic ones, these are just not applicable for anything more than order of magnitude estimates at this scale. 5 and 6 are usually good approximations, but at least 6 has to be taken into account if CD happens exactly when a species (here electrons and positrons) heat the photon bath. For 1 and 2 the errors were less than order 1 % for $x/\xi \gtrsim 3$, which means they are usually really good approximations, at least for all the parameters considered in this section.

When the dust settles, we see that this model can give rise to both late KD and correct relic density. We can also add a self interaction term, as is discussed briefly in Bringmann et al., 2016, but this would only lead to a constant self interaction, which is at best problematic if you want to address small scale problems (see Sec. 3.3.2).

Chapter 9

$SU(N)$ Model

Models where DM is charged under some $SU(N)$ gauge group have been considered several times in the literature (Buen-Abad, Marques-Tavares, and Schmaltz, 2015; Lesgourgues, Marques-Tavares, and Schmaltz, 2016; Cyr-Racine et al., 2015). We, however, want to look at the possibility of late KD in such models.

We will mostly consider fermionic DM, but the results for a complex scalar are very similar, as we show in Bringmann et al., 2016. We will build on the results from Bringmann et al., 2016, but will go into more detail on some important points.

9.1 Elastic Scattering Amplitude

The DM - DR elastic scattering in this model can happen in both the s, u and t-channels, as is shown in Fig. 9.1. The total amplitude for elastic scattering

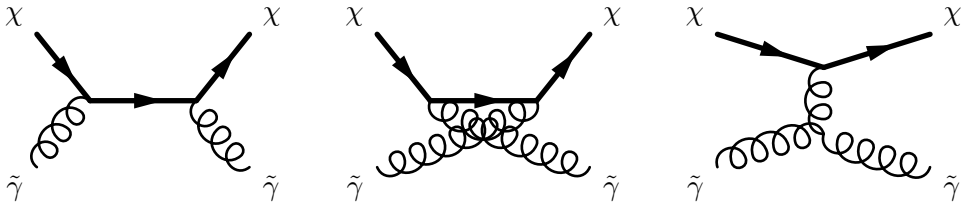

FIGURE 9.1: Diagrams contributing to the process $\chi\gamma \to \chi\gamma$ (to leading order). We see that scattering in both s (left), u (middle) and t-channels (right) is possible.

is given by

$$
\begin{aligned}
&i\mathcal{M}_{\chi\gamma\to\chi\gamma} = i(\mathcal{M}_s + \mathcal{M}_u + \mathcal{M}_t) \\
&= \frac{\epsilon_\mu(k_1)\epsilon^*_\nu(k_2)\bar{u}(p_2)\left(-ig\gamma^\nu T^b_{jl}\right)(\not{k}_2 + \not{p}_2 + m_\chi)\left(-ig\gamma^\mu T^a_{li}\right)u(p_1)}{s - m_\chi^2} \\
&\quad + \frac{\epsilon_\mu(k_1)\epsilon^*_\nu(k_2)\bar{u}(p_2)\left(-ig\gamma^\mu T^a_{jl}\right)(\not{p}_2 - \not{k}_1 + m_\chi)\left(-ig\gamma^\nu T^b_{li}\right)u(p_1)}{u - m_\chi^2} \\
&\quad + g\epsilon_\mu(k_1)\epsilon^*_\nu(k_2)f^{abc}\Big[g^{\nu\sigma}(2k_2 - k_1)^\mu + g^{\mu\sigma}(2k_1 - k_2)^\nu - g^{\mu\nu}(k_1 + k_2)^\sigma\Big] \\
&\quad \times \left(\frac{(p_1 - p_2)_\rho (p_1 - p_2)_\sigma}{t} - g_{\rho\sigma}\right)\bar{u}(p_2)\Big(-ig\gamma^\rho T^c_{ji}\Big)u(p_1)/\left[t - m^2_{\tilde{\gamma}}\right],
\end{aligned}
\tag{9.1}
$$

where p_1 and k_1 are the momenta of the incoming χ and $\tilde{\gamma}$ respectively, while p_2 and k_2 are the corresponding outgoing momenta. We have also allowed for the possibility that the gauge symmetry is broken by giving $\tilde{\gamma}$ a non-zero mass.

Ultra-relativistic $\tilde{\gamma}$

If we assume that $m_\chi \gg \omega \gg m_{\tilde{\gamma}}$, where ω is the energy of the incoming $\tilde{\gamma}$ particle, we get the following leading term for the t-averaged amplitude squared (Bringmann et al., 2016)

$$\langle|\mathcal{M}_{\chi\gamma\to\chi\gamma}|^2\rangle_t \approx \frac{18g^4 C_F C_A^2 m_\chi^2 \ln\left(4\omega^2/m_{\tilde{\gamma}}^2\right)}{\omega^2}, \tag{9.2}$$

where $C_F \equiv (N^2-1)/2N$ and $C_A \equiv N$. We see that this expression diverges, albeit only logarithmically, as $m_{\tilde{\gamma}} \to 0$. This divergence comes from the pole in the t-channel propagator, which makes the integral over t diverge at $t = 0$, unless $\tilde{\gamma}$ has a finite mass.

Even if there is no explicit mass therm for the $\tilde{\gamma}$ gauge bosons, the amplitude will not actually diverge in this limit. This is because the gauge bosons will acquire a thermal mass of the order $m_{\tilde{\gamma}}^{\text{Debye}} \sim gT_{\tilde{\gamma}}$. Since $\omega \sim T$ the logarithm should just give approximately a constant.

Relativistic or Non-Relativistic $\tilde{\gamma}$

If we do not assume that $\tilde{\gamma}$ is ultra-relativistic, but assume just that $m_\chi \gg m_{\tilde{\gamma}}, \omega$, we get the expression

$$\langle|\mathcal{M}_{\chi\gamma\to\chi\gamma}|^2\rangle_t = \frac{2g^4 C_F C_A^2 m_\chi^2}{m_{\tilde{\gamma}}^2}\left[F(w) + \mathcal{O}\left(\frac{m_{\tilde{\gamma}}}{m_\chi}\right)\right], \tag{9.3}$$

where $w \equiv \omega/m_{\tilde{\gamma}}$ and we have defined

$$\begin{aligned} F(w) = &\Bigg[-68w^6 + 36w^4 + 56w^2 - 24 \\ &+ \left(36w^4 + 13w^2 - 30\right) w^2 \log\left(4w^2 - 3\right)\Bigg] \\ &\times \frac{1}{w^2\left(w^2-1\right)^2\left(4w^2-3\right)}. \end{aligned} \tag{9.4}$$

Despite appearances, this expression is, in fact, finite as $w \to 1$, which means that it does not have any singularities (since we clearly need $w \geq 1$).

9.2 Kinetic Decoupling

As we see from Fig. 5.4 and the associated discussion, since the matrix element of this model scales like $n = -2$, KD "never" happens for this model. By this we mean that KD never happens, in the radiation dominated phase, while the assumptions $m_\chi \gg \omega \gg m_{\tilde{\gamma}}$ are valid. What is happening here is that, as long as we are in the radiation dominated phase, $n = -2$ implies

that both $\gamma(T_{\tilde{\gamma}})$ and $H(T)$ scale like T^2, meaning that we are either *always* in equilibrium or *never* in equilibrium, depending on the model parameters[1].

If the gauge symmetry in not broken ($m_{\tilde{\gamma}} = m_{\tilde{\gamma}}^{\text{Debye}}$), then, assuming the model parameters are such that we get equilibrium, KD will not happen until the universe becomes matter dominated. This possibility, however, is ruled out by observations, since the cutoff in the matter power spectrum would be at a very large mass (if we assume $T_{\text{kd}} \sim$ eV we get $M_{\text{cut}} \sim 10^{16}\ M_\odot$ which is about ten thousand times heavier than the Milky way galaxy!), meaning that there would be almost no galaxies today.

Another possibility is that the interaction is not strong enough to keep DM in thermal equilibrium, but somewhat weaker. This case is studied in Buen-Abad, Marques-Tavares, and Schmaltz, 2015, and results in a suppression of all scales that enter the horizon during radiation domination, but not the exponential cutoff we would get from full equilibrium. These effects, though interesting, are not the within the scope of this thesis.

Introducing a constant mass for $\tilde{\gamma}$ that becomes relevant at keV-scales, however, gives us something that looks more like the standard picture of KD. We must however make an assumption about what happens to $\tilde{\gamma}$ after it becomes non-relativistic. We will here look at two simple cases.

9.2.1 Massive $\tilde{\gamma}$ with Chemical Equilibrium

If we assume that $\tilde{\gamma}$ is kept in chemical equilibrium with some other species, lets call it ϕ, then the number density of $\tilde{\gamma}$ will be exponentially suppressed when it becomes non-relativistic. The exponential suppression of the number density leads very quickly to KD of χ. We will not go into detail about the interaction between $\tilde{\gamma}$ and ϕ, other than to require that it must not give rise to strong interactions between χ and ϕ. This, for example rules out the possibility of ϕ being in the fundamental representation of the $\tilde{\gamma}$ gauge group[2].

Momentum Transfer Rate, $\gamma(T_{\tilde{\gamma}})$

Using Eq. 5.22 and using the dimensionless parameters $w \equiv \omega/m_{\tilde{\gamma}}$ and $z \equiv T_{\tilde{\gamma}}/m_{\tilde{\gamma}}$ we can write the momentum transfer rate for this model

$$\gamma(T_{\tilde{\gamma}}) = \frac{1}{12\pi g_\chi} \frac{\alpha_N^2 m_{\tilde{\gamma}}^2}{m_\chi} I(z) \tag{9.5}$$

where $\alpha_N \equiv \sqrt{N^2-1}g^2/4\pi$, $g_\chi = 4N$ and

$$I(z) \equiv \int_1^\infty dw \frac{1}{e^{w/z}-1} \partial_w \Big[(w^2-1)^2 F(w)\Big]. \tag{9.6}$$

When we solve the BE for KD (Eq. 5.8) our time variable is the photon temperature, we see that apart from this, the process of KD only depends

[1] We should note that $\gamma(T_{\tilde{\gamma}})$ scales like $T_{\tilde{\gamma}}^2$, which deviates from T^2 if ξ changes, but this is usually a small and temporary effect, and $\gamma(T_{\tilde{\gamma}})$ will soon scale like T^2 again.

[2] This is not entirely correct. If ϕ is in the fundamental representation of the gauge group, and we allow $\tilde{\gamma}$ to be significantly heavier ($\sim$ MeV), we would get a model that looks a lot like one of the 3-particle models (B22) in Bringmann et al., 2016, which is certainly a viable model, but not really what we are interested in studying here.

on two dimensionful parameters from the model

$$a \equiv \frac{\alpha_N^2 m_{\tilde{\gamma}}^2}{m_\chi}, \tag{9.7}$$

$$b \equiv \frac{m_{\tilde{\gamma}}}{\xi}. \tag{9.8}$$

Writing the momentum transfer rate in terms of these new parameters we get simply

$$\gamma(T, a, b) = \frac{a}{12\pi g_\chi} I(T/b). \tag{9.9}$$

In Fig. 9.2 we compare the momentum transfer rate to the Hubble rate for some typical values of a and b.

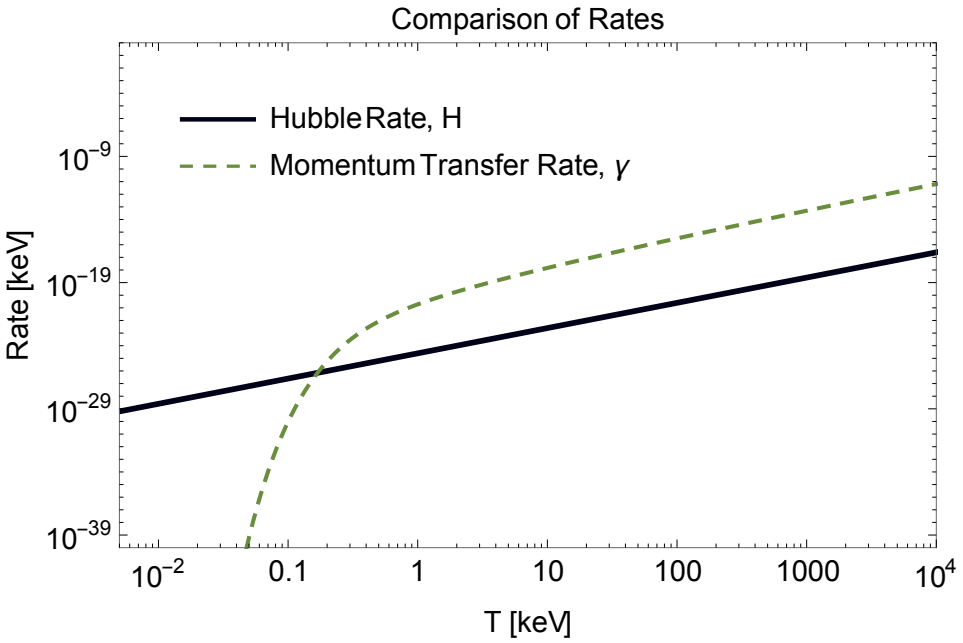

FIGURE 9.2: Comparison of momentum transfer rate, $\gamma(T_{\tilde{\gamma}})$, and expansion rate, $H(T)$. Here $a = \alpha_N^2 m_{\tilde{\gamma}}^2/m_\chi = 10^{-20}$ keV and $b = m_{\tilde{\gamma}}/\xi = 2$ keV. We see that at high temperatures the two rates scale almost the same way, but as $\tilde{\gamma}$ becomes non-relativistic, the momentum transfer rate quickly drops due, mainly, to the exponential suppression of the $\tilde{\gamma}$ number density. This means that we get $T_{\rm kd} \sim m_{\tilde{\gamma}}$ with only a very weak dependence on the rest of the parameters.

It is clear that any change in the model parameters, $m_\chi, m_{\tilde{\gamma}}, g, N$ and ξ, that leave a and b invariant will not change $T_{\rm kd}$. This makes it much easier to map the whole parameter space. In Fig. 9.3 we have plotted the combinations of a and b that lead to a cutoff mass of $M_{\rm cut} = 10^{10} M_\odot \equiv M_{10}$. Translating this result back to the model parameters we can include constraints from self interaction as well, see Fig. 9.4 (Bringmann et al., 2016).

Evolution of ξ

Up until now, we have disregarded the change in ξ as $\tilde{\gamma}$ annihilate to ϕ. This can be neglected if $\tilde{\gamma}$ is highly non-relativistic at KD, by the same sort

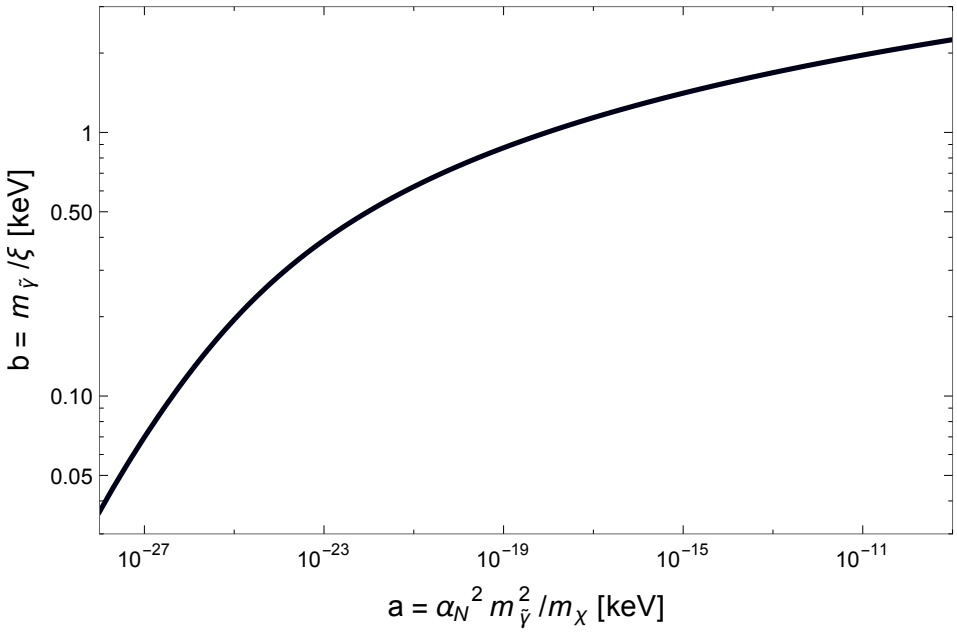

FIGURE 9.3: Relation between the two parameters $a = \alpha_N^2 m_{\tilde{\gamma}}^2/m_\chi$ and $b = m_{\tilde{\gamma}}/\xi$ needed to get the cutoff mass $M_{\text{cut}} = 10^{10} M_\odot \equiv M_{10}$ from KD. This corresponds roughly to $T_{\text{kd}} \approx 67$ eV. KD only depends on the value of these two combinations of model parameters, so this single plot is a complete map of the parameter space. The disadvantage is that not that clear how to interpret a and b physically. We therefore also include the plot from Bringmann et al., 2016, using more transparent parameters, and also including constraints from self-interaction (see Fig. 9.4).

of argument as in Sec. 4.2.2. If, however, we want to consider the value of ξ e.g. compared to the lower bound in Eq. 6.20, we would need to use the value of ξ while $\tilde{\gamma}$ are relativistic. On the other hand, when comparing to the CMB-constraints we would like to use the value of ξ after $\tilde{\gamma}$ are fully annihilated.

Defining ξ_I as the value of ξ when $\tilde{\gamma}$ is fully relativistic, and ξ_0 the value when annihilation is completed we get the following expression (using Eq. 6.19)

$$\frac{\xi_0}{\xi_I} = \left(\frac{g_\phi + 3(N^2-1)}{g_\phi}\right)^{1/3}. \tag{9.10}$$

Assuming for simplicity that $g_\phi = 1$, and that $\xi_I = 0.33$, which is the lower bound assuming the dark sector was in equilibrium with the visible sector at some early time, and the visible sector only consists of the SM particles (Eq. 6.20), we get

$$\xi_0^{N=2} \approx 0.71, \tag{9.11}$$

$$\xi_0^{N=3} \approx 1. \tag{9.12}$$

Both of these values are in some tension with CMB measurements (Planck Collaboration et al., 2015). Increasing g_ϕ will, while it decreases ξ_0, only increase ΔN, meaning that the possibility of this model combined with the

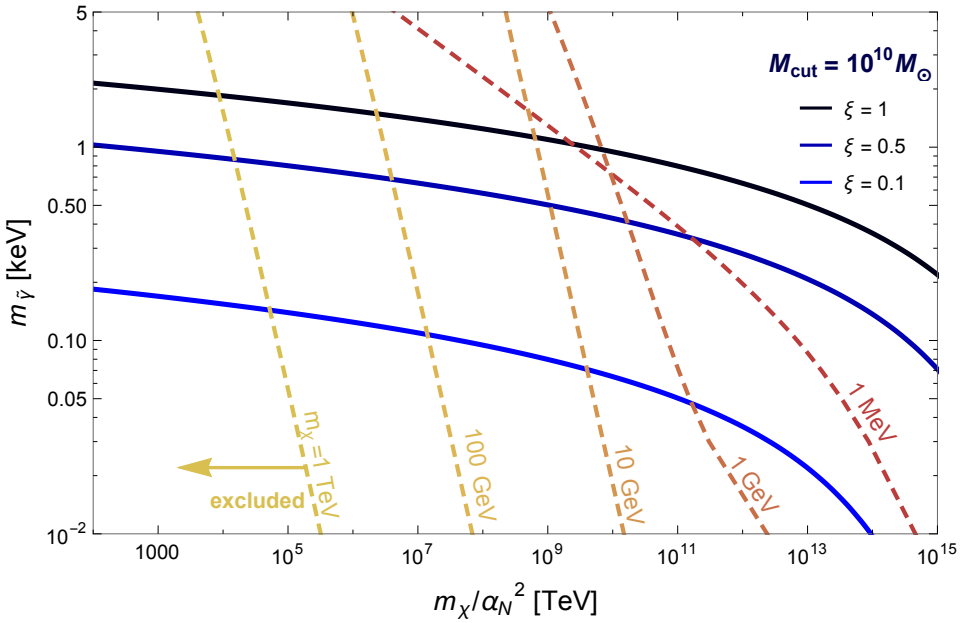

FIGURE 9.4: Plot of model parameters required for late KD ($M_{\rm cut} = M_{10}$), for a fermion χ, scattering with light $SU(N)$ gauge vectors $\tilde{\gamma}$ (solid lines). Also includes constraints from χ self-interaction mediated by $\tilde{\gamma}$ for different m_χ (dashed lines). Everything to the left on the dashed lines is excluded. For the self-interaction constraints we assumed $N = 2$. Larger values of N lead to weaker constraints. Figure taken from Bringmann et al., 2016.

assumption that the dark sector and the visible sector were in thermal equilibrium at some time, is at least in some tension with observations. Allowing for entropy violation could alleviate this tension.

9.2.2 Massive $\tilde{\gamma}$ without Chemical Equilibrium

The simpler assumption than the one we looked at in the previous section would be to assume that the dark sector only consists of χ and $\tilde{\gamma}$. In this case when $\tilde{\gamma}$ becomes non-relativistic, there is no exponential suppression of the number density. This is because there are no processes to maintain chemical equilibrium, since $2\tilde{\gamma} \to \tilde{\gamma}$ is not kinematically allowed.

However, when $\tilde{\gamma}$ becomes non-relativistic, the temperature scales as $T_{\tilde{\gamma}} \propto 1/a^2$ and this means that $T_\chi \propto 1/a^2$ as well.

Let us assume that $\tilde{\gamma}$ decouples, meaning no more interactions (except for the few interactions with χ), at some temperature $T_{\rm d}$ while relativistic, then we can use the solution to the collisionless BE (Eq. 2.33). The results should not change qualitatively if kinetic equilibrium is maintained until after $\tilde{\gamma}$ becomes non-relativistic. We then get

$$f_{\tilde{\gamma}}(p,T) = \frac{1}{\exp\left(\sqrt{T_{\rm d}^2 p^2/T^2 + m_{\tilde{\gamma}}^2}/\xi_{\rm d} T_{\rm d}\right) - 1}. \tag{9.13}$$

Using this, we can calculate the momentum transfer rate, as well as the evolution of $T_{\tilde{\gamma}}$, see Fig. 9.5.

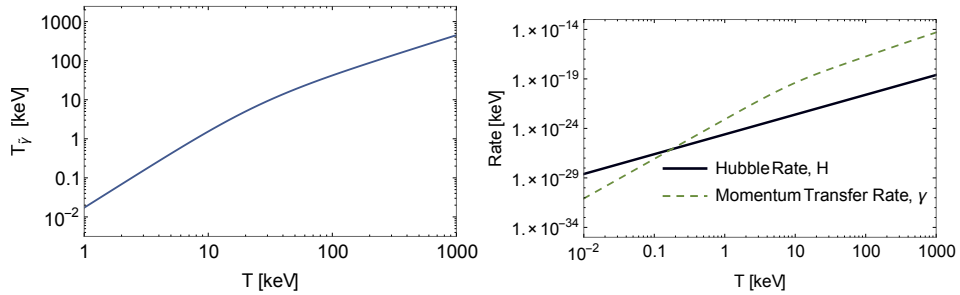

FIGURE 9.5: Left: Figure showing the evolution of the temperature of $\tilde{\gamma}$ as it becomes non-relativistic. Since χ will have the same temperature, we will, if we define KD as the time where the two asymptotic curves meet, get a get a KD temperature of about $T_{\text{kd}}^{\text{scaling}} \sim 30$ keV. Right: Figure comparing the momentum transfer rate, $\gamma(T_{\tilde{\gamma}})$, with the expansion rate, $H(T)$. If we define KD as the time when these two rates are equal, we get a KD temperature of about $T_{\text{kd}}^{\text{rates}} \sim 0.1$ keV. This shows that, even though the two definitions of KD usually gives (roughly) the same results, they are based on different phenomena, and in this special case gives wildly different results.

Conflicting Definitions of Kinetic Decoupling

In this thesis we have used a definition of KD that relies on the scaling of the DM temperature, defining (roughly) T_{kd} as the temperature where T_χ starts to scale like a^{-2}, lets call this temperature $T_{\text{kd}}^{\text{scaling}}$. But what if the temperature of the heat bath itself starts to scale like a^{-2}, like what happens to $\tilde{\gamma}$ after it becomes non-relativistic. In this case, there is plenty of interactions between χ and $\tilde{\gamma}$ even after what we define as KD.

There is another definition of T_{kd}, lets call it $T_{\text{kd}}^{\text{rates}}$, that better captures what we actually mean by kinetic decoupling. KD should be when there are essentially no interaction with the heat bath, we can use this and define $T_{\text{kd}}^{\text{rates}}$ as the temperature at which the expansion rate equals the momentum transfer rate

$$H(T_{\text{kd}}^{\text{rates}}) = \gamma(T_{\text{kd}}^{\text{rates}}). \tag{9.14}$$

In almost all cases $T_{\text{kd}}^{\text{rates}} \sim T_{\text{kd}}^{\text{scaling}}$, so it is usually not that important what definition we use, but here we get very different results for the two definitions. It is also clear that, in this case, it is the definition based on the rates that corresponds best to what we usually mean by KD.

What is M_{cut}

On the other hand, what we really want to know here is not the temperature of KD, but rather, what is the mass of the cutoff in the matter power spectrum.

This is a more complicated question, and we would need to solve the full perturbed Eistein-Boltzmann equations in order to answer this. This is beyond the scope of this thesis, but would make for an interesting future project.

Let us, however, ask how the Jeans scale k_J compares to the Hubble scale aH after $\tilde{\gamma}$ becomes non-relativistic. Let us assume that this happens

while we are still in the radiation dominated phase. We then get

$$\frac{k_J}{aH} \sim \frac{1}{c_s}\sqrt{\frac{\rho_\chi}{\rho_\gamma}} \sim \sqrt{\frac{m_{\tilde{\gamma}}}{\xi T}\frac{a}{a_{\text{eq}}}} \sim \left(\frac{a}{a_{\text{eq}}}\right)^{3/2}\sqrt{\frac{m_{\tilde{\gamma}}}{\xi T_{\text{eq}}}}, \tag{9.15}$$

where a_{eq} corresponds to the scale factor at matter-radiation equality and we have used $c_s^2 \sim \xi T/m_{\tilde{\gamma}}$. Equating this expression to 1 we get

$$T_{\text{cut}} \sim \left(\frac{m_{\tilde{\gamma}} T_{\text{eq}}^2}{\xi}\right)^{1/3}, \tag{9.16}$$

suggestion that the Jeans length becomes smaller than the horizon at some time between $T = m_{\tilde{\gamma}}/\xi$ and $T = T_{\text{eq}}$.

I must stress that this is only a very crude order of magnitude estimate, however, it does indicate that scales entering the horizon even after $\tilde{\gamma}$ becomes non-relativistic are also suppressed, and only modes that enter the horizon after $T \sim T_{\text{cut}} \ll m_{\tilde{\gamma}}/\xi$ remain unsuppressed. So it is more reasonable to replace T_{kd} by T_{cut} in Eq. 5.30, than to put in either $T_{\text{kd}}^{\text{scaling}}$ or $T_{\text{kd}}^{\text{rates}}$.

Relic Density of $\tilde{\gamma}$

A serious problem for this model, however, is the relic density of $\tilde{\gamma}$. Since, under the assumption in this section, $\tilde{\gamma}$ undergoes CD while relativistic, we get a direct relation between $m_{\tilde{\gamma}}$ and $\Omega_{\tilde{\gamma}}$ from Eq. 4.13

$$m_{\tilde{\gamma}} = 1.56\text{ eV}\left(\frac{g_{*S}^v(T = m_{\tilde{\gamma}}/\xi)}{g_{\tilde{\gamma}}^{\text{eff}}}\right)\xi(T = m_{\tilde{\gamma}}/\xi)^{-3}\left(\frac{\Omega_{\tilde{\gamma}}h^2}{0.1188}\right). \tag{9.17}$$

This is a problem if we want $T_{\text{cut}} \sim 100$ eV, since we have $m_{\tilde{\gamma}}/\xi \gtrsim T_{\text{cut}}$. If we want $\Omega_{\tilde{\gamma}} \lesssim 0.1\Omega_\chi$, we will need $\xi \lesssim 0.1$, which would probably require either a violation of entropy conservation, or a situation where the dark and visible sectors were never in thermal equilibrium.

9.3 Summary

We have studied the SU(N) model (with fermionic DM), as a representative of the 2-particle models with an enhanced scattering amplitude from the t-channel. These models differ from the "standard" case in that the analytic solution for T_{kd} is not applicable. In these models, since $n \leq -2$, we do not get KD as long as $\tilde{\gamma}$ is relativistic, so the process of KD is crucially dependent on when and how $\tilde{\gamma}$ becomes non-relativistic. In this chapter we have considered two different cases for what happens to $\tilde{\gamma}$ when it becomes non-relativistic.

First we assumed that annihilation to another species ϕ, keeps $\tilde{\gamma}$ in chemical equilibrium. In this case the number density of $\tilde{\gamma}$ becomes exponentially suppressed as it becomes non-relativistic, leading quickly to KD. This possibility can lead to late KD while avoiding the self interaction constraints for a wide range of model parameters.

Second we assumed that $\tilde{\gamma}$ was already decoupled from the heat bath and was simply free streaming. In this case the (comoving) number density of $\tilde{\gamma}$ is constant, but the effective temperature of $\tilde{\gamma}$ decreases quickly after $\tilde{\gamma}$ becomes non relativistic. Although we can still calculate $T_{\rm kd}$ using whatever definition we want, it is no longer clear that this temperature corresponds directly to the cutoff in the linear matter power spectrum, the way that it usually does. In order to investigate this, we would need to solve the full perturbed BE's and look at the power spectrum. This is beyond the scope of this thesis, but would make for an interesting future project.

For slightly different reasons, both these possibilities require a very low value for ξ in order to be consistent with cosmology, which is hard, but not impossible, to achieve from a model building perspective.

Part IV

Discussion and Conclusion

Chapter 10

Discussion

In this chapter we will discuss some aspects of the models we have been considering. First we will give a brief discussion of the main results. Not only from this thesis but also from Bringmann et al., 2016. Then we will discuss the plausibility of these kinds of models and why we would want to go beyond the CDM paradigm in the first place.

10.1 Discussion of Results

After looking at all the simplest DM models we see that late KD is possible in quite a few of these models. For the 2-particle models the constraints from self-interaction limited the number of possibilities severely (see Tab. 7.1), but for the 3-particle models all of the models we studied had at least some part of the parameter space that was allowed.

The ways of achieving an enhanced elastic scattering amplitude from putting a virtual particle on shell is fairly straightforward, although it was a bit surprising that the leading contributions to the scattering amplitude in the s/u-channels canceled exactly in all the 2-particle models we considered.

Another important point to note is that in some cases, we did not need an enhanced scattering amplitude, but could achieve late KD simply by reducing the DM mass. The prime example of this being the 4-point coupling scalar model discussed in Sec. 8. As we showed for this model, however, some care needs to be used when calculating the relic density of light DM $m_\chi \lesssim$ MeV.

It is interesting to consider what happens when the DM mass in these kinds of models approach the masses associated with WDM candidates. One of the reasons is that we need to know what happens to WDM with $\xi \ll 1$. We are not aware of this case being studied in the literature at all, although it seems plausible that a lower temperature leads to less free streaming and such would allow for lighter WDM for small ξ, but a more careful analysis of this possibility would be interesting.

t-channel enhancements in the 2-particle models also leads to very interesting behavior, where the scattering amplitude increases as the temperature drops. This means that KD is typically related to $\tilde{\gamma}$ becoming non-relativistic. The process and significance of KD also depends crucially on whether $\tilde{\gamma}$ stays in chemical equilibrium when it becomes non-relativistic or not, as we discussed in Ch. 9.

In Aarssen, Bringmann, and Pfrommer, 2012 a DM model for late KD is introduced, that can (possibly) address both the missing satellite problem, the cusp/core problem and the too big to fail problem simultaneously,

as well as producing the correct relic density. The natural combination of these features makes this model very attractive. In Bringmann et al., 2016 we show that this model actually fits into a larger class of models with essentially the same phenomenology. Some other models are also similar to these models but with elastic scattering that is independent of the energy of $\tilde{\gamma}$. It would be interesting to study i detail how the full results would differ in these two classes of models.

We also find a class of 3-particle models in the s/u-channels that can give late KD, but do not naturally give rise to strong self-interaction that could address the cusp/core or too big to fail problems.

10.2 Unitarity

Some of the elastic scattering amplitudes, particularly for 2-particle models in the t-channel, become enormously enhanced. This should make us ask questions about unitarity. Unitarity is typically studied in the ultra-relativistic limit (see e.g. Kahlhoefer et al., 2016), which is very far from the kinematic situation in these elastic scatterings, so it is unclear how relevant the usual discussion is for us.

A detailed analysis of unitarity would typically involve a partial wave expansion of our scattering amplitude, which is far beyond the scope of this thesis. However, a reasonable first step to see if our results are physical, would be to calculate the first loop correction and compare that to our tree-level result. Another member of our collaboration did this calculation for the fermion-scalar 2-particle model in the t-channel (from Bringmann et al., 2016). That calculation showed that the tree-level result completely dominated the amplitude for all relevant model parameters, which is at least a good sign.

A more thorough study of unitarity in this kinematic limit would be both helpful and interesting for the kind of model building we are doing.

10.3 Plausibility

10.3.1 Input vs Output

In (at least almost) all cases we need some light heat bath particle to scatter off. This usually means that we need to explicitly add a new particle in addition to the SM particles. For the 3-particle models we also need to add a mediator particle.

When assessing the plausibility of a given model, one of the main thing to consider is the amount of "input" and compare it to the amount of "output" you get back. As an example let us consider CDM. If we simply assume that there exists some new particle species which is non-relativistic at low temperatures, is somehow produced in the early universe to give a current relic density of about 5 times the density of baryons and interacts weakly with itself and the SM, then we can explain the whole breath of independent branches of evidence summarized in 3.1.

While it is unreasonable to expect any model to be as successful as the CDM model, we should still take into account the amount of input and output when assessing our models for plausibility.

These considerations mean that, all else being equal, 2-particle models are preferred to 3-particle models. Also, a model with less free parameters is also preferred. The fact that we find 2-particle models that can give rise to late KD is then encouraging. However, the t-channel enhanced models, while they can achieve an interesting strength of the self interaction, cannot (except perhaps for very light DM masses) be thermally produced without invoking some other interaction or mechanism. Also, in order to achieve late KD we typically need to fine-tune the mass of $\tilde{\gamma}$. If we further assume that $\tilde{\gamma}$ stays in chemical equilibrium when it becomes non-relativistic, this means that we even need to introduce another particle to the model.

In Aarssen, Bringmann, and Pfrommer, 2012 the heat bath particles are the SM neutrinos, meaning that, even though we would classify this as a 3-particle model, we only need to introduce one new particle, the mediator, in addition to DM itself. Another nice feature about this is that, since we know the neutrino temperature, ξ is fixed, meaning that we have one less free parameter.

It is hard, and perhaps not very useful, to rank these different models by plausibility. However, we should always have these thoughts in the back of our mind, when working on model building.

10.3.2 Considerations on the Value of ξ

If the dark and visible sectors are in equilibrium at high temperatures, the value of ξ can be calculated exactly at any time if we know what is going on in both the dark and visible sectors, and assuming entropy is conserved.

As we showed in Sec. 6.2, if we assume that the dark and visible sectors decouple before any of the SM particles heat the photon bath, then the lower bound on ξ is given roughly by $\xi_{\text{min}}^{\text{SM}} \approx 0.33$.

This value can be compared to the 1σ bound on N_{eff} from CMB which gave an upper bound of e.g. $\xi \lesssim 0.39$ for a single Dirac fermion DR species.

We see that the range of values for ξ is very limited. We should also note that the value for $\xi_{\text{min}}^{\text{SM}}$ assumes that no particles heat the dark heat bath. If χ and possibly other particles in the dark sector heat the dark bath after the two sectors decouple, then $\xi_{\text{min}}^{\text{SM}}$ should be multiplied by a factor $[(g_{\tilde{\gamma}} + g_{\chi} + g_{\text{other}})/g_{\tilde{\gamma}}]^{1/3}$, making it even worse.

We see that the possibility of DR is severely limited if we assume both that the dark and visible sectors were once in thermal equilibrium, and that entropy is conserved after the two sectors decoupled. This begs the question about what happens if we assume that the dark and visible sectors were never in equilibrium.

Discussing how possible reheating models, or other high temperature mechanisms can give rise to two completely decoupled sectors with different temperatures is beyond the scope of this thesis, but we may in the not too distant future get to the point where something like this might be required in order to have DR. If such a mechanism is indeed required, then that at least makes the idea of DR somewhat less plausible, and it would make the prospects of DM detection entirely hopeless.

10.4 Why go Beyond CDM? Or, If it Ain't Broke, Don't Fix it

As discussed in Sec. 3.1 the CDM paradigm has been extremely successful. A wide range of independent evidence all point to the existence of large amounts of new non-relativistic matter interacting through the gravitational force.

Since the very simple CDM model is so successful, it begs the question as to why we would want to add more complications on top, like DR or self-interactions. Is this like adding epicycles to a simple and beautiful model?

This objection misses a large point, which is that the reason for bringing up these more involved DM models (mainly small scale problems in ΛCDM) are largely independent from the main evidence for DM. This means that even if these new DM models were not able to address the small scale problems, or if the small scale problems were solved in some other way (e.g. by using baryonic physics), this would not be a significant blow to the CDM paradigm.

Rather if some more complicated DM model, like the ones we are considering in this thesis, could (potentially) address the small scale problems, this would just be a nice additional feature, making these models of DM more attractive as compared to other models of DM. Whether or not these additional features are compelling enough to justify adding the new baggage (new particles, interactions etc) onto the simple CDM paradigm, is a matter of judgement.

A nice thing about models with late KD, that we should also consider, is that they provide us with new ways to look for DM. Since these acoustic oscillations change the dark matter power spectrum, precise measurements of the power spectrum at these scales could potentially detect these effects. Also, if we detect some non-zero value for ΔN, that would be evidence for dark radiation.

It also has to be noted that we expect in any case that DM is part of some, more complete, beyond-SM model of particle physics. Therefore understanding the particle nature and interactions of DM is a very important step towards understanding which direction to go for beyond-SM physics. This means that mapping out the different possibilities of physics in the dark sector has some value completely independently of small scale problems in ΛCDM.

Conclusion

The search for models that can lead to late KD in Bringmann et al., 2016 must be said to be a success. In addition to recovering working models for late KD in the literature, we see that these were in many cases just part of a broader class of similar models. We also discover some new types of models not considered in the literature before. The potential in some of these models to solve all the three small-scale problems we have mentioned, as well as producing the correct relic density, is at the very least promising.

The scalar 4-point coupling model is very interesting. Both because it maps onto essentially any effective theory of $\chi - \tilde{\gamma}$ interactions that leads to a scattering that is independent of the energy of $\tilde{\gamma}$, but also because it is such a simple model and yet still seems viable. Calculating the KD temperature in this model is very simple, but when trying to obtain both late KD and the correct relic density we see that we need very small DM masses ($m_\chi \lesssim$ MeV). In this region we cannot trust the analytic expression we used for the relic density, since the assumption that χ is non-relativistic at CD is not as certain anymore. However, after analyzing all the approximations that usually go into calculations of relic density, and doing a full numerical calculation, we find that the model is actually very viable.

The second model we have looked into in this thesis is the model where a fermionic DM transforms in the fundamental representation of an $SU(N)$ gauge theory. This model, like other 2-particle models where the elastic $\chi - \tilde{\gamma}$ scattering is dominated by the t-channel, gave rise to the interesting behavior where KD does not happen until $\tilde{\gamma}$ becomes non-relativistic. As we discussed, these models raise questions about how we should actually define KD, and how KD is related to the cutoff in the power spectrum, M_{cut}. Also this model seems to require very small values of ξ, which, as we discussed in the precious chapter, is hard to achieve when building a complete consistent model.

An interesting future project would be to solve the perturbed BE's for one of the 2-particle models in the t-channels. Since, as we discussed in Sec. 9.2.2, it is not entirely clear how the suppression in the matter power spectrum would look in those models.

Looking into early universe mechanisms to produce a dark sector that is completely decoupled from the visible sector, would also be an interesting area of study. This could tell us more about how easy it is to obtain small values for ξ, and may also give us suggestions for what the dark sector could look like.

Part V

Appendices

Appendix A

Quantum Field Theory

Quantum field theory (QFT) is, together with special and general relativity, the crowning achievements of theoretical physics in the last century. It describes how the fundamental (and non-fundamental) particles of nature behave and interact, and it describes how the physics at different energy scales is related. Here we give a very brief theoretical introduction to a few of the main aspects of QFT.

A.1 Classical Field Theory

In classical mechanics we derive the equations of motion for any system from an action principle. The configurations of the system change in the way that extremizes the action, S.

For a classical field the action principle leads us to the *Euler-Lagrange equations*, which govern evolution of the fields ϕ_a, given by

$$\frac{\partial \mathcal{L}}{\partial \phi_a} - \partial_\mu \left(\frac{\partial \mathcal{L}}{\partial \left(\partial_\mu \phi_a \right)} \right) = 0, \tag{A.1}$$

where ϕ_a are the fields of the theory and $\mathcal{L}(\phi_a)$ is the Lagrangian density, i.e. the function that is integrated over spacetime to give the action, S.

It is often useful to divide the Lagrangian into two parts, the *free* Lagrangian, $\mathcal{L}_0$, and the *interaction* Lagrangian, $\mathcal{L}_I$ such that

$$\mathcal{L} = \mathcal{L}_0 + \mathcal{L}_I. \tag{A.2}$$

The free part of the Lagrangian is usually the part that leads to linear equations of motions for the fields, while the interaction Lagrangian contains higher order terms, and terms mixing different fields.

A.2 Quantum Field Theory

To describe the fundamental particles of nature we use QFT. In QFT, the time evolution of a state (in the interaction picture) is given by the time evolution operator $U(t, t_0)$

$$|\Psi(t)\rangle = U(t, t_0)|\Psi(t_0)\rangle, \tag{A.3}$$

where

$$U(t, t_0) = T \exp\left(-i \int_{t_0}^{t} H_I(t')dt' \right), \tag{A.4}$$

where T stands for *time ordering* and where $H_I = -\mathcal{L}_I$ is the interaction Hamiltonian in the interaction picture. Here we use the exponential simply as a shorthand for its series expansion.

When looking at scattering we want to study what happens to some initial state, $|i\rangle$, presumably of particles moving towards each other, to a final state, $|f\rangle$, presumably of particles moving away from each other. Such a process is described by the S-matrix, defined by

$$\lim_{t_\pm \to \pm\infty} \langle f|U(t_+, t_-)|i\rangle \equiv \langle f|S|i\rangle. \tag{A.5}$$

Using this we can define the scattering amplitude $\mathcal{M}$ by

$$\langle f|S|i\rangle = i\mathcal{M}_{i\to f}\,(2\pi)^4\delta^{(4)}(p_f - p_i), \tag{A.6}$$

where p_i and p_f are the momenta of the initial and final states respectively. In order for this approach to work, we need to assume that H_I is "small", in the sense that the series in Eq. A.4 converges quickly. In this case we can get a good approximation to S by treating Eq. A.4 as a perturbation series, and taking the leading terms. If this is the case we can calculate $\mathcal{M}$ by drawing the Feynman diagrams, corresponding to each term in the series expansion of Eq. A.4, and using the Feynman rules derived from the corresponding Lagrangian (see e.g. Peskin and Schroeder, 1995).

A.3 Particles

Since our relativistic quantum theories should be Lorentz-invariant, the Lorentz-group has a unitary (or anti-unitary) representation on our Hilbert space (Wigner, 1939). We can write the action of the Lorentz group on all the quantum fields in our theory by the unitary operator, $U(\Lambda)$ (for an active transformation)

$$U^\dagger(\Lambda)\phi_a(x)U(\Lambda) = D_{ab}(\Lambda)\phi_b(\Lambda^{-1}x). \tag{A.7}$$

We can now choose to rearrange the fields in order to block-diagonalize the matrix D. Each of the blocks would then correspond to an irreducible representation of the Lorentz-group. We usually call these irreducible representations of the Lorenz-group the *particles* of the theory. Note that although $U(\Lambda)$ is unitary, $D(\Lambda)$ is not (in general).

The next question to ask is then, what form can these matrices D_{ab} take, as this will tell us what kinds of particles we can have.

The trivial (singlet) representation, where $D = 1$, is called the scalar field

$$U^\dagger(\Lambda)\phi(x)U(\Lambda) = \phi(\Lambda^{-1}x). \tag{A.8}$$

The vector field is another simple case, in this representation $D = \Lambda$, the regular Lorentz transformation matrices.

$$U^\dagger(\Lambda)\phi^\mu(x)U(\Lambda) = \Lambda^\mu{}_\nu\phi^\nu(\Lambda^{-1}x). \tag{A.9}$$

In general, the matrix $D(\Lambda)$ must be writable on the form

$$D_{ab}(\Lambda) = \exp\left(\frac{i}{2}\omega_{\alpha\beta}\mathcal{M}^{\alpha\beta}_{ab}\right), \tag{A.10}$$

where $\mathcal{M}^{\alpha\beta}$ has to satisfy the commutation relations

$$\left[\mathcal{M}^{\mu\nu}, \mathcal{M}^{\alpha\beta}\right] = i\left(\eta^{\nu\beta}\mathcal{M}^{\mu\alpha} + \eta^{\mu\alpha}\mathcal{M}^{\nu\beta} - \eta^{\mu\beta}\mathcal{M}^{\nu\alpha} - \eta^{\nu\alpha}\mathcal{M}^{\mu\beta}\right). \tag{A.11}$$

Another important representation is the spinor representation

$$D_{ab}(\Lambda) = \exp\left(-\frac{i}{4}\omega_{\alpha\beta}\sigma^{\alpha\beta}_{ab}\right) \equiv S_{ab}(\Lambda), \tag{A.12}$$

where $\sigma^{\mu\nu} \equiv \frac{i}{2}\left[\gamma^{\mu}, \gamma^{\nu}\right]$ obeys the commutation relations in Eq. A.11, where γ^{μ} obays the *Clifford Algebra* given by

$$\{\gamma^{\mu}, \gamma^{\nu}\} = 2\eta^{\mu\nu}, \tag{A.13}$$

and where η is the Minkowski metric.

We usually label the different particles by their spin. The scalar, spinor and vector representations corresponds to particles with spin 0, $1/2$ and 1 respectively. These three representations actually describe all the known elementary particles in the universe.

Appendix B

Gauge Boson Polarization Sums

The treatment of gauge boson polarization in non-abelian gauge theories requires some care. We will here summarize the main issues and find ways to treat polarization sums of external gauge bosons consistently.

When considering polarization vectors it is natural to choose an orthonormal basis such that (with a slight abuse of notation since λ and λ' are not Lorentz indices)

$$\sum_{\lambda\lambda'} g^{\lambda\lambda'} \epsilon^{*\mu}_{\lambda'} \epsilon^{\nu}_{\lambda} = g^{\mu\nu}, \tag{B.1}$$

where the sum is over all (four) polarizations.

If gauge bosons were described using all polarizations, then our life would be simple, but since there is a large redundancy in using a four vector to describe a gauge boson, we need to be careful to distinguish between physical and unphysical degrees of freedom.

B.1 Massless Gauge Bosons

If the gauge symmetry is unbroken the gauge bosons have two physical polarization degrees of freedom. Since a general (Lorentz) vector has four degrees of freedom, we must somehow remove two of them.

One approach would be to just use a basis of the two transverse polarization states, and ignore the unphysical time-like and longitudinal polarizations. For a boson traveling in the z-direction, the transverse polarization vectors are given by

$$\epsilon^{\mu}_{-} \equiv \frac{1}{\sqrt{2}}(0, 1, -i, 0), \tag{B.2}$$

$$\epsilon^{\mu}_{+} \equiv -\frac{1}{\sqrt{2}}(0, 1, +i, 0), \tag{B.3}$$

where we have chosen to use circularly polarized basis vectors.

The polarization sum is then given by (for a boson traveling in the z-direction)

$$\sum_{\lambda=+,-} \epsilon^{*\mu}_{\lambda}(k) \epsilon^{\nu}_{\lambda}(k) = \begin{pmatrix} 0 & 0 & 0 & 0 \\ 0 & 1 & 0 & 0 \\ 0 & 0 & 1 & 0 \\ 0 & 0 & 0 & 0 \end{pmatrix}. \tag{B.4}$$

We can generalize this to a boson traveling in any direction

$$\sum_{\lambda=T} \epsilon_\lambda^{*i}(k)\epsilon_\lambda^j(k) = \delta^{ij} - \frac{k^i k^j}{|\mathbf{k}|^\mathbf{2}}, \tag{B.5}$$

where T denotes transverse polarizations.

While this new expression is rotationally covariant, it is certainly not Lorentz covariant. This is a perfectly valid approach to use, but a general covariant formalism is usually much easier to deal with.

Note also that none of these expressions are gauge-invariant. They amount to choosing a specific gauge, called the *transverse gauge*.

B.1.1 Axial Gauge

The axial gauge is obtained by adding the following gauge-fixing term to the Lagrangian (De Wit and Smith, 1986, p. 439)

$$\mathcal{L}_{\text{axial}} = -\frac{1}{2\xi}(n \cdot A)^2, \tag{B.6}$$

where A is the gauge field, n is an arbitrary four vector and ξ is an arbitrary gauge fixing parameter.

In this gauge we can write the sum over transverse polarizations in a fully covariant way[1]

$$\sum_{\lambda=T} \epsilon_\lambda^{*\mu}\epsilon_\lambda^\nu = -g^{\mu\nu} + \frac{n^\mu k^\nu + n^\nu k^\mu}{(n \cdot k)} - \frac{n^2 + \xi k^2}{(n \cdot k)^2} k^\mu k^\nu. \tag{B.7}$$

We can make this simpler by specifying a gauge. If we choose $\xi \to 0$ and $n^2 = 0$, we get the *light cone gauge*. With this gauge choice the sum over transverse polarizations is simply

$$\sum_{\lambda=T} \epsilon_\lambda^{*\mu}(k)\epsilon_\lambda^\nu(k) = -g^{\mu\nu} + \frac{n^\mu k^\nu + n^\nu k^\mu}{(n \cdot k)}. \tag{B.8}$$

We can see that, for a boson travelling in the z-direction, if we choose $n^\mu = (1, 0, 0, -1)$ we recover Eq. B.4.

If we are calculating a specific process involving two external gauge bosons with momenta k_1 and k_2, it is very useful to simply choose $n = k_2$ (or k_1), since we already have expressions involving k_2 and it already satisfies $k_2^2 = 0$. This gives us e.g.

$$\sum_{\lambda=T} \epsilon_\lambda^{*\mu}(k_1)\epsilon_\lambda^\nu(k_1) = -g^{\mu\nu} + \frac{k_2^\mu k_1^\nu + k_2^\nu k_1^\mu}{(k_2 \cdot k_1)}. \tag{B.9}$$

B.1.2 Ghosts

Another way to deal with the unphysical polarizations is to introduce ghosts to cancel these contributions. Using the approach of Faddeev and Popov

[1] Here we see one drawback of this gauge, namely the singularity at $n \cdot k = 0$, but unless you are integrating over all k this should be avoidable.

(Faddeev and Popov, 1967), we can add the following terms to the Lagrangian

$$\mathcal{L}_{\text{FP}} = -\frac{1}{2\xi}(\partial \cdot A)^2 + \bar{c}(-\partial^\mu D_\mu)c, \tag{B.10}$$

where the first term is the gauge-fixing term, and the second term is the kinetic term for the ghosts.

The ghosts, c, are not physical particles, but are introduced to cancel out the unphysical polarizations of the gauge bosons. The ghosts have a number of interesting properties. They transform in the adjoint representation of the gauge group, like the gauge bosons, they transform like a scalar under Lorentz transformations, but they obey Fermi-Dirac statistics.

From the Lagrangian we can derive Feynman rules for the ghosts (see e.g. Peskin and Schroeder, 1995, p. 515), so we can include them in scattering processes. This allows us, for external gauge bosons, to use the replacement

$$\sum_{\lambda=T} \epsilon^{*\mu}_\lambda(k)\epsilon^\nu_\lambda(k) \to -g^{\mu\nu} \tag{B.11}$$

if we also sum over ghosts in the same external states.

At tree level, the ghosts only appear in external states, and they are included formally as if they were extra degrees of freedom for the gauge bosons. However, we must remember to use Fermi-Dirac statistics when permuting two external ghosts. In addition, when calculating the squared diagrams, we need to include a factor $(-1)^{n/2}$, where n is the number of ghosts in the diagram (Nachtmann, 1990, p. 489). This can lead to what appears to be negative probabilities, but these are needed to cancel out the contribution from the unphysical polarization states we included when making the replacement in Eq. B.11.

B.2 Massive Gauge Bosons

If the gauge symmetry is broken, by giving the gauge boson a mass, dealing with the polarizations actually becomes simpler. A massive vector boson has three physical polarizations, two transverse, and one longitudinal.

Using Eq. B.1 we can find the sum of the three physical polarizations

$$\sum_{\lambda=T,L} \epsilon^{*\mu}_\lambda(k)\epsilon^\nu_\lambda(k) = -g^{\mu\nu} + \epsilon^{*\mu}_0(k)\epsilon^\nu_0(k), \tag{B.12}$$

where L and 0 corresponds to the longitudinal and time-like polarization vectors respectively.

The time-like polarization is proportional to the momentum (as can be seen by moving to the rest frame), and its normalization is fixed by Eq. B.1

$$\epsilon^\mu_0(k) = \frac{k^\mu}{m}. \tag{B.13}$$

This gives us, for the polarization sum of an external massive gauge boson

$$\sum_{\lambda=T,L} \epsilon^{*\mu}_\lambda(k)\epsilon^\nu_\lambda(k) = -g^{\mu\nu} + \frac{k^\mu k^\nu}{m^2}. \tag{B.14}$$

Bibliography

Aarssen, Laura G. van den, Torsten Bringmann, and Christoph Pfrommer (2012). "Is dark matter with long-range interactions a solution to all small-scale problems of ΛCDM cosmology?" In: *Phys. Rev. Lett.* 109, p. 231301. arXiv: 1205.5809 [astro-ph.CO].

Abazajian, K. and S. M. Koushiappas (2006). "Constraints on sterile neutrino dark matter". In: Phys. Rev. D 74.2, 023527, p. 023527. eprint: astro-ph/0605271.

Arneodo, F. (2013). "Dark Matter Searches". In: *ArXiv e-prints*. arXiv: 1301.0441 [astro-ph.IM].

Arnold, P. and L. G. Yaffe (1995). "Non-Abelian Debye screening length beyond leading order". In: Phys. Rev. D 52, pp. 7208–7219. eprint: hep-ph/9508280.

Askew, A. et al. (2014). "Searching for dark matter at hadron colliders". In: *International Journal of Modern Physics A* 29, 1430041, p. 30041. arXiv: 1406.5662 [hep-ph].

Balberg, Shmuel, Stuart L. Shapiro, and Shogo Inagaki (2002). "Selfinteracting dark matter halos and the gravothermal catastrophe". In: *Astrophys. J.* 568, pp. 475–487. arXiv: astro-ph/0110561 [astro-ph].

Bezrukov, F., H. Hettmansperger, and M. Lindner (2010). "keV sterile neutrino Dark Matter in gauge extensions of the Standard Model". In: *Phys. Rev.* D81, p. 085032. arXiv: 0912.4415 [hep-ph].

Binder, Tobias et al. (2016). "Matter Power Spectrum in Hidden Neutrino Interacting Dark Matter Models: A Closer Look at the Collision term". In: arXiv: 1602.07624 [hep-ph].

Birkedal, A. et al. (2006). "Little Higgs dark matter". In: Phys. Rev. D 74.3, 035002, p. 035002. eprint: hep-ph/0603077.

Blok, W. J. G. de (2010). "The Core-Cusp Problem". In: *Adv. Astron.* 2010, p. 789293. arXiv: 0910.3538 [astro-ph.CO].

Bolz, M., A. Brandenburg, and W. Buchmüller (2001). "Thermal production of gravitinos". In: *Nuclear Physics B* 606, pp. 518–544. eprint: hep-ph/0012052.

Borriello, A. and P. Salucci (2001). "The dark matter distribution in disc galaxies". In: MNRAS 323, pp. 285–292. eprint: astro-ph/0001082.

Boylan-Kolchin, M. et al. (2009). "Resolving cosmic structure formation with the Millennium-II Simulation". In: MNRAS 398, pp. 1150–1164. arXiv: 0903.3041 [astro-ph.CO].

Boylan-Kolchin, Michael, James S. Bullock, and Manoj Kaplinghat (2011). "Too big to fail? The puzzling darkness of massive Milky Way subhaloes". In: *Mon. Not. Roy. Astron. Soc.* 415, p. L40. arXiv: 1103.0007 [astro-ph.CO].

Bringmann, T. (2009). "Particle models and the small-scale structure of dark matter". In: *New Journal of Physics* 11.10, 105027, p. 105027. arXiv: 0903.0189.

Bringmann, T. and S. Hofmann (2007). "Thermal decoupling of WIMPs from first principles". In: J. Cosmology Astropart. Phys. 4, 016, p. 016. eprint: hep-ph/0612238.

Bringmann, T. et al. (2016). "Suppressing structure formation at dwarf galaxy scales and below: late kinetic decoupling as a compelling alternative to warm dark matter". In: *ArXiv e-prints*. arXiv: 1603.04884 [hep-ph].

Bringmann, Torsten (2011). "Indirect dark matter searches: A mini-review". In: *PoS* EPS-HEP2011, p. 061.

Bringmann, Torsten, Jasper Hasenkamp, and Jörn Kersten (2014). "Tight bonds between sterile neutrinos and dark matter". In: *JCAP* 1407, p. 042. arXiv: 1312.4947 [hep-ph].

Buen-Abad, M. A., G. Marques-Tavares, and M. Schmaltz (2015). "Non-Abelian dark matter and dark radiation". In: Phys. Rev. D 92.2, 023531, p. 023531. arXiv: 1505.03542 [hep-ph].

Carroll, Sean M. (2004). *Spacetime and geometry: An introduction to general relativity*. San Francisco, USA: Addison-Wesley 513 p. ISBN: 0805387323, 9780805387322.

Chu, X. and B. Dasgupta (2014). "Dark Radiation Alleviates Problems with Dark Matter Halos". In: *Physical Review Letters* 113.16, 161301, p. 161301. arXiv: 1404.6127 [hep-ph].

Cowsik, R. and J. McClelland (1972). "An Upper Limit on the Neutrino Rest Mass". In: *Phys. Rev. Lett.* 29 (10), pp. 669–670.

Cushman, P. et al. (2013). "Snowmass CF1 Summary: WIMP Dark Matter Direct Detection". In: *ArXiv e-prints*. arXiv: 1310.8327 [hep-ex].

Cyr-Racine, F.-Y. et al. (2015). "ETHOS - An Effective Theory of Structure Formation: From dark particle physics to the matter distribution of the Universe". In: *ArXiv e-prints*. arXiv: 1512.05344.

Dasgupta, B. and J. Kopp (2014). "Cosmologically Safe eV-Scale Sterile Neutrinos and Improved Dark Matter Structure". In: *Physical Review Letters* 112.3, 031803, p. 031803. arXiv: 1310.6337 [hep-ph].

De Wit, B. and J. Smith (1986). *Field Theory in Particle Physics Volume 1*. Revised version in preparation, available online. Amsterdam, Netherlands: North-Holland.

Dodelson, S. (2003). *Modern Cosmology*. ISBN: 9780122191411. Academic Press.

Dodelson, S. and L. M. Widrow (1994). "Sterile neutrinos as dark matter". In: *Physical Review Letters* 72, pp. 17–20. eprint: hep-ph/9303287.

Dubinski, J. and R. G. Carlberg (1991). "The structure of cold dark matter halos". In: ApJ 378, pp. 496–503.

Faddeev, L. D. and V. N. Popov (1967). "Feynman Diagrams for the Yang-Mills Field". In: *Phys. Lett.* B25, pp. 29–30.

Gelmini, G. B. (2015). "TASI 2014 Lectures: The Hunt for Dark Matter". In: *ArXiv e-prints*. arXiv: 1502.01320 [hep-ph].

Gondolo, P. and G. Gelmini (1991). "Cosmic abundances of stable particles: improved analysis." In: *Nuclear Physics B* 360, pp. 145–179.

Gorenstein, Paul and Wallace Tucker (2014). "Astronomical Signatures of Dark Matter". In: *Adv. High Energy Phys.* 2014, p. 878203.

Hooper, D. and S. Profumo (2007). "Dark matter and collider phenomenology of universal extra dimensions". In: Phys. Rep. 453, pp. 29–115. eprint: hep-ph/0701197.

Jiang, Fangzhou and Frank C. van den Bosch (2015). "Comprehensive Assessment of the Too-Big-to-Fail Problem". In: *Mon. Not. Roy. Astron. Soc.* 453.4, pp. 3575–3592. arXiv: 1508.02715 [astro-ph.CO].

Kahlhoefer, F. et al. (2016). "Implications of unitarity and gauge invariance for simplified dark matter models". In: *Journal of High Energy Physics* 2, 16, p. 16. arXiv: 1510.02110 [hep-ph].

Klypin, Anatoly A. et al. (1999). "Where are the missing Galactic satellites?" In: *Astrophys. J.* 522, pp. 82–92. arXiv: astro-ph/9901240 [astro-ph].

Ko, P. and Y. Tang (2014). "$\nu\Lambda$MDM: A model for sterile neutrino and dark matter reconciles cosmological and neutrino oscillation data after BICEP2". In: *Physics Letters B* 739, pp. 62–67. arXiv: 1404.0236 [hep-ph].

Kodama, H. and M. Sasaki (1984). "Cosmological Perturbation Theory". In: *Progress of Theoretical Physics Supplement* 78, p. 1.

Kolb, Edward W. and Michael S. Turner (1990). "The Early Universe". In: *Front. Phys.* 69, pp. 1–547.

Kravtsov, Andrey V., Oleg Y. Gnedin, and Anatoly A. Klypin (2004). "The Tumultuous lives of Galactic dwarfs and the missing satellites problem". In: *Astrophys. J.* 609, pp. 482–497. arXiv: astro-ph/0401088 [astro-ph].

Lesgourgues, J. et al. (2013). *Neutrino Cosmology*. Cambridge University Press. ISBN: ISBN 9781107013957.

Lesgourgues, Julien, Gustavo Marques-Tavares, and Martin Schmaltz (2016). "Evidence for dark matter interactions in cosmological precision data?" In: *JCAP* 1602.02, p. 037. arXiv: 1507.04351 [astro-ph.CO].

Loeb, A. and N. Weiner (2011). "Cores in Dwarf Galaxies from Dark Matter with a Yukawa Potential". In: *Physical Review Letters* 106.17, 171302, p. 171302. arXiv: 1011.6374 [astro-ph.CO].

Meszaros, P. (1974). "The behaviour of point masses in an expanding cosmological substratum". In: *Astron. Astrophys.* 37, pp. 225–228.

Milgrom, M. (2010). "New Physics at Low Accelerations (MOND): an Alternative to Dark Matter". In: *American Institute of Physics Conference Series*. Ed. by J.-M. Alimi and A. Fuözfa. Vol. 1241. American Institute of Physics Conference Series, pp. 139–153. arXiv: 0912.2678 [astro-ph.CO].

Mo, Houjun, Frank van den Bosch, and Simon White (2010). *Galaxy Formation and Evolution*. Cambridge University Press, 840 p. ISBN: 978-0-521-85793-2.

Moustakas, L. A. and R. B. Metcalf (2003). "Detecting dark matter substructure spectroscopically in strong gravitational lenses". In: MNRAS 339, pp. 607–615. eprint: astro-ph/0206176.

Nachtmann, O. (1990). *Elementary Particle Physics: Concepts and Phenomena*.

Navarro, J. F., C. S. Frenk, and S. D. M. White (1996). "The Structure of Cold Dark Matter Halos". In: ApJ 462, p. 563. eprint: astro-ph/9508025.

Nollett, Kenneth M. and Gary Steigman (2015). "BBN And The CMB Constrain Neutrino Coupled Light WIMPs". In: *Phys. Rev.* D91.8, p. 083505. arXiv: 1411.6005 [astro-ph.CO].

Pathria, R.K. and P.D. Beale (2011). *Statistical Mechanics*. Academic Press. ISBN: ISBN 9780123821881.

Peskin, Michael E. and Daniel V. Schroeder (1995). *An Introduction to quantum field theory*. Reading, USA: Addison-Wesley 842 p. ISBN: 9780201503975, 0201503972.

Petraki, K. and R. R. Volkas (2013). "Review of Asymmetric Dark Matter". In: *International Journal of Modern Physics A* 28, 1330028, p. 1330028. arXiv: 1305.4939 [hep-ph].

Planck Collaboration et al. (2015). "Planck 2015 results. XIII. Cosmological parameters". In: *ArXiv e-prints*. arXiv: 1502.01589.

Pospelov, M. and T. ter Veldhuis (2000). "Direct and indirect limits on the electro-magnetic form factors of WIMPs". In: *Physics Letters B* 480, pp. 181–186. eprint: hep-ph/0003010.

Preskill, John, Mark B. Wise, and Frank Wilczek (1983). "Cosmology of the Invisible Axion". In: *Phys. Lett.* B120, pp. 127–132.

Riemer-Sorensen, Signe, David Parkinson, and Tamara M. Davis (2013). "What is half a neutrino? Reviewing cosmological constraints on neutrinos and dark radiation". In: *Publ. Astron. Soc. Austral.* 30, e029. arXiv: 1301.7102 [astro-ph.CO].

Rocha, M. et al. (2013). "Cosmological simulations with self-interacting dark matter - I. Constant-density cores and substructure". In: MNRAS 430, pp. 81–104. arXiv: 1208.3025.

Saro, A. et al. (2013). "Toward Unbiased Galaxy Cluster Masses from Line-of-sight Velocity Dispersions". In: ApJ 772, 47, p. 47. arXiv: 1203.5708.

Steigman, G., B. Dasgupta, and J. F. Beacom (2012). "Precise relic WIMP abundance and its impact on searches for dark matter annihilation". In: Phys. Rev. D 86.2, 023506, p. 023506. arXiv: 1204.3622 [hep-ph].

Stetson, Peter B. (1994). "The Center of the core - cusp globular cluster M15: CFHT and HST Observations, ALLFRAME reductions". In: *Publ. Astron. Soc. Pac.* 106, p. 250.

Tang, Yong (2016). "Interacting Scalar Radiation and Dark Matter in Cosmology". In: *Phys. Lett.* B757, pp. 387–392. arXiv: 1603.00165 [astro-ph.CO].

Taoso, M., G. Bertone, and A. Masiero (2008). "Dark matter candidates: a ten-point test". In: J. Cosmology Astropart. Phys. 3, 022, p. 022. arXiv: 0711.4996.

The Fermi-LAT Collaboration et al. (2013). "Dark Matter Constraints from Observations of 25 Milky Way Satellite Galaxies with the Fermi Large Area Telescope". In: *ArXiv e-prints*. arXiv: 1310.0828 [astro-ph.HE].

Tulin, S., H.-B. Yu, and K. M. Zurek (2013). "Beyond collisionless dark matter: Particle physics dynamics for dark matter halo structure". In: Phys. Rev. D 87.11, 115007, p. 115007. arXiv: 1302.3898 [hep-ph].

van den Aarssen, L. G., T. Bringmann, and Y. C. Goedecke (2012). "Thermal decoupling and the smallest subhalo mass in dark matter models with Sommerfeld-enhanced annihilation rates". In: Phys. Rev. D 85.12, 123512, p. 123512. arXiv: 1202.5456 [hep-ph].

van Uitert, E. et al. (2012). "Constraints on the shapes of galaxy dark matter haloes from weak gravitational lensing". In: A&A 545, A71, A71. arXiv: 1206.4304.

Vogelsberger, M. et al. (2015). "ETHOS - An Effective Theory of Structure Formation: Dark matter physics as a possible explanation of the small-scale CDM problems". In: *ArXiv e-prints*. arXiv: 1512.05349.

Vogelsberger, Mark, Jesus Zavala, and Abraham Loeb (2012). "Subhaloes in Self-Interacting Galactic Dark Matter Haloes". In: *Mon. Not. Roy. Astron. Soc.* 423, p. 3740. arXiv: 1201.5892 [astro-ph.CO].

Weinberg, Steven (2008). *Cosmology*. Oxford, UK: Oxford Univ. Pr. 593 p.

Wigner, Eugene P. (1939). "On Unitary Representations of the Inhomogeneous Lorentz Group". In: *Annals Math.* 40. [Reprint: Nucl. Phys. Proc. Suppl.6,9(1989)], pp. 149–204.

Zavala, Jesús, Mark Vogelsberger, and Matthew G. Walker (2013). "Constraining self-interacting dark matter with the Milky Way's dwarf spheroidals". In: *Monthly Notices of the Royal Astronomical Society: Letters*.

Zwicky, F. (1933). "Die Rotverschiebung von extragalaktischen Nebeln". In: *Helv. Phys. Acta* 6, pp. 110–127.